University of the Pacific Theses and Dissertations

Graduate School

2019

Fliposomes with a pH-sensitive conformational switch for anticancer drug delivery against triple negative breast cancer

Yifan Lu
University of the Pacific, y_lu5@u.pacific.edu

Follow this and additional works at: https://scholarlycommons.pacific.edu/uop_etds

    Part of the Pharmacy and Pharmaceutical Sciences Commons

FLIPOSOMES WITH A PH-SENSITIVE CONFORMATIONAL SWITCH FOR ANTICANCER DRUG DELIVERY AGAINST TRIPLE NEGATIVE BREAST CANCER

by

Yifan Lu

A Dissertation Submitted to the

Graduate School

In Partial Fulfillment of the

Requirements for the Degree of

DOCTOR OF PHILOSOPHY

Thomas J Long School of Pharmacy and Health Sciences
Pharmaceutical and Chemical Sciences

University of the Pacific
Stockton, CA

2019

FLIPOSOMES WITH A PH-SENSITIVE CONFORMATIONAL SWITCH FOR
ANTICANCER DRUG DELIVERY AGAINST TRIPLE NEGATIVE BREAST CANCER

by

Yifan Lu

APPROVED BY:

Dissertation Advisor: Xin Guo, Ph.D.

Committee Member: Xiaoling Li, Ph.D.

Committee Member: Melanie Felmlee, Ph.D.

Committee Member: Dongxiao Zhang, Ph.D.

Committee Member: Qinliang Zhao, Ph.D.

Department Chair: William K. Chan, Pharm.D., Ph.D.

Dean of Graduate School: Thomas Naehr, Ph.D.

FLIPOSOMES WITH A PH-SENSITIVE CONFORMATIONAL SWITCH FOR
ANTICANCER DRUG DELIVERY AGAINST TRIPLE NEGATIVE BREAST CANCER

DEDICATION

This dissertation is dedicated to my wife and lovely kids for their love and support, and is also dedicated to my beloved mom.

ACKNOWLEDGMENTS

I would like to express my sincere gratitude to my advisor Dr. Xin Guo for his continuous guidance and support during the years of my graduate studies. I had the distinct pleasure of working with him, especially enjoyed the environment of freedom he created in the lab. I must say thanks to Dr. Guo for bearing me so many unsuccessful trials with all the resources. It was a great experience to work with him on so many promising projects. I can always get help, insight and encouragement from him. His advice on both research and my personal life have been invaluable.

I would also like to thank acknowledge my committee member Dr. Xiaoling Li. Without him, I probably wouldn't know the Pacific and PCSP program. Appreciate all the extended discussions and valuable suggestions in my research and my career. I really appreciate his participation to my dissertation committee and enjoyed working under his guidance to develop my leadership. I want to thank Dr. Melanie Felmlee for all help she provided in my research, tremendous input and suggestions in my animal study. She is the master in terms of animal technology. I learned so much from her, especially passion and techniques for the scientific research. In the same way, I would like to thank Dr. Qinliang Zhao for all help and support in my research as well as my life. She is always there whenever I need help. Special thanks are due to Dr. Dongxiao Zhang who is an industrial leader and set a great example to me. He gave invaluable suggestions and input to our project. I am honored to have all of them on my dissertation committee. I would like to give my thanks to Dr. Bhaskara Jasti for his suggestion in joint group meeting, Dr. James Uchizono for his guidance and help in research and all student activities, Dr. William K. Chan for allowing me use so many instruments in their lab, Dr. John Livesey for providing the facilities as well as detailed training for my research, Dr. Lisa

Wrischnik for so many suggestions and guidance on confocal microscopy. I also want to thank Kathy Kassab and Lynda Davis for taking care me as a child.

I would like to thank Guo's group members both past and present. Especially thanks to Dr. Shen Zhao, who is my partner in the project and a close friend in my life. Without him, we can't start the project. Mallika Vadlamudi, she is always here when I need help. Glad to work with her in the research as well as in our AAPS student chapter. I am sincerely grateful for the time Yingbo spent for my research as the most reliable partner. Xinyu Pei, Ruiqi Huang, Zhongyue Yuan, Zizhao Xu's contribution in 3D MCS and animal study is unforgettable. I'm glad make so many friends through the boring research time. I want to thank Dr. Siwen Wang, Dr. Yujuan Zheng, Dr. Yu Zheng, Dr. Zhu Zhou, Poonam Dattani, Hunan Li, Chao Feng, Weizhou Yue, Jieyun Cao, Jinyun Chen, Yujie Yang, Hao Wei, Zhixin Lu, Michael Ng, Fang Liu, Kevin Zhang, Dengpan Liang, Jingda Wang, Md Zahir Uddin, Ryan Murray, Michael Pastor, Sven Hackbusch, Ronnie Ruyonga, Patrick Batoon, for their help in my research and the happiness they brought to my life.

Finally, I would like to thank my family. Their unconditional love supports, prepares and strengths me to walk through this tough but invaluable journey.

Fliposomes with a pH-sensitive conformational switch for anticancer
drug delivery against triple negative breast cancer

Abstract

by Yifan Lu

University of the Pacific
2019

Cancer is the second leading cause of death in the US and worldwide, accounting for 16% of deaths worldwide in 2015. Of more than 100 types of cancers affecting humans, breast cancer is the most common cancer among women and is the second leading cause of death in women. Triple negative breast cancer (TNBC) is a subtype of breast carcinomas defined by the lack of the expression of estrogen receptor (ER), progesterone receptor (PR) and human epidermal growth factor receptor (HER2 /neu). The prognosis and survival of TNBC patients remains the poor due to the lack of effective targeted therapy.

Nanotechnology-based drug delivery systems, such as liposomes, are widely investigated to enhance anticancer efficacy by concentrating the drug molecules in the tissues of interest and by altering the pharmacokinetic profile. Taking advantage of the pH gradient in the tumor microenvironment, pH-triggered release is a promising strategy to enhance the anticancer efficacy of drug delivery systems against TNBC. Previously, a strategy in our lab has been developed to render saturated and pegylated liposomes pH-sensitive: protonation-induced conformational switch of lipid tails, using trans-2-aminocyclohexanol lipids (TACH, flipids) as a molecular trigger. Based on previous work in our lab, pH-sensitive liposomes (fliposomes) composed of C-16 flipids with amine group of morpholine (MOR) and azetidine (AZE) demonstrated optimized triggered release in response to the tumor's low pH microenvironment.

In this study, different preparation methods were developed and optimized to produce viable fliposomes with high doxorubicin (DOX) encapsulation efficiency. *In vitro* release assays were established and validated to accurately reflect pH-triggered release of fliposomes. The physicochemical properties of DOX-loaded fliposomes were characterized and their pH-dependent release were investigated. Factors influencing the desirable attributes of liposomes, such as size, pH-sensitivity, stability and drug-loading capacity were explored. Based on these characterizations, central composite design (CCD) was utilized to optimize the formulation of fliposome with two critical factors, flipids and cholesterol.

Cell viability assays on traditional monolayer and innovative three-dimensional multicellular spheroids (3D MCS) of TNBC cell lines were conducted to evaluate the anticancer efficacy of the resultant fliposomes *in vitro*. The constructed 3D MCS carried heterogeneously distributed live and apoptotic cells, as well as acidity inside the 3D MCS based on confocal microscopic imaging studies. The distribution and penetration of DOX-loaded fliposomes into 3D MCS was imaged by confocal microscopy in comparison to DOX-loaded non pH-sensitive liposomes and free DOX. As a result, fliposome manifested superior anticancer activity against TNBC 3D MCS by efficient penetration into 3D MCS, followed by tuning up the release rate of the anticancer agent DOX.

A TNBC orthotopic xenograft model was established by transplanting TNBC into the murine mammalian fat pad, which maintains the organ-specific tumor microenvironment of the original organ. A pilot pharmacokinetic study was conducted in order to correlate the pH response and stability properties with the *in vivo* stability of the optimized AZE-C16 fliposome. The antitumor efficacy was comparable between free DOX and DOX-loaded stealth liposome with tumor volumes of ~ 80-90% of the control treatment 32 days post first dose. In contrast, the

DOX-loaded fliposome, especially MOR-C16 fliposome, exhibited a significantly higher antitumor efficacy and delayed progression compared to free DOX and stealth liposome treatments.

Taken together, DOX-loaded fliposomes were successfully prepared and optimized for *in vivo* application. They were able to achieve superior activity against TNBC *in vitro* and *in vivo*, facilitated by enhanced release of the anticancer drug DOX after penetration inside TNBC tumor.

TABLE OF CONTENTS

LIST OF TABLES

Table

LIST OF FIGURES

Figure

LIST OF ABBREVIATIONS

ADC	Antibody-drug conjugate
ANOVA	Analysis of variance
AZE	Azetidine
CCD	Central composite design
CDX	Cell-derived xenografts
Chol	Cholesterol
$C_{12}E_8$	Octaethylene glycol monododecyl ether
DFS	Disease-free survival
DMEM	Dulbecco's Modification of Eagle's Medium
DMSO	Dimethyl sulfoxide
DLPC	1,2-dilauroyl-sn-glycero-3-phosphocholine
DMPC	1,2-dimyristoyl-sn-glycero-3-phosphocholine
DPPC	1,2-dipalmitoyl-sn-glycero-3-phosphocholine
DSPC	1,2-distearoyl-sn-glycero-3-phosphocholine
DOPC	1,2-dioleoyl-sn-glycero-3-phosphocholine
DOX	Doxorubicin
ECG	Electrocardiography
ECM	Extracellular matrix
EE	Encapsulation efficiency
EPR	Enhanced permeability and retention
ER	Estrogen receptor
GEMM	Genetically engineered mouse models
HEPES	2-[4-(2-hydroxyethyl)piperazin-1-yl]-ethanesulfonic acid
HER2	Human epidermal growth factor receptor
HPLC	High-performance liquid chromatography

LUV	Large unilamellar vesicles
MCS	Multicellular spheroids
MES	2-(N-morpholino)ethanesulfonic acidc1
MLV	Multilamellar vesicles
MOR	Morpholine
NEEA	Non-Essential Amino Acid
OS	Overall survival
pCR	Pathologic complete response
PDI	Polydispersity Index
PDX	Patient-derived xenografts
PE	Phosphatidylethanolamine
PEG	Polyethylene glycol
POPC	1-palmitoyl-2-oleoyl-glycero-3-phosphocholine
QC	Quality control
RED	Rapid Equilibrium Dialysis
RES	Reticuloendothelial system
ROS	Reactive oxygen species
PBS	Phosphate buffered saline
PR	Progesterone receptor
RSM	Response surface methodology
SD	Standard deviation
SEM	Standard error of mean
SUV	Small unilamellar vesicle
TACH	Trans-2-aminocyclohexanol
TEA	Triethanolamine
T_m	Transition temperature
TNBC	Triple negative breast cancer

TOP II	Topoisomerase II
Tris	2-Amino-2-(hydroxymethyl)propane-1,3-diol
ULA	Ultra-low attachment

Chapter 1: Introduction

1.1 Statement of the Problem

 1.1.1 Triple negative breast cancer (TNBC). Cancer is a large group of related diseases that involves rapid and abnormal proliferation of cells with the potential to spread and invade surrounding tissues [1]. Cancer is the second leading cause of death in the US and worldwide, accounting for 16% of deaths worldwide in 2015 [2]. About 1.7 million new cases of cancer and about 609,640 deaths have been estimated in the US for the year 2018 [1]. Of more than 100 types of cancers affecting humans, breast cancer is the most common cancer among women and is the second leading cause of death in women, exceeded only by lung cancer [3]. Clinically, breast cancers can be divided into various subtypes by stage, pathology, grade or the expression level of specific receptors [4, 5]. Triple negative breast cancer (TNBC), a subtype accounting for approximately 15% to 20% of all breast carcinomas, is defined by the lack of expression of the estrogen receptor (ER), the progesterone receptor (PR) and the human epidermal growth factor receptor (HER2 /neu) [4, 6, 7]. It was reported that TNBC is much more common in younger women and in women of African ancestry in addition to exhibiting more BRCA1 mutations [8]. Although the population of TNBC is not the largest among various subtypes of breast cancer, the prognosis for TNBC remains the poorest because it is more aggressive and not responsive to targeted therapies that are effective to other subtypes of breast cancer. Among breast cancer patients, those with TNBC have the poorest prognosis and the shortest life span [7].

 1.1.2 Treatment choices and chemotherapy. Patients with TNBC cannot benefit from hormone therapy because the cancer is ER/PR-negative; they cannot benefit from Herceptin-based therapy because the cancer cells are HER2-negative. Therefore, surgery, radiation therapy

and chemotherapy, individually or in combination, are the only available options for the TNBC patients.

Surgery and radiotherapy are available options to patients with other subtypes of breast cancer. Basically, there are 2 types of breast cancer surgery: lumpectomy and mastectomy, of which the aim is to remove the entire tumor from the breast. Radiotherapy is typically conducted in the TNBC patient following the surgery, more often in women having lumpectomy (breast conserving surgery). It was reported that TNBC patients with the BRCA1 gene mutation are potentially highly radiosensitive and benefit more from the radiotherapy [9].

Chemotherapy, individually or in combination with surgery or radiotherapy is predominantly given to the patients with both early stage and advanced TNBC although there are no standard guidelines for TNBC chemotherapeutic treatment [5, 10]. Generally, there are different categories of chemotherapies based on the mechanism, including microtubule stabilizers, DNA replication inhibitor, cell proliferation inhibitor and targeted therapies [10, 11].

Microtubule stabilizers are a group of microtubule-targeting agents that bind to microtubules and increase the quantity of cellular microtubules by breaking the dynamics of tubulin polymer during the mitotic stage of the cell cycle [12, 13]. Taxanes, including paclitaxel and docetaxel, exhibit more potency against TNBCs than receptor-positive breast cancers. It was reported that TNBC patients who received the treatment of fluororacil, epirubicin, and cyclophosphamide (FEC) followed by weekly paclitaxel for 8 week benefit more than the patient receiving FEC only [14].

Platinum compounds play a major role in treating TNBC. Carboplatin and cisplatin form crosslinks within and between double-stranded DNA, which inhibits DNA replication. Hence, platinums can overcome the DNA repair cascade caused by the BRCA mutation, making them

the primary option for the TNBC patient with BRCA mutation [15]. Although Zhang *et al.* reported the cisplatin-based treatment have the best efficacy against TNBC, the platinums are still recommended to be used with other chemotherapeutic drug to achieve better efficacy [16].

Anthracyclines, such as doxorubicin and epirubicin, are some of the most common and most active drugs for the breast cancer treatment. It was found that the pathologic complete response (pCR), disease-free survival (DFS) and overall survival (OS) are improved with the use of neoadjuvant chemotherapy, in which anthracycline-based regimen is frequently utilized. Carey *et al.* reported that doxorubicin and cyclophosphamide treatment showed better clinical sefficacy on TNBC patients than non-TNBC patients [17]. In addition, DNA damage caused by anthracycline can also bypass the effect of BRCA mutation [18]. 57.1% vs 29% pCR rates were found between BRCA1 mutated and wild type TNBC patients after being treated with anthracycline and taxane regimens, respectively [19].

In addition, targeted chemotherapy, which aims at particular growth factor or receptor is also widely used in the treatment of TNBC. Examples of targeted therapy include PARP inhibitors, angiogenesis inhibitors, EGFR inhibitors, TK inhibitors and mTOR inhibitors [10]. Immunotherapy, such as checkpoint inhibitors, has also emerged to improve the outcome of advanced-stage TNBC in combination with chemotherapy [20].

1.1.3 Doxorubicin: Pros and cons. Doxorubicin (DOX or DXR) (Figure 1.1), which was first extracted from the actinobacteria *Streptomyces peucetius* var. *caesius*, is one of the most commonly used anthracyclines [21]. DOX belongs to the antibiotic category of cytotoxic anticancer drugs [22]. DOX is indicated in the treatment of various cancers including breast cancer, ovarian cancer, lung cancer, neuroblastoma, gastric cancer, Hodgkin lymphoma and acute lymphocytic leukemia[23-25]. It is administrated by an intravenous injection through

catheter to prevent extravasation and is often used in a combination with other chemotherapy drugs [17, 19, 26].

C$_{27}$H$_{29}$NO$_{11}$
Exact Mass: 543.17
Mol. Wt.: 543.52
m/e: 543.17 (100.0%), 544.18 (30.9%), 545.18 (6.8%), 546.18 (1.1%)
C, 59.66; H, 5.38; N, 2.58; O, 32.38
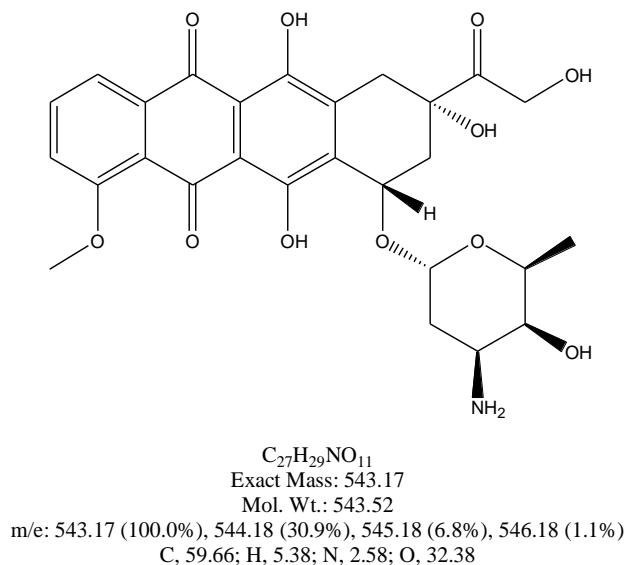
Figure 1.1. Chemical Structure of Doxorubicin

The cytotoxicity of DOX is cell cycle-nonspecific but peaks in the S phase. Several mechanisms have been proposed to explain the anticancer activity of DOX, of which two major ones are widely accepted (Figure 1.2). One is inhibition of macromolecular biosynthesis by intercalation into DNA and another is cell membrane damage through the generation of free radicals and reactive oxygen species (ROS) [27-29]. The intercalation of DOX into DNA causes inhibition of the function of the topoisomerase II (TOP II) complex, an enzyme responsible for relaxing supercoils in DNA during transcription [27, 30, 31]. Regarding free radical generation, DOX is reduced by the ubiquitous oxidoreductases to form unstable DOX-semiquinone radicals, which carry out one-electron reduction of molecular oxygen to generate reactive oxygen species (ROS) that lead to lipid peroxidation and membrane damage, DNA damage and oxidative stress, eventually triggering apoptotic pathways of cell death [29, 32].
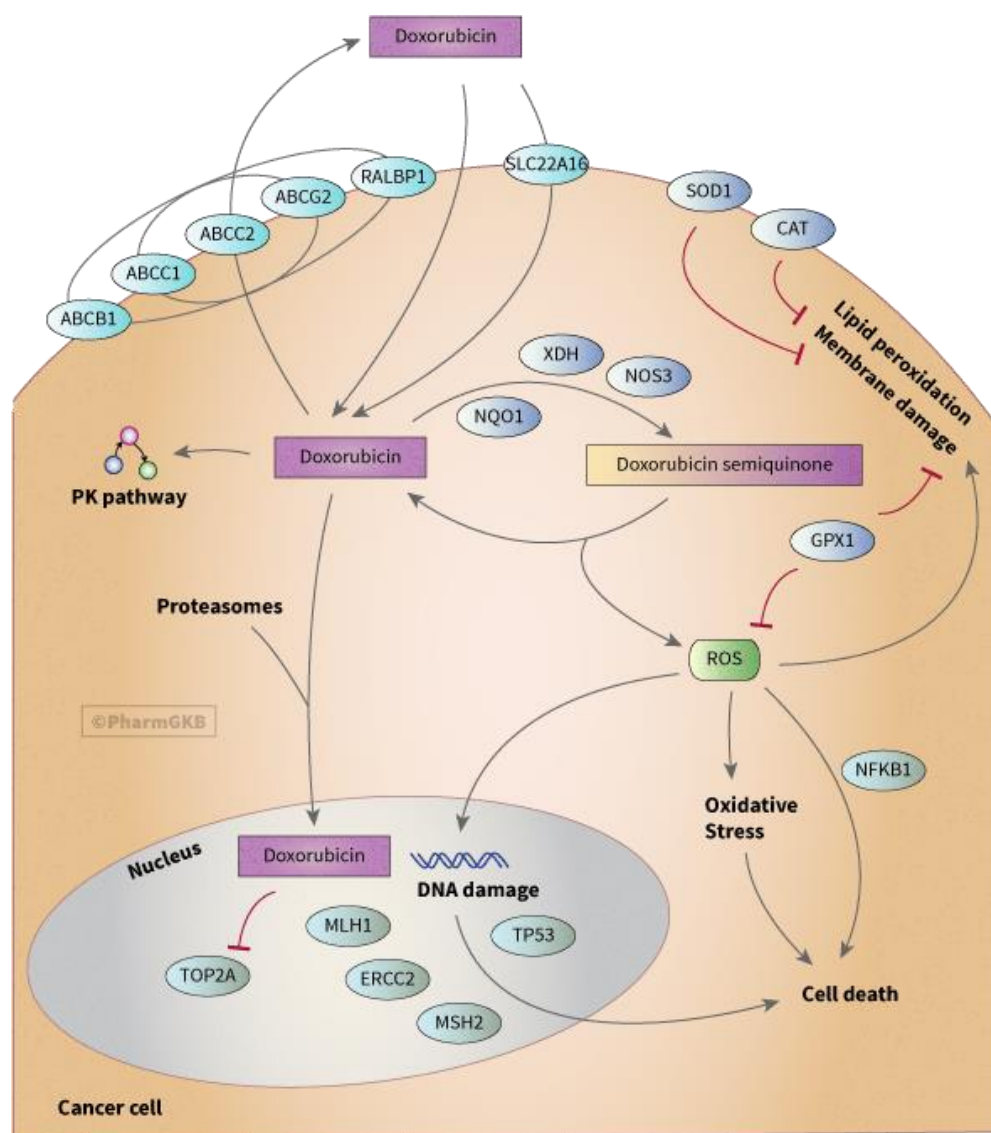
Figure 1.2. Mechanism of action of doxorubicin (candidate genes involved in the action of doxorubicin in a stylized cancer cell) [33].

After the approval of DOX in 1974, it took 20 years to see the approval of paclitaxel for metastatic breast cancer [34]. The ability to arrest the cell cycle at all stages and the broad-spectrum antineoplastic activity makes DOX most widely used in cancer therapy. However, the clinical use of DOX is still restricted by several side effects (Table 1.1), especially dose-dependent cardiotoxicity [35, 36]. The development of liposomal DOX was based on the

rationale, that the DOX encapsulated inside liposome cannot extravasate in areas with tight

capillary junctions such as heart muscle but can escape where the vasculature is not tighty

jointed such as in solid tumors [37]. Hence, the first nanotechnology-based drug Doxil® carries

less cardiotoxicity than the free DOX, and was approved in 1995 [38].

Table 1.1. Adverse effects associated with doxorubicin [37]

Category	Adverse events
Hematologic	Bone marrow depression especially of neutrophils and platelets
Dermatologic	Photosensitivity, itching, rash
Gastrointestinal	Nausea, vomiting, oral ulceration, lopecia, diarrhea
Cardiovascular	
Acute cardiotoxicity	Tachycardia, hypotension and various Electrocardiography (ECG) changes due to arrhythmia
Chronic cardiotoxicity	Cardiomyopathy leading to congestive cardiac failure
Renal	Glomerular atrophy and increase glomerular permeability

Another practical reason leading us to select DOX as a cargo drug is its unique spectral

property. DOX is a fluorescent molecule which is typically excited at 485 nm and emits high

quantum yield fluorescence between 560 - 590 nm. Such a long wavelength allows us to

conduct visualized experiments to investigate the DOX's distribution *in vitro*.

1.1.4 Barriers in drug delivery to TNBC. TNBC is considered as a malignant solid

tumor, which is an abnormal growth of cells that forms a mass in a solid tissue. The

physiological characteristics of a solid tumor (Figure 1.3) are distinct from normal tissue,

including neovasculature, interstitial pressure, and multiple gradients of nutrients, oxygen and

therapeutic agents. Newly formed blood vessels are structurally and functionally abnormal [39].

The distribution of blood vessels in a solid tumor is also heterogeneous, ranging from well

perfused periphery to avascular necrotic core, which increases the difficulty to sufficiently deliver anticancer agents into all the cancer cells. In addition, the high interstitial pressure in tumors compared to normal tissues leads to a net outward flow from the core of the tumor. It was reported that the elevated interstitial fluid pressure of a solid tumor may aggravate the gradients of angiogenic factor that are released into the surrounding tissues [40]. Furthermore, the abnormal lymphatic function, the elevated interstitial hydraulic conductivity as well as the collapse of tumor lymphatic drainage are the main causes of the interstitial fluid pressure inside the solid tumor [40].

To exert its activity, an anticancer drug has to avoid quick clearance and distribute sufficiently to the blood vessels of a tumor, then permeate through the tumor blood vessels efficiently, then translocate through the interstitial matrix to penetrate deep into the tumor [41]. The extravasation and the penetration are largely affected by the physiochemical properties of the compound, such as size, charge, and solubility in water and lipids. The penetration and transport through the tumor interstitium are mainly controlled by diffusion, which is governed by concentration gradient. However, ionization of the drug molecule in the tumor microenvironment will increase its interaction with the extracellular matrix and thus hamper diffusion. One example would be doxorubicin, a weak base, getting protonated and then stuck in the acidic organelles and interstitium. The transport of larger molecules is mainly governed by convection, which depends on the hydraulic conductivity and pressure difference. Specifically, extravasation of macromolecules will be drastically decreased by the high interstitial fluid pressure of the solid tumor. Furthermore, the well interconnected structure of extracellular matrix, such as collagen, will decrease the penetration of high-molecular-weight drugs [42]. All

those characters in solid tumor are all present in TNBC and create a dreadful barrier to the delivery of anticancer drugs against TNBC.
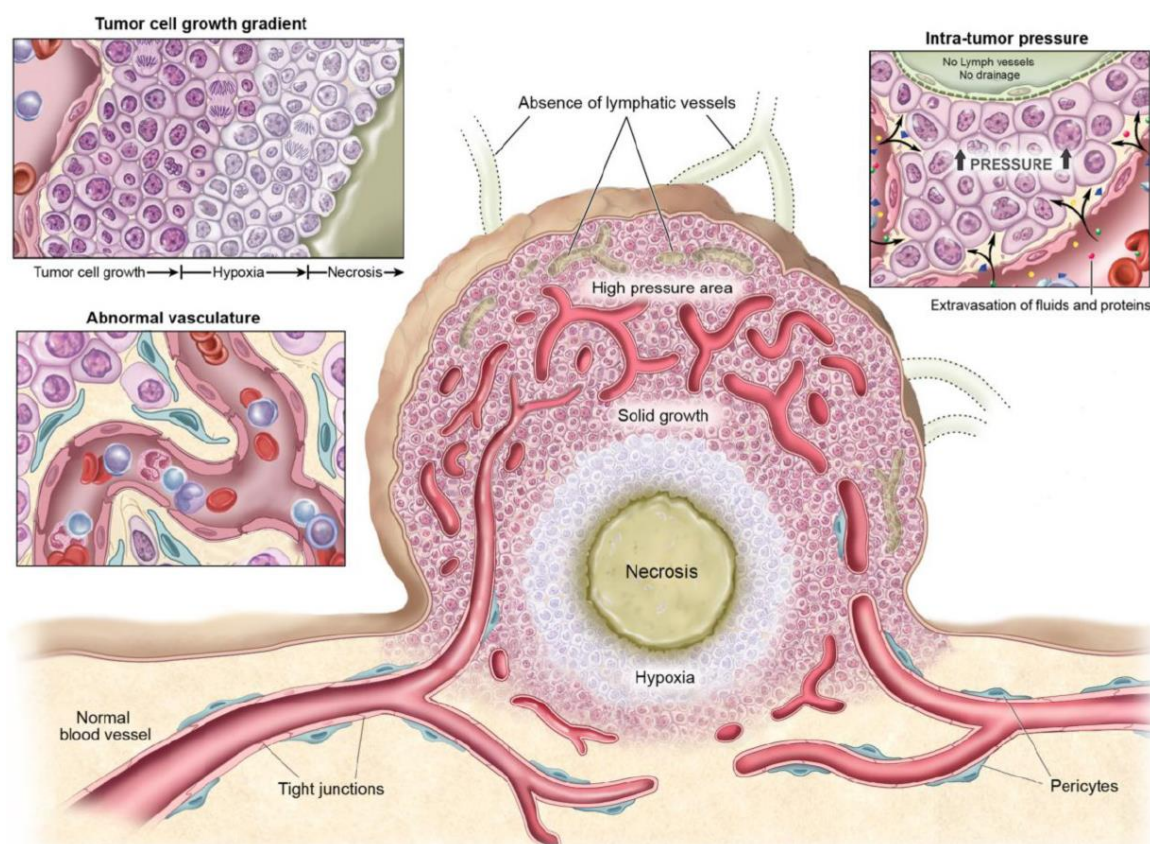
Figure 1.3. Physiological Characteristics of Tumor Tissue and Vasculatures [43]

1.2 Strategies for Effective Delivery of Doxorubicin to Solid Tumors

1.2.1 Targeted delivery. An ideal drug delivery system has to overcome the above mentioned barriers in order to improve therapeutic efficacy and to minimize adverse effects of the cargo drug. Targeted drug delivery provides one of the solutions by modifying the pharmacokinetics profile, especially the distribution of anticancer agents. Generally, there are two broad classes of drug targeting, namely passive targeting and active targeting [44, 45].

1.2.1.1 Passive targeting. Passive targeting, also called physical targeting, achieves the

desired accumulation of therapeutic agent at the target site by catering the physicochemical

properties of the drug delivery system to the distinctive characteristics of the pathologic

tissue/organ. The enhanced permeation and retention (EPR) effect, one of mechanisms of

passive targeting (Figure 1.4), was proposed in 1986 as an innovative strategy to deliver

macromolecular drugs to tumors [46]. The enhanced permeation of nanocarriers or

macromolecules at the tumor site is caused by tumor vascular leakage while the enhanced

retention occurs due to the impaired lymphatic drainage within neoplastic tissues [47]. The cut-

off size of the permeabilized vasculature varies, but 200 nm in diameter or below is generally

accepted for the solid tumor vasculature [48]. Nevertheless, an extended period of circulation in

the blood is required for this type of drug delivery system to achieve sufficient accumulation in

the tumor. Besides keeping the molecular weight above 40 kDa to circumvent renal filtration,

the common way to keep the nano-drug delivery system in the blood stream is to disguise them

by grafting their surface with polyethylene glycol (PEG). This hydrophilic polymer minimizes

the adsorption of serum proteins to prevent opsonization and thus hinder their recognition and

clearance by the reticuloendothelial system (RES) [49]. Generally, the higher average molecular

weight of PEG leads to longer systemic circulation time, except that liver clearance is found to

be enhanced when the average molecular weight of PEG goes over above 50 kDa [50]. In

addition, prolonged circulation makes it possible to maintain therapeutic concentrations of drug

or drug delivery system in the blood for a relatively long time even after a single dose.
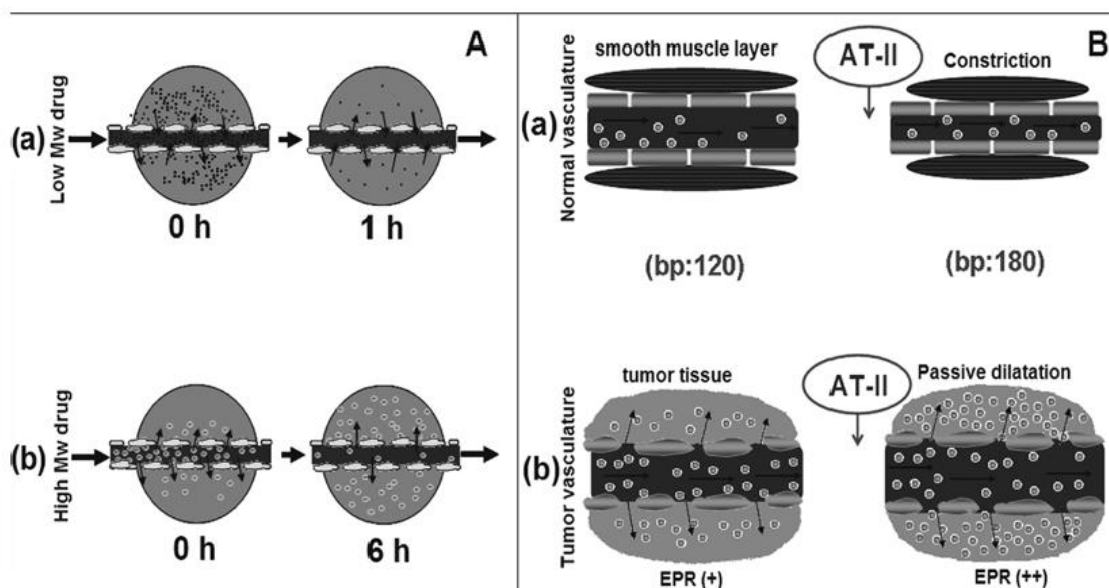
Figure 1.4. Diagrammatic representation of EPR effect [51].

It must be noted that there are several challenges in passive targeting for anticancer drug delivery. First, the EPR effect varies by the different structures of various tumors. For instance, hepatic and renal carcinoma show relatively strong EPR effect due to the high vascular density, while pancreatic and prostate cancers show less EPR effect [46]. In addition, the heterogeneity within one solid tumor also creates an imbalance of the EPR effect. It is reported that the central necrotic area of metastatic cancers doesn't exhibit the EPR effect due to the lack of vasculature [52, 53]. This phenomenon makes penetration the limiting step to achieve the desired therapeutic efficacy. Furthermore, tumor growth rate and tumor size in animal models are not comparable to that in humans, leading to differences of EPR effect between tumor and tumor xenografts [54]. Rodent tumor models always have tumors at least 5 mm in diameter during the late stage and a larger tumor is more likely to have hypovascular areas in the necrotic core. Moreover, the resistance of the capillary wall to the move of macromolecules or drug delivery

system getting into tumor interstitial space, which is significantly greater than subsequent

resistance, is a noticeable factor that affects the outcome of the EPR effect [55].

1.2.1.2 Active targeting. In general, active targeting involves coupling specific targeting

ligands to the surface of the drug carrier so that it can selectively bind to target receptors

expressed on the surface of particular cell, tissue or an organ [56, 57]. The strong interaction

between the ligand and receptor is so selective that the unwanted non-specific binding in

peripheral tissues and toxicity will be reduced. Because some receptors manifest higher

expression in the tumor cells or tumor vasculature cells than normal cells, a solid tumor is highly

likely to get benefits of active targeting therapy. It is also reported that the activation of

receptor-mediated endocytosis by such specific binding can suppress multidrug resistance

because it circumvents drug efflux by P-glycoprotein [58]. Tremendous effects were put into

developing novel targeted delivery systems for diagnostic and therapeutic applications in various

diseases. The active targeting ligands that are exploited in those systems include antibodies,

antibody fragments, aptamers, peptides, proteins and some small molecules which are known as

receptor ligands [59]. Currently, antibody-drug conjugates (ADCs), which currently represent

the leading class of biopharmaceutical drugs, is an eminent example of the active targeting

strategy. All the four approved ADC products are utilized to treat various types of cancer, which

suggests the great clinical response to this strategy of treating cancer. Unfortunately, TNBC is

so far known to have no potential target receptor to take advantage of active targeting.

1.2.2 Liposomes. As one of the nanocarriers, liposomes are nano-sized vesicles

composed of amphiphilic molecules such as phospholipids, which form a closed bilayer structure

that encloses a central aqueous compartment [60-62] (Figure 1.5). Liposomes have a spherical

shape with the size ranging from 20 nm to a few microns in diameter. Typically, the hydrophilic

drug molecules can be encapsulated in the aqueous core while lipophilic drugs can be incorporated in the lipid bilayer (Figure 1.6), which enables liposomes to deliver a variety of cargo molecules including small molecules, proteins, nucleotides and even plasmids [61]. Liposomes can be categorized into the following types based on the numbers of concentric lipid bilayers and the size: multilamellar vesicle (MLV), small unilamellar vesicle (SUV) and large unilamellar vesicle (LUV) [63].

From the perspective of biomedical application, liposomes consist of biocompatible material which won't cause severe allergic or toxic reactions and will eventually be broken down through biological pathways [64]. Liposomes can protect the entrapped cargo molecules, especially proteins and nucleotides from the inactivating effect of the physiological media [44]. It was also reported that liposomes can fuse with the cell surface to deliver agents into cell [65]. From the perspective of clinical application, liposomes are capable of altering the bio-distribution and the rate of clearance of the contents entrapped, which results in the drastic change of the pharmacokinetic parameters [64]. The physicochemical properties of the liposome, such as size, surface charge and steric stabilization are the main factors affecting the pharmacokinetic profile. Besides these features, the surface of the liposomes can be grafted with various molecules to enhance their stability in blood circulation and/or to increase their specific targeting to certain cells/tissues. The first liposomal pharmaceutical product Doxil® (Janssen Products, LP, Horsham, PA) was approved by the FDA to treat Kaposi's sarcoma and breast cancer in 1995 and 2003, respectively [38, 66]. There are currently more than ten marketed liposomal products and hundreds of new products are in various stages of clinical trials.
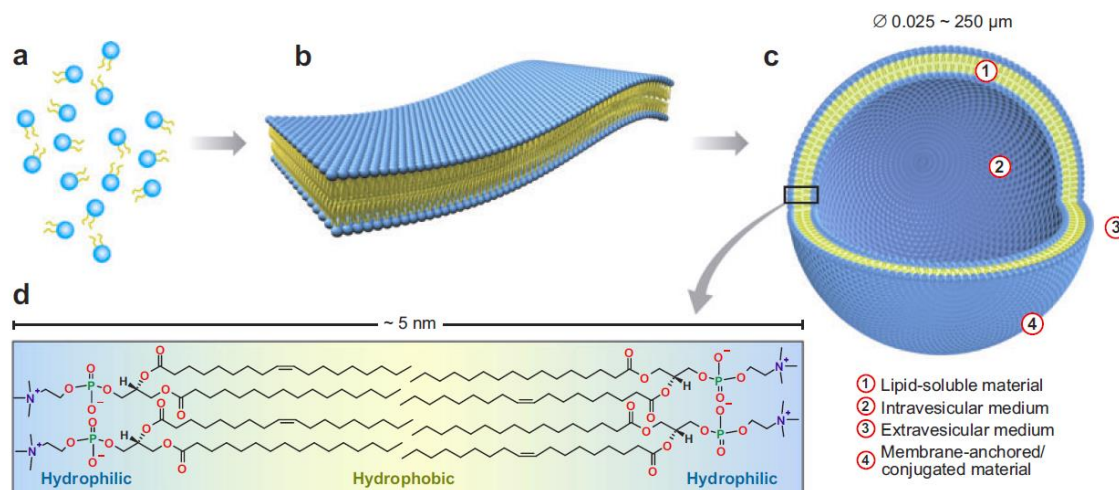
Figure 1.5. The self-assembly of individual amphiphilic lipids (a) to bilayer (b) and then to closed liposomes (c). A single bilayer is typically ~5 nm thick and consists of neatly arranged individual lipid molecules with their hydrophilic heads facing the internal and external aqueous media and their hydrophobic tails packed inside the bilayer (d) [67].
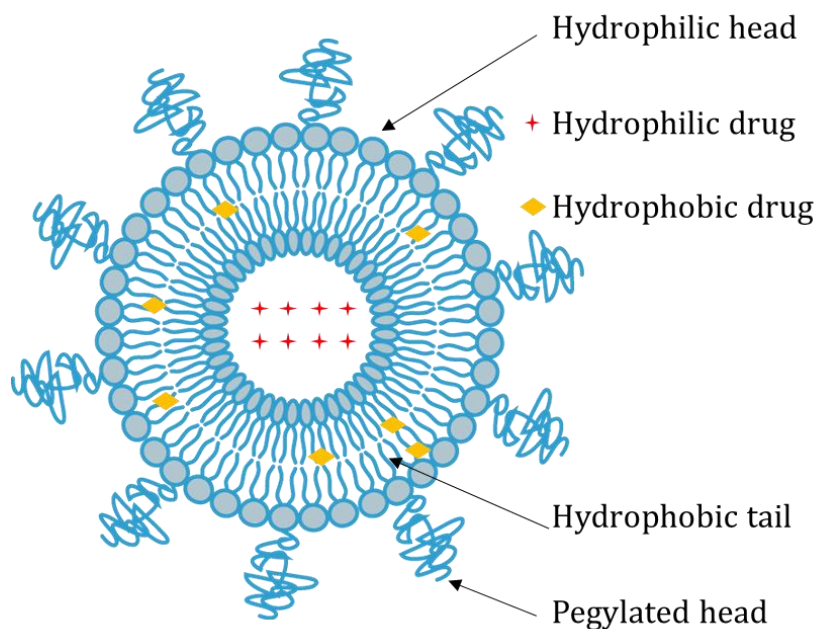
Figure 1.6. Drug loading in liposome: soluble hydrophilic drugs are entrapped into the aqueous interior of the liposome (✛), while poorly soluble hydrophobic drugs are localized in the liposomal membrane (◆)

1.2.2.1 Conventional liposomes. Conventional liposomes, sometimes termed classical liposomes or 1st generation liposomes, are made up of neutral and/or negatively charged phospholipids and cholesterol. Some of these formulations are on the market already, such as Ambisome® (Gilead Sciences, Foster City, CA), Daunoxome® (Gilead Sciences) and Myocet® (Elan Pharmaceuticals Inc., Princeton, NJ). It was observed that conventional liposomes are rapidly captured by cells of the RES and eliminated from blood circulation, leading to their relative short half-life [68]. This *in vivo* attribute of conventional liposomes was exploited to develop antiparasitic and antimicrobial drugs in order to treat infections because both the liposomes and the pathogen cells accumulate to the RES [69, 70]. It was also reported that increasing size of conventional liposomes would enhance uptake in the RES, primarily in the liver, leading to more rapid hepatic clearance [71]. Furthermore, it was found that drug leakage from conventional liposomes is associated with their interaction with high and low density lipoproteins in the plasma, especially when the conventional liposome does not carry cholesterol in the lipid membrane [72, 73]. As mentioned above, the application of conventional liposome is limited when the target site is beyond RES.

1.2.2.2 Stealth liposomes. The incorporation of saturated phospholipids with high transition temperature (T_m) and cholesterol into the bilayer structure still cannot fully overcome the *in vivo* stability issue caused by opsonization. In order to target tissues other than the RES system, liposomes need to minimize interaction with the RES so as to prolong their half life in blood circulation. Several strategies in this regard have been developed. The surface of the liposome can be grafted with monosialoganglioside [74] to generate new "stealth liposomes" with a more hydrophilic surface [75] that decrease the liposomes's interaction with RES. The most popular and successful method to generate "stealth liposomes" is to coat the liposome

surface with hydrophilic polymers, such as poly (ethylene glycol) (PEG). The basic mechanism

is that the hydrophilic polymer molecules with a flexible chain occupy the space adjacent to the

surface of liposome and thus form a steric protective layer to hinder the binding of other

macromolecules such as opsonin, thereby slowing down the liposomes' recognition by the RES

and subsequent clearance [62, 64, 72]. Moreover, it was reported that the PEG chains on the

liposome surface provide strong repulsion between membranes to prevent liposome aggregation,

thus improving the stability of formulations [76]. In this way, the EPR effect can be enhanced

due to the sufficient time available for the stealth liposomes to accumulate in the solid tumor,

which results in improvements in the therapeutic outcomes compared to conventional liposome.

As an example, Doxil® as a representative of stealth liposome was approved to treat AIDS-

related Kaposi's sarcoma.

      1.2.2.3 Stimuli-responsive liposomes. It must be kept in mind that only the drug

molecules that are released from liposomes can exert their biological function. Thus, the

therapeutic efficacy of liposome formulations can improve only when the rate of drug release

from liposomes is elevated at the target tumor [77, 78]. The stability of PEGylated liposomes

may not always favor more biological effect, especially if it does not increase the distribution of

the cargo drug molecules inside the target cells. An ideal liposomal drug delivery system should

remain stable during blood circulation until it is delivered to the disease site, and then elevate the

release of its cargo drug molecules in response to a specific stimulus at the target site. The

stimulus can be internal or external. The former is endogenous stimuli presented in various

physiological environments, such as low endosomal pH [79], raised temperature at inflammatory

tissue [80] and specific enzymes in a particular microenvironment [81]. The latter is the stimuli

from external sources, which include ultrasounds [82], light [83], magnetic field [84] and electric field [85]. Typically, the application of external stimuli requires particular facilities.

If a stimuli-responsive lipid component is incorporated into the stealth liposome, the liposome can then be developed into a "smart" delivery system to achieve controlled release as a "magic bullet".

1.2.3 pH-sensitive lipids and fliposomes. Among the above mentioned stimuli, pH gradients have been widely investigated because they are present at various organs, tissues and cell levels within body (Figure 1.7) [86]. It is widely recognized that the acidic extracellular microenvironment is the most prevalent attribute among various types of tumors except for blood carcinomas. Generally speaking cancer cells have an intracellular pH (pH_i) of 7.4 and a lower extracellular pH (pH_e) of ~6.7 while the reverse pattern is observed in normal cells (pH_i= ~7.2 and pH_e= ~7.4) [87]. As the solid tumor grows, cancer cells become farther from the basement membrane and vasculature, leading to the low oxygen supply. The high consumption of energy required for cancer cell survival is compensated by the upregulation of glycolysis [88-90]. Simultaneously, HIF-1α expression is activated and promotes the activation of multiple genes including those encoding pH regulators, leading to the overexpression of Na^+-H^+ exchanger NHE1 of the SLC9A family and the monocarboxylate - H^+ efflux cotransporters MCT1 and MCT4 of the SLC16A family [87, 88] (Figure 1.8). All these pathways, together with the absence of lymphatic drainage contribute to the acidification of the tumor microenvironment. It was reported that decreased pH_e is associated with a tumor's escape from immune detection and eventually cancer progression and metastasis [90, 91]. Furthermore, at subcellular level the pH in endosomes and lysosomes can reach as low as 4.5-5.5 [92].
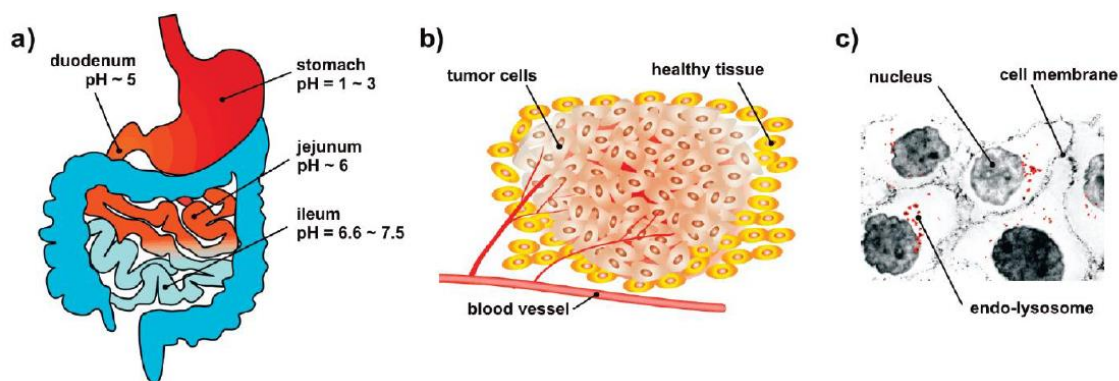
Figure 1.7. Examples of different physiological pHs available for pH-sensitive drug delivery targeting. a) Targeting at the organ level: the GI tract is characterized by a pH gradient. b) Targeting at the tissue level: solid tumors exhibit an acidic extracellular microenvironment. c) Targeting at the cellular level: endo-lysosomes are more acidic compared to the cytoplasm (shown in red) [86].
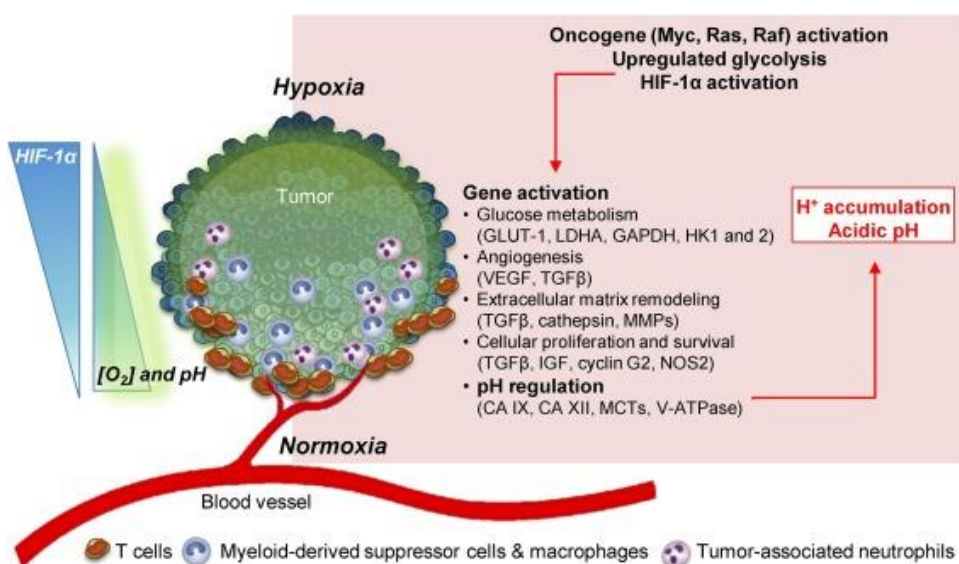
Figure 1.8. Mechanisms of pH decrease in the tumor microenvironment [88]

As mentioned above, pH gradient could be an excellent trigger to elevate the release of therapeutic agent from stimuli-response liposomes. Most of the reported work on pH-sensitive liposomes takes advantage of the dramatically more acidic environment of endosomes/lysosomes [93, 94]. While the pH in the tumor interstitium is slightly lower than the one in blood, it is rarely below 6.5, which makes it difficult for the pH-sensitive liposomes to release more drugs

[95]. Many approaches have been tried to render stealth liposomes pH-sensitive, including incorporation of pH-sensitive fusogenic peptides [96, 97], coating the liposomes with polyanions [98, 99] and incorporation of the phase transition lipid PE [100].

Various pH-sensitive lipids were designed and synthesized previously in our lab [101, 102]. A conformationally controlled molecular switch has been designed to destabilize the liposome membrane in response to a pH drop and was reported by our group and collaborators [103][104]. The mechanism of the membrane destabilization is that an intramolecular hydrogen bond between the protonated amine group and its neighboring hydroxyl group induces a conformational change of the cyclohexane ring in the lipid, leading to the axial positional transformation of the lipid tails [105] (Figure 1.9). In stealth liposome comprising such pH-sensitive lipids, the conformational switch can destabilize the lipid bilayer, thus increasing the rate of content release (Figure 1.10). Lipids with this kind of conformational switch are named "flipids" and the liposomes containing flipids are called "fliposomes" [106-108]. In order to fulfill the prerequisite of stability, flipids with saturated hydrocarbon chains at the length of 16 carbons were selected to develop fliposomes for the treatment of TNBC. With preliminary data, flipids with amine group of morpholine (estimated pKa in methanol = 4.9) and azetidine (estimated pKa in methanol = 6.8) (Figure 1.11) fit into the narrow range of pH gradient in tumor microenvironment for the TNBC treatment [104].
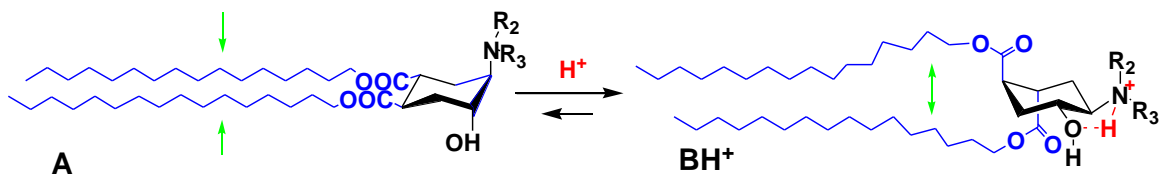
Figure 1.9. Mechanism of pH-Triggered conformational switch in flipid.
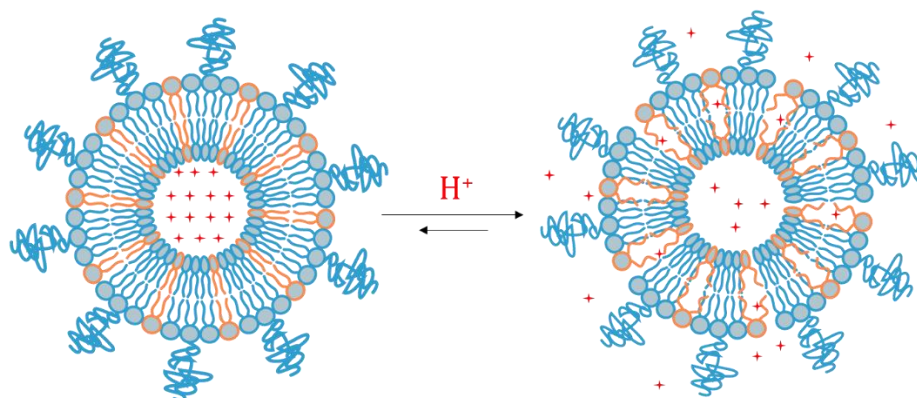
Figure 1.10. Perturbation of lipid bilayer and drug release induced by pH-Triggered conformational switch

MOR-C16   Est. pKa 4.9

$C_{44}H_{83}NO_6$
Exact Mass: 721.62
Mol. Wt.: 722.13

AZE-C16   Est. pKa 6.8

$C_{43}H_{81}NO_5$
Exact Mass: 691.61
Mol. Wt.: 692.11
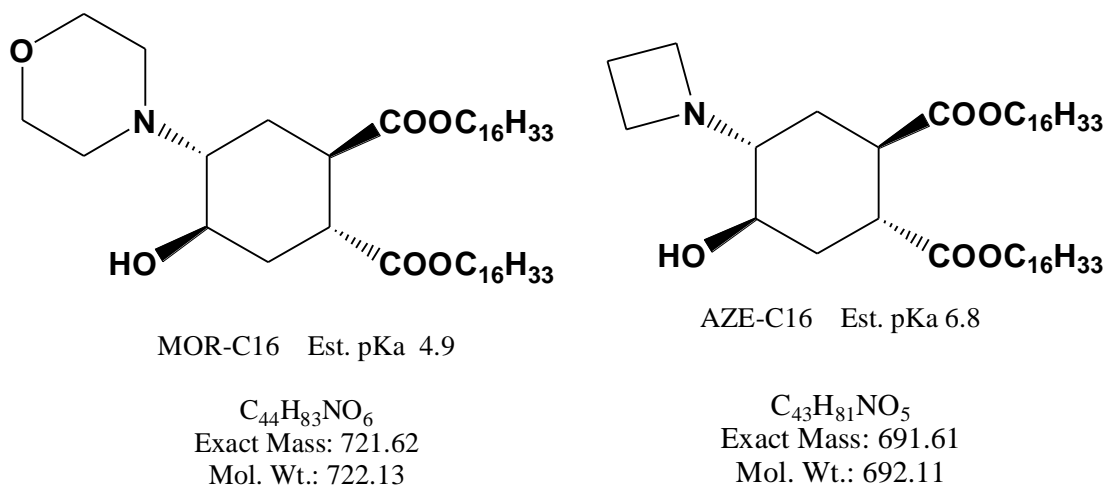
Figure 1.11. Chemical structure and Estmated pKa in methanol of MOR-C16 and AZE-C16 [104]

1.3 Hypothesis and Specific Aims

Based on the foregoing review of the literature, we hypothesize that pH-triggered release from liposomes can improve physical targeting, consequently the efficacy of doxorubicin against triple negative breast cancer. Accordingly, select fliposomes loaded with doxorubicin were prepared by different methods and characterized *in vitro* to investigate the triggered release in response to the acidic pH that mimics the acidic tumor microenvironment. The optimization of select fliposome was conducted to further fulfill the prerequisite for *in vivo* application.

Afterwards, the anticancer efficacy of the resultant fliposomes was evaluated in both 2D monolayer TNBC cells and in 3D MCS of TNC cells *in vitro*. Finally, the anticancer activity of select flipsomes were also evaluated in an orthotopic xenograft model of TNBC. The comparison of anticancer efficacy *in vitro* and *in vivo* between fliposome and corresponding non pH-sensitive liposomes was conducted to evaluate the improvement due to pH-triggered release.

Chapter 2: Preparation and Characterization of pH-sensitive Fliposome

2.1 Introduction: Strategies to Prepare pH-sensitive Liposomes

It is widely known that liposomes are mainly composited with natural and/or synthetic lipids, which are classified as amphiphilic molecules. Once those molecules are exposed to aqueous solution, they tend to form aggregated complexes so as to minimize entropically unfavorable interactions between their hydrophobic moieties and the surrounding water molecules. Numerous techniques and methods have been developed to prepare liposome formulations since their discovery by Bangham et al in 1965 [109]. The formation of liposomes requires a sufficient amount of energy to form a thermodynamic system, therefore dispersion is the key step with various techniques. Accordingly, liposomal preparation falls into two categories: mechanical dispersion methods and solvent dispersion methods [110-113].

The mechanical dispersion methods include the following types: thin-film lipid hydration, sonication, freeze-thawing, and membrane extrusion. These methods could be performed individually or in combination depending on the nature of the formulation components. Thin-film hydration was originally invented by Bangham [109], in which the mixture of lipids was first dispersed in an organic solvent. Then the solvent was removed under vacuum to obtain a thin layer of lipid film deposited at the bottom of flask. Hydration buffer was added under agitation at a temperature above the lipid transition temperature (T_m) [109]. By this method, multilamellar liposomes (MLVs) with size ranging from 0.5 µm to 5 µm could be obtained. Typically, further size reduction was required to attain smaller and uniformly sized formulations. Sonication is one of the methods to reduce the size. A bath or probe tip sonicator is required for producing small unilamellar vesicles (SUV). However, sonication can degrade the lipids and the encapsulated compounds, in addition to the drawback of decreasing the

liposomes' internal volume [110]. The process of quick freezing and slow thawing forms unilamellar vesicles by reorganizing the structure of SUV[114, 115]. Extrusion through polycarbonate filters with different pore size above T_m is another method widely implemented to reduce the liposome size.

The commonly used solvent dispersion methods are solvent injection and reverse phase evaporation [113]. The solvent injection method involves dissolution of the desired lipids into an organic solvent (ethanol or ether), then the injection of the organic solvent into aqueous media to form the liposomes. The difference between the two organic solvent is the method to remove. Ether is removed by evaporation at elevated temperature or under reduced pressure, while ethanol is removed by dialysis or diafiltration because it is miscible with water. Both of the injection methods have the disadvantage of heterogeneity of the resultant formulation. The reverse phase evaporation method results in the fusion of micelles into liposomes during the evaporation of the organic solvent. When the gel eventually collapses after evaporation, some of the phospholipids form bilayer structures around the residual micelle to form liposomes. This method has the advantage of high loading efficiency by creating a higher aqueous space-to-lipid ratio, while carrying the disadvantage of possible degradation of the lipids and the loading content by sonication during the micelles' formation [112, 113]. Solvent dispersion could be combined with appropriate mechanical dispersion to form smaller and more homogenous liposomes.

In addition, new large-scale liposome preparation techniques, such as spray-drying, freeze-drying and microfluidics, have emerged in response to the demand for industrial scale production. Several modified ethanol injection methods have been applied to large scale liposome manufacturing [116].

In this study, a sequential combination of mechanical dispersion methods including lipid film hydration, freeze-thawing, and finally membrane extrusion was well-established in our group. Moreover, we have established the ethanol injection method because it is widely used in industrial production. The procedure of the method includes ethanol injection followed by diafiltration. In addition, sonication was also involved before drug loading in case that the size of resultant after extrusion was not small enough. The aim of this chapter's studies is to establish robust preparation method of DOX-loaded fliposome.

2.2 Materials and Methods

2.2.1 Materials. The lipids 1,2-dipalmitoyl-sn-glycero-3-phosphocholine (DPPC), 1,2-distearoyl-sn-glycero-3-phosphocholine (DSPC), N-palmitoyl-sphingosine-1-(succinyl[methoxy(polyethylene glycol)2000]) (PEG-ceramide (2000)), 1,2-dipalmitoyl-sn-glycero-3-phosphoethanolamine-N-[azido(polyethylene glycol)-2000 (DPPE-PEG (2000)) were purchased from Avanti Polar Lipids, Inc. (Alabaster, AL, USA). Cholesterol, copper(II) D-gluconate, octaethylene glycol monododecyl ether (detergent OGME/C12E8), Dowex® 50WX-4, 2-Amino-2-(hydroxymethyl)propane-1,3-diol (Tris) and triethanolamine (TEA) were purchased from Sigma-Aldrich. Doxorubicin Hydrochloride was purchased from Biotang (Waltham, MA, USA). Calcein, sucrose and 2-[4-(2-hydroxyethyl)piperazin-1-yl]-ethanesulfonic acid (HEPES) were purchased from Fisher Scientific. All other organic solvent and chemicals were purchased from Sigma Aldrich, Fisher Scientific or VWR.

2.2.2 Preparation of DOX-loaded liposomes.

2.2.2.1 Preparation of DOX-loaded liposomes by thin-film hydration coupled with freeze-annealing-thawing. Generally, empty liposomes were prepared with thin-film hydration, followed by extrusion based on prior reports [102, 108]. Chloroform and dichloromethane

solutions of various lipids were mixed in a 25 mL round bottom pear-shaped flask. The traces of

organic solvent were removed by evaporation on a Buchi rotavapor and further drying in high

vacuum overnight at room temperature. The thin-film of lipids at the bottom of the flask was

hydrated with 30 mM HEPES buffer (pH 7.4) containing 300 mM $MnSO_4$ or 375 mM TEA

buffer (pH 8.0) containing 100 mM Cu-Gluconate in a 60 °C water bath. The flask was filled

with argon followed by parafilm sealing. Intermittent agitation and vortexing were applied to

facilitate the hydration to obtain a liposome suspension of 20 mM total lipids. The liposome

suspension was followed by freeze-annealing-thawing procedure (sequentially immersion in

liquid nitrogen, ice-and-water mixture and 60 °C water bath until the temperature was

equilibrated respectively) for seven times. Then the liposome suspension was sequentially

extruded at least eleven times through 400 nm, 200 nm and 100 nm polycarbonate membranes

(Nucleopore Corp., Pleasanton, CA, USA) using a hand-held Mini-extruder (Avanti Polar Lipids

Inc., Alabaster, AL, USA) or three times using a high-pressure nitrogen Lipex® extruder

(TRANSFERRA Nanosciences Inc., Burnaby, B.C., Canada) at 60 °C.

In order to establish a transmembrane metal salt gradient, the extruded liposomes were

run through a Sephadex G-75 size exclusion column (SEC) (Sigma Aldrich, St. Louis, MO,USA)

which was pre-equilibrated with isotonic buffer containing 5 mM HEPES and 140 mM saline

(pH 7.4) or 10 mM Tris in 10% sucrose solution (pH 8.0). Doxorubicin was dissolved in the

same isotonic buffer at the concentration of 2 or 4 mg/mL. After passing through SEC, the

empty liposome suspension was promptly mixed with the previously described DOX solution in

1:1 volume/volume ratio and incubated at 60 °C for 40 minutes [117]. The cation-exchange

resin Dowex® 50WX-4 (Sigma Aldrich, St. Louis, MO, USA) was pretreated as previously

reported [118] and was mixed with liposome preparation at weight ratio of resin: DOX = 60 :1

and gently shaken for 25 minutes at room temperature. During the incubation period, the positively charged, free DOX binds to the Dowex resin, while the entrapped DOX remains associated with the liposomes. The Dowex was removed from the DOX-loaded liposomes by filtration of the mixture through 25 gauge syringe needle. The resultant liposome preparations were stored at 4 °C in brown glass vials that were filled with argon until further studies.

2.2.2.2 Preparation of DOX-loaded liposome by ethanol injection. The desired lipids were dissolved into absolute ethanol above the lipids transition temperature (60°C). The 30 mM HEPES buffer (pH 7.4) containing 300 mM $MnSO_4$ or 375 mM TEA buffer (pH 8.0) containing 100 mM Cu-Gluconate was equilibrated at 60°C in a hot water bath. Then the lipid ethanol solution was injected into aqueous media. Liposomes formed spontaneously with mild shaking and agitation. The solution was sequentially passed 3 times through polycarbonate membranes of 400, 200, 100 nm pore size using a high pressure nitrogen Lipex® extruder (TRANSFERRA Nanosciences Inc., Burnaby, B.C., Canada) at 60°C. The unloaded $MnSO4$/Cu-Gluconate were removed by hollow-fiber diafiltration (MicroKros Spectrum Laboratories, Inc., Rancho Dominguez, CA, USA) to establish the transmembrane metal salt gradient and to eliminate ethanol from the formulation out of safety concern. The resultant liposomes were concentrated by hollow-fiber diafiltration to a lipid concentration of 15~20 mM, then mixed with the previously described DOX solution in 1:1 volume/volume ratio and incubated at 60 °C for 40 minutes. Purification was as described in 2.2.2.1.

2.2.3 Preparation of liposomes encapsulating calcein. Chloroform and dichloromethane solutions of various lipids (Table 2.3) were mixed in a 25 mL round bottom pear-shaped flask. The organic solvent was removed by evaporation on a Buchi rotavapor followed by further drying in high vacuum overnight at room temperature. The thin-film of

lipids at the bottom of the flask was hydrated with 100 mM Calcein (pH 7.4) in a 60 °C water bath. The flask was filled with argon, capped and sealed with parafilm. Intermittent agitation and vortex were applied to facilitate the hydration and obtain a liposome suspension of 20 mM total lipids. The liposome suspension was freeze-annealing-thawing (sequentially immersion in liquid nitrogen, ice-and-water mixture and 60 °C water bath until the temperature was equilibrated respectively) for seven times. Then the liposome suspension was sequentially extruded at least eleven times through 200 nm and 100 nm polycarbonate membranes (Nucleopore Corp., Pleasanton, CA, USA) using a high pressure nitrogen Lipex® extruder (TRANSFERRA Nanosciences Inc., Burnaby, B.C., Canada) at 60° C. The resultant liposome suspension was passed through a Sephadex G-75 size exclusion column pre-equilibrated with isotonic saline containing 5 mM HEPES at pH 7.4 to remove the unencapsulated calcein. The liposome preparations were stored at 4°C in brown glass vials that were filled with argon.

2.2.4 Physicochemical characterizations of liposomes. The sizes and ζ-potential of the liposome preparations were measured by photon correlation spectrometry and electrophoresis mobility under applied voltage, respectively, using Zetasizer ZS 90 (Malvern Instruments Ltd., Malvern, UK).

2.2.5 Quantitation of DOX concentration and encapsulation efficiency of DOX-loaded liposomes. An aliquot (10 µL) of DOX-loaded liposome was lyzed with 90 µL lysing buffer (90% isopropanol containing 0.075 M HCl) [119]. The fluorescence of solution was measured at 485 nm (excitation) and 590 nm (emission) on the Synergy HT microplate reader (Biotek, Winooski, VT, USA). The concentration of DOX was quantified from a calibration curve of DOX standard solutions (1, 2, 5, 10, 20, 50, 100 µg/ml) which were operated under the

same lyzing procedure. The encapsulation efficiency (EE) of liposome preparation can be

calculated by the formula:

$$EE = \frac{DOX\ amount\ entrapped\ inside\ of\ the\ formulation}{DOX\ amount\ added\ for\ the\ drug\ loading} \times 100\%$$

2.3 Results and Discussion

2.3.1 Size, ζ-potential and polydispersity index (PDI) of liposome formulations.

After preparation by either thin-film hydration or ethanol injection, the liposomes of various

compositions presented similar average sizes, smaller than 200 nm after passing through 100 nm

polycarbonate membranes. The Polydispersity Index (PDI) of all preparations was lower than

0.3, which is the key indicator of homogeneity of colloids. No detectable ζ-potential for all

formulations suggested neutral charge of the whole system at pH 7.4, which would be expected

from the neutrally charged lipid components of the liposomes. The average size, PDI and

encapsulation efficiency of selected DOX-loaded liposomes are shown in Table 2.1.

Table 2.1. Size, PDI and EE of DOX-loaded liposomes by different preparation methods

Liposome	Molar Ratio	Method	Size (nm)	PDI.	EE (%)
MOR-C16/DPPC/PEG-DPPE	25/70/5	Thin-film	170.5	0.064	100
AZE-C16/DPPC/PEG-DPPE	25/70/5	Thin-film	119.8	0.165	86
MOR-C16/DSPC/Chol/PEG-Ceramide	30/40/25/5	Thin-film	189.1	0.188	88
MOR-C16/DSPC/Chol/PEG-Ceramide	30/40/25/5	EtOH Inj.	129.6	0.261	94
DPPC/Chol/PEG-Ceramide	50/45/5	Thin-film	110.2	0.097	65
DPPC/Chol/PEG-Ceramide	50/45/5	EtOH Inj.	124.9	0.220	56

It is widely acknowledged that the size of drug delivery systems has prominent influence on their pharmacokinetics profile and tissue distribution [120]. For tumor treatment, nanocarriers with only size lower than 150 nm can get into the tumor interstitium by escaping from the fenestrated capillaries of solid tumors [120-122]. However, 200 nm is the cut-off size for the drug delivery system to take advantage of the EPR effect for tumor treatment [46, 123]. It is reported that nanocarriers with size ranging from 100 to 150 nm were not able to extravasate into normal tissues in kidney, lung and heart [120, 122]. In this study, we have developed robust preparation methods and procedures to strictly control the size of liposomes under 200 nm. Therefore, all of these liposomes could serve as a viable nano-drug delivery system for anticancer treatment.

2.3.2 Encapsulation efficiency (EE) of DOX-loaded liposomes. As shown in Table 2.1, the encapsulation efficiencies of DOX-loaded liposomes achieved 80% to 100% payload with concentration ranging from 1 mg/ml to 2 mg/ml by the remote loading method except for the conventional liposome with DPPC, Cholesterol and PEG-lipids.

To be sufficient for animal studies, 2 mg/ml or higher DOX concentration in the final formulation was the goal for the all preparations. For the payload drug Doxorubicin, remote loading, also known as active loading, was a well-established procedure to achieve high loading efficiency and a high enough concentration. The transmembrane ion gradient was the driving force to pump the payload drug molecules into the liposome aqueous core, while their precipitation with either sulfate or metal ion enables high payload retention. Besides pH gradient, ammonium sulfate gradient is the most commonly utilized method in the industry manufacture. Metal salt, such as manganese sulfate or copper gluconate were reported to achieve similar loading ability by forming metal-doxorubicin complex which is favored when the

intraliposomal pH >6.5 [60, 124]. In this project we utilized either the manganese sulfate or the copper gluconate gradient for the remote DOX loading since it circumvented the low pH of the ammonium sulfate solution during the drug loading.

2.3.3 Comparison of different preparation procedure.

2.3.3.1 Mini-extruder versus nitrogen Lipex extruder. As shown in Table 2.2, no significant difference in the liposome size was observed after using either a mini-extruder or a nitrogen Lipex extruder. The mini-extruder is ideal for a sample whose volume is smaller than 1 ml. However, the optimal lipid concentration for this method was 10 mM for better size and PDI. In comparison, the Lipex extruder could be used to prepare 1-10 ml sample in one batch and could operate with up to 50 mM lipid concentration to achieve higher drug concentrations in the final formulation. In addition, Lipex extrusion is the industry standard, which can be scaled up to prepare 100-800 ml formulations by GMP standards for early clinical development. In this project, early discovery of liposome composition employed the mini-extruders while later larger scale liposome preparations for animal studies or formulation optimization employed a Lipex extruder.

Table 2.2. Size, PDI and EE of DOX-loaded liposomes prepared by different extruders

Liposome	Lipid Conc. (mM)	Molar Ratio	Extruder	Size (nm)	PDI.	EE (%)
DPPC/Chol/PEG-Ceramide	10	50/45/5	Mini	110.2	0.097	65
DPPC/Chol/PEG-Ceramide	20	50/45/5	Lipex	120.4	0.086	92

2.3.3.2 Thin-film hydration versus ethanol injection. There is no qualitative difference observed between the size of the liposomes made from the two different methods, as shown in

Table 2.1. Generally thin-film hydration had better PDI value, which indicated better homogeneity of the liposome system. The slight increase of PDI was probably caused by the procedure of liposome concentration for drug loading after the diafiltration. After a composition was selected, detailed operation procedure with higher lipid concentration was optimized. Because ethanol injection method is more practical and commonly used in industry manufacture, it can be scaled up for manufacturing when reproducibility of the method is established.

2.3.3.3 Manganese sulfate versus copper gluconate. There is no difference observed between two metal salt for remote loading, as shown in Table 2.3. Because $MnSO_4$ is not compatible with alkaline pH and will precipitate at pH = 8.0, copper gluconate is optimal for AZE fliposome formulation where the AZE lipid has an amine of pKa 6.8[125].

Table 2.3. Size, PDI and EE of DOX-loaded liposomes remote loading with different metal salt

Liposome	Molar Ratio	Metal Salt	Size (nm)	PDI.	EE (%)
MOR-C16/DPPC/PEG-Ceramide	50/45/5	$MnSO_4$	182.4	0.309	100
MOR-C16/DPPC/PEG-Ceramide	50/45/5	Cu-Gluconate	157.0	0.283	100

2.3.4 Characterization of calcein-loaded liposome. Calcein was utilized as a model liposome cargo molecule to verify the release profile. All the selective liposomes had size range 140 ~ 170 nm with small PDI to indicate homogeneous liposome preparations, as shown in Table 2.4.

Table 2.4. Size, PDI and EE of Calcein-loaded liposomes

Liposome	Molar Ratio	Size (nm)	PDI.
AZE-C16/DSPC/Chol/PEG-Ceramide	33/38/25/5	168.2	0.219
MOR-C16/DPPC/PEG-Ceramide	25/70/5	144.3	0.150
DPPC/Chol/PEG-Ceramide	55/40/5	145.4	0.088
DPPC/Chol/PEG-Ceramide	70/25/5	153.1	0.068

2.4 Summary

The pH-sensitive fliposomes were successfully prepared by thin film hydration and ethanol injection. The traditional proton gradient or ammonium gradient method to remote load DOX into liposomes creates acidic environment, which is not compatible with pH-senstivie fliposomes. The metal ion remote loading method was developed to circumvent the increasing proton concentration. Fliposomes carried high encapsulation efficiency (>80%), small mean particle size (<200 nm) and small PDI (<0.3), indicating the robust preparation procedure. The quality of liposomes, indicated by size, PDI, varies among different batches, suggesting that optimization of preparation procedure is needed if fliposomes move to the step of scale-up and manufacture.

Chapter 3: Establishment of a Release Assay to Evaluate pH-sensitivity of Fliposome *in vitro*.

3.1 Introduction

In the process of product development, the *in vitro* drug release from an oral dosage form, known as dissolution testing, is an essential step to illustrate the quality of the product and to forecast its *in vivo* performance [126]. Dissolution testing was first established back to 1950s and accepted by the United States Pharmacopeia (USP) in 1970 [127]. Generally, the formulation under the test is deposited into the apparatus and exposed to a releasing media, ideally at sink condition. During certain time of agitation at 37°C, such as stirring of paddle or basket, the released drug was sampled and quantified. There is also a flow-through dissolution system known as USP apparatus 4, which is utilized to perform dissolution testing in order to fit the requirement for sustained-release formulations. Through *in vitro–in vivo* correlations/relationships (IVIVC/IVIVR), the dissolution testing could be utilized to predict the drug candidate's performance *in vivo* and served as critical data for drug development. For instance, a highly soluble drug that was developed in an immediate release formulation could be bio-waived because the standardized dissolution testing result is sufficient according to the FDA regulatory guidance [126].

For complex parenteral formulations, such as liposomes and nanoparticles, the release assay is even more important in order to achieve altered pharmacokinetics. The release assay is widely utilized in the therapeutics of oncology. By means of nano-drug delivery system, prolonged circulation of the drug is achieved to enhance intratumoral accumulation of chemotherapy agent through the EPR effect. After the drug's accumulation inside the target tumor, its anticancer activity could be optimized by manipulating the rate of release from the

delivery system. Therefore, the accuracy of the release assay is prerequisite to optimize the properties of the delivery system, such as sufficient stability in circulation and quick release at the target site.

In our lab, a release assay based on the fluorophores ANTS/DPX was used to characterize liposomes consisting of TACH lipids and to investigate the impact of TACH lipids' amine head groups on the liposomes' pH sensitivity [102]. The assay mainly served as proof of concept for the liposomes' pH-sensitivity. For applications in drug delivery, it's more reasonable to evaluate the release with the cargo drug instead of ANTS/DPX. In addition, the newly designed C16 TACH lipids have longer hydrocarbon tails and are used in liposomes in combination with saturated phospholipids, which drastically raises the transition temperature (T_m) of the resultant liposome formulation. Therefore, substantial changes of the release profile and the response to lower pH are anticipated, which make it essential to develop a more reliable release assay for DOX-loaded liposomes under this study. The aim of this chapter's studies is to establish reliable release assay to evaluate pH-sensitive release of fliposome *in vitro*.

3.2 Materials and Methods

3.2.1 Materials. Rapid Equilibrium Dialysis (RED) Device was purchased from Thermofisher. Octaethylene glycol monododecyl ether (detergent OGME/$C_{12}E_8$) and Dowex® 50WX-4 were purchase from Sigma Aldrich. Acetic acid, D(+)-Glucose, 2-[4-(2-hydroxyethyl)piperazin-1-yl]-ethanesulfonic acid (HEPES) and 2-(N-morpholino)ethanesulfonic acid (MES) were purchased from Fisher Scientific. Doxorubicin Hydrochloride was purchased from Biotang (Waltham, MA, USA). BioBeads SM-2 was purchased from Bio-rad (Hercules, CA).

3.2.2 Equilibrium microdialysis. Equilibrium microdialysis [128] by the Rapid Equilibrium Dialysis (RED) Device (MWCO = 8,000) was utilized to establish release assay according to the manufacturer's recommendations. Isotonic buffers with different pH were prepared as the following: pH 7.4 and 7.0 (100 mM HEPES, 92.6 mM glucose), pH 6.5 and 6.0 (100 mM MES, 92.6 mM glucose), pH 5.5, 5.0, 4.5 and 4.0 (100 mM acetic acid, 92.6 mM glucose). 100 µL of Dox-loaded fliposome or non pH-sensitive liposome preparation was added into sample chamber while 300 µL of buffer with different pHs described above was added into the buffer chamber. The RED plate with samples were covered with sealing tape and incubated for dialysis at 37°C at approximately 200 rpm on an orbital shaker for overnight (14 hour). An aliquot of the solution in both sample chamber and buffer sample was taken for concentration determination. All measurements are in triplicates. The percent of DOX released from liposomes at different time points was calculated using the following equation.

$$\% \text{ Dox released} = \left[1 - \frac{(C_s - C_b) \times V_s}{C_i V_s}\right] \times 100\%$$

Where, V_s = Volume of sample chamber, C_s = concentration of Dox in sample chamber, C_b = concentration of Dox in buffer chamber, C_i = initial liposomal Dox concentration added to sample chamber.

3.2.3 Indirect resin adsorption method. Liposomal formulations and a buffer of defined pH were added at v/v ratio of 1:7 into an amber glass vial. The glass vial containing the sample was incubated at 37°C at approximately 100 rpm on an orbital shaker overnight (14 hour). 50 µL of supernatant of the releasing solution was aliquoted and transferred into a 1.5 mL centrifuge tube filled with Dowex 50WX4 resin (Dowex : Dox = 60 : 1, wt : wt). The centrifuge tube was agitated for 20 minutes, allowing the released doxorubicin to be completely adsorbed by the resin. Then 10 µL supernatant was aliquoted for analysis after 2 minutes centrifuge at 200

rpm. All measurements are in triplicate. The percent of DOX released from liposomes at different time points was calculated using the following equation.

$$\% \text{ Dox released} = \frac{(C_i V_i - C_s V_s)}{C_i V_i} \times 100\%$$

Where, V_s = Volume of total solution after incubation, C_s = concentration of Dox of supernatant (unreleased), C_i = initial liposomal DOX concentration added, V_i = initial volume of liposomal DOX added.

3.2.4 Fluorescent dequenching method. In order to capture the kinetic profile of drug release from liposomes, a more convenient and rapid release assay than Indirect Resin Absorption is necessary. Doxorubicin has a fluorophore functional group which is excited at 490 nm and emits fluorescence at 590 nm. It is suggested that the fluorescence of doxorubicin is also self-quenched at high concentrations because of the large overlap between the absorption and the emission spectra [129, 130]. Therefore, doxorubicin release could be reflected by the dequeching of its fluorescence as the molecules move from its high concentration inside the liposome to low concentration outside.

Each liposomal sample (2 µL) was added into 198 µL of different buffer in a black 96 well plate. The fluorescent measurement of doxorubicin as the baseline of no release was recorded by the Synergy HT microplate reader (Biotek, Winooski, VT, USA) at 485 nm (excitation) and 590 nm (emission) promptly after sample addition. The plate was sealed with tape and incubated at 37 °C on an orbital shaker at approximately 100 rpm. At incremental time points (1, 3, 6, 12, 24, 48 h), the fluorescent intensity of each sample was measured. At the end of experiment, 10 µl detergent ($C_{12}E_8$) was added to fully lyse the Dox-loaded liposomes to obtain the fluorescent intensity of complete release (F_{x-100}). The release percentage was calculated as following,

$$\% \text{ Dox released} = \frac{F_t - F_0}{F_{x-100} - F_0} \text{ x } 100\%$$

Where F_t is the fluorescence intensity of a given time point and F_0 is the baseline fluorescence intensity upon sample addition, F_{x-100} is the fluorescence intensity of liposome that is 100% lysed.

3.2.5 Direct resin adsorption method. Dowex 50WX4 resin or Bio-beads resin was mixed with a buffer-diluted sample of liposomal doxorubicin in an amber glass vial at the ratio of resin : Dox = 200 : 1 or 1000:1 (wt : wt), respectively. The mixture was incubated at 37°C on an orbital shaker at approximately 100 rpm. At incremental time points (0, 3, 6, 12, 24, 36, 48 h), 10 µl supernatant of each sample was aliquoted and transferred into 90 µl lysing buffer (90% isopropanol containing 0.075 M HCl) to quantify DOX. All measurements were in triplicates. The percentage of DOX released from liposomes at different time points was calculated using the following equation.

$$\% \text{ Dox released} = (1 - \frac{C_s V_s}{C_i V_i}) \times 100\%$$

Where, V_s = Volume of total solution after incubation, C_s = concentration of Dox of supernatant (unreleased), C_i = initial liposomal DOX concentration added, V_i = initial volume of liposomal DOX added.

3.2.6 pH-Triggered release of calcein-loaded fliposmes. Each sample (20 µl) of calcein-loaded liposomes was added into 180 µl of different pH buffer solutions (defined in Section 3.2.2) in a black 96 well plate. The plate was covered with sealing tape and incubated at 37°C on an orbital shaker at approximately 100 rpm. At different time points (0, 1, 2, 4, 6, 9, 12, 24, 36, 48 h), the fluorescence of each well was measured on the Synergy HT microplate reader (Biotek, Winooski, VT, USA) (Ex. = 495 nm and Em. = 515 nm). At the end of experiment,

10 µl detergent ($C_{12}E_8$) was added to completely disrupt the bilayer of liposomes and release calcein for the 100% release measurement. All measurements are in triplicate. The release percentage was calculated as following,

$$\text{Dox released} = \frac{F_t - F_0}{F_{x-100} - F_0} \text{ x } 100\%$$

Where F_t is the fluorescence intensity of a given time point and F_0 is the fluorescence intensity of initial time point upon sample additiion, F_{x-100} is the fluorescence intensity of liposome that was 100% lysed.

3.3 Results and Discussion

3.3.1 Equilibrium microdialysis. Selected liposome formulations (DPPC:PEG-DPPE = 95:5, MOR-C16:DPPC:PEG-DPPE = 25:75:5, AZE-C16:DPPC:PEG-DPPE = 25:75:5) were utilized to establish and validated this release assay. The percentage of pH-triggered release of liposomes at four different pH was shown in Table 3.1.

Table 3.1. Release percentage of selected DOX-loaded liposomes by Equilibrium Microdialysis

pH	DPPC	MOR-C16	AZE-C16
6.0	41.33	37.30	47.09
6.5	36.24	28.32	33.62
7.0	36.83	10.36	40.40
7.4	16.45	26.16	40.78

All selected liposomes showed certain extent of pH-sensitivity by exhibiting elevated release at lower pH. In the meantime, the equilibrium of release could be achieved even within 2 hours with increased rpm for shaking. However, large amount of red stains was observed on the dialysis membrane, which indicated remarkable mass loss during the dialysis process. The

average recovery rate among all sample is ~ 72.2%. Furthermore, recovery rate of free

doxorubicin at concentration 250 μg/ml, 500 μg/ml and 1000 μg/ml was 16.17%, 26.31% and

33.87% respectively following the same procedure with pH 7.4 buffer. This phenomenon could

be explained by the interaction between positive charged doxorubicin and cellulose membrane of

dialysis tube [131]. Therefore, equilibrium microdialysis was not appropriate for release assay

of doxorubicin.

      3.2.2 Indirect resin adsorption method. Select liposomes with different compositions

Tach-C16:DPPC:PEG-DPPE = 25:75:5) were utilized to establish and validate this release assay.

The percentage of pH-triggered release of liposomes at defined pH after 14 hour incubation at 37

°C is shown in the Figure 3.1. Among all pH-sensitive lipids, MOR-C16 showed the largest

difference in leakage between physiological environment (pH 7.4) and tumor microenvironment

(pH 6.0), which made it one of our leading TACH lipids for further investigation. In addition,

AZE-C16 has a pKa value around 6.8, which encouraged us to further investigate the lipid for

quick response to drop of pH.
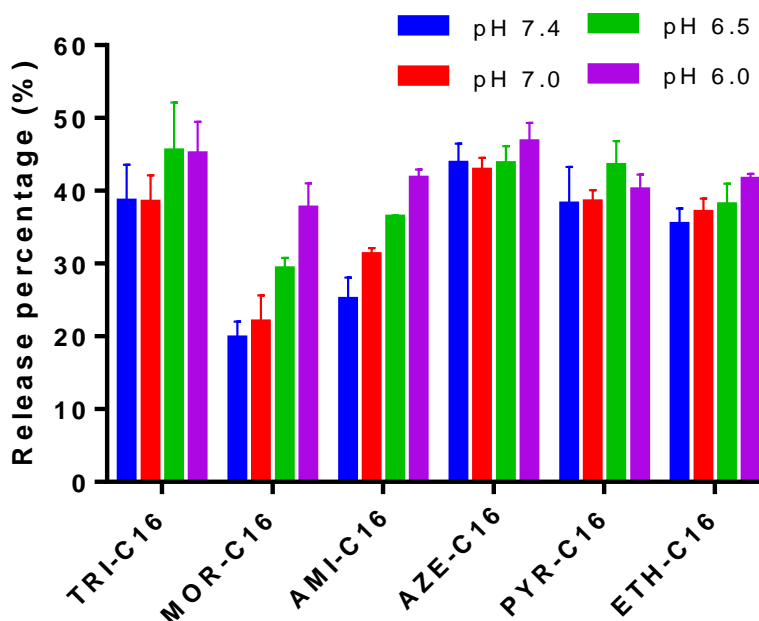
Figure 3.1. Release Percentage of DOX-loaded fliposomes over 14h at defined pHs, 37°C by Indirect Resin adsorption methods. Data presented as mean ± SD, N = 3.

Dowex 50WX4 is a strong cation-exchange resin which could adsorb positively charged doxorubicin upon their release from liposomes. Therefore, Dowex 50WX4 is used to remove residual free doxorubicin after active loading of liposomes [132]. For liposome release assay, the aqueous solution in the vial is a mixture of released free doxorubicin and unreleased doxorubicin entrapped inside of liposome after incubation. When the mixture solution was then agitated with Dowex resin, the released, free doxorubicin would be adsorbed by resin, thus allowing the measurement of doxorubicin still trapped in the liposome formulation. Because the fliposomes are typically neutrally charged and have a size (~100 nm) much larger than the pores on the resins (~ 10 nm), the resins would not significantly influence the release of the liposomes by directly interacting with them. However, the drawback of this method includes its tedious procedure to recover the formulation with the unreleased doxorubicin and its inability to recover the whole mass balance.

3.2.3 Fluorescent dequenching method. Selected liposomes with different

compositions were utilized to establish and validate this release assay. The kinetics of pH-

triggered release of liposomes at defined pH over 48 hour incubation at 37 °C was tracked and is

shown in the Figure 3.2. The pH-sensitive liposomes (MOR-C16:DSPC:Chol:PEG-

Ceramide=30:40:25:5) showed different release profile depending on the pH while the

conventional liposome (DPPC:Chol:PEG-Ceramide= 50:45:5) maintained the same pattern of

leakage at all pHs from 4.0 to 7.4. However, we observed the controversial response to lowered

pH at two different pH ranges. As shown in Figure 3.2 over 48 hours and Figure 3.3 at 24 hour,

fliposome had more leakage at more acidic pH range from 4.0 to 5.5. However, the trend was

reversed at pH range from 6.0 to 7.4.
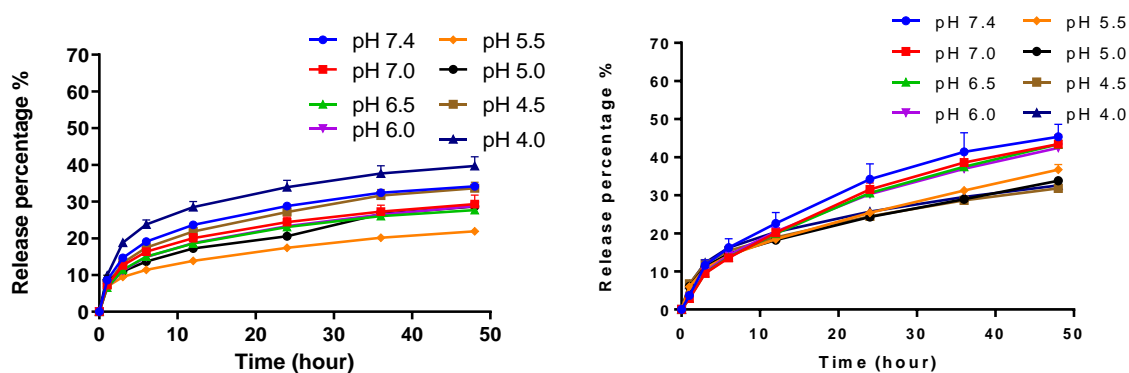
Figure 3.2. Release Percentage of DOX-loaded liposomes (Left: pH-sensitive fliposome MOR-C16:DSPC:Chol:PEG-Ceramide=30:40:25:5, Right: pH-insensitive liposome DPPC:Chol:PEG-Ceramide= 50:45:5) over 48h at defined pHs, 37°C by Fluorescent dequenching methods. Data presented as mean ± SD, N = 3.
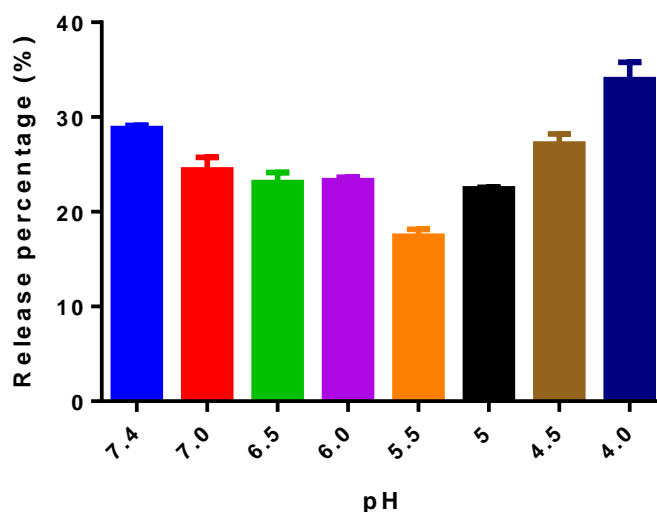
Figure 3.3. Release Percentage of DOX-loaded fliposomes (MOR-C16:DSPC:Chol:PEG-Ceramide=30:40:25:5) at 24h at defined pHs, 37°C by Fluorescent dequenching methods. Data presented as mean ± SD, N = 3.

It was reported that Doxorubicin is not stable at neutral pH, 37°C, with a degradation rate constant of 0.0174 (1/hour) [131]. The degradation rate decreases as the pH of the buffer decreases. The remaining percentage of doxorubicin (125 µg/ml) after incubation at four pHs, 37 °C in our experiments conformed with the literature (Table 3.2). Therefore, the released doxorubicin will gradually degrade over the whole process to cause an underestimation of the complete release (F_{x-100}), the more close to 7.4, the more the underestimation. All these findings suggested the limitation of the florescent dequenching method to evaluate release in response to different pHs, even though it was the most convenient method to obtain kinetic release profile of liposomes if artefacts from the degradation can be mitigated.

Table 3.2. Doxorubicin remaining in solution at 37°C over 12 h at pH 6.0, 6.5, 7.0 and 7.4 (n = 3).

pH	7.4	7.0	6.5	6.0
Remain %	68.82±1.47	76.94±2.10	89.98±8.35	94.57±3.06

3.2.4 Direct resin adsorption methods. Direct resin adsorption was optimized in order to precisely obtain the kinetic release profile of the DOX-loaded liposomes. The advantage of this method is that it balances the ease of the operation procedure and the accuracy of the assay. The percentage of pH-triggered release of liposomes (Table 3.3) at defined pHs over 48 hour incubation at 37 °C was tracked and shown in the Figure 3.4. The pH-sensitive liposomes with AZE-C16 gave the most response upon the drop of pH, while those with MOR-C16 had less change of the release percentage. The conventional liposome showed no difference of release among all pH from 4.5 to 7.4.

Table 3.3. Composition and characterization of selected DOX-loaded liposomes for direct resin adsorption method

Liposome	Mole ratio	Size (nm)	PDI.
AZE : Chol : PEG-Ceramide	50:45:5	301.8	0.377
MOR : Chol : PEG-Ceramide	50:45:5	258.8	0.347
DPPC : Chol : PEG-Ceramide	50:45:5	112.6	0.122
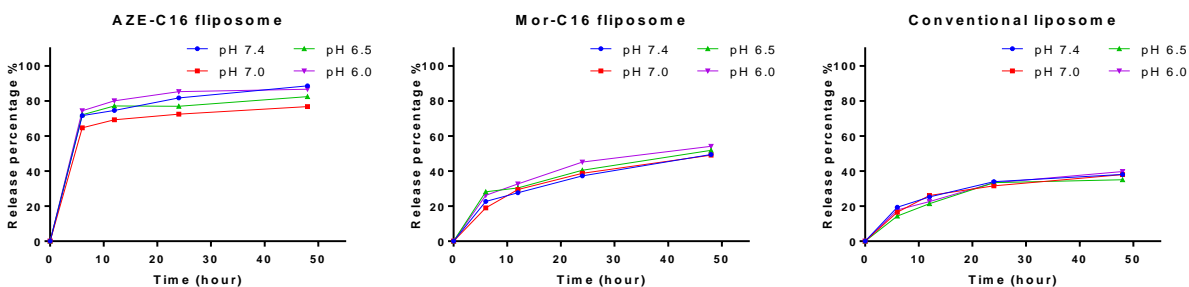
Figure 3.4. Release Percentage of DOX-loaded fliposomes over 48 h at defined pHs, 37°C by Direct Resin adsorption methods.

Dowex 50WX4 is a strong cation-exchange resin which can adsorb free, positively charged doxorubicin. Bio-Beads SM-2 Resin is composed of neutral, macroporous polystyrene beads which are widely used as adsorbent in hydrophobic interaction chromatography. The aromatic rings of doxorubicin could interact with those nonpolar polymeric beads, leading to the adsorption. Both of resins have the pore size below 10 nm, allowing doxorubicin molecules to be trapped inside for adsorption. The fliposomes are typically composed of neutral lipids and larger than 100 nm in diameter so the interference by resin on the fliposome release could be considered insignificant. Therefore, the direct resin adsorption method would be an acceptable method, by which the release profile would be correctly monitored and the procedure would be practical to run large numbers of samples. However, the drawback of this method was the inability to recover the whole mass balance due to practical feasibility.

3.2.5 pH-Triggered release of calcein-loaded fliposmes. In order to validate the release profile of DOX-loaded fliposomes, we studied the pH-dependent leakage of fliposomes by measuring their release of a self-quenching fluorophore, Calcein at pHs 7.4, 7.0, 6.5 and 6.0, 37°C over time. The fluorescence of Calcein was measured and then normalized against the fluorescence of the lysed liposome sample after adding detergent. The pH-triggered release of calcein over 48 hours from select calcein-loaded fliposomes are shown in Figure 3.5. The fliposomes exhibited increased release at lower pH, while the conventional liposome maintained the similar release profile regardless of pH. The DOX-loaded and calcein-loaded fliposomes demonstrated the same the pH-sensitivity trends as shown in Figure 3.6.
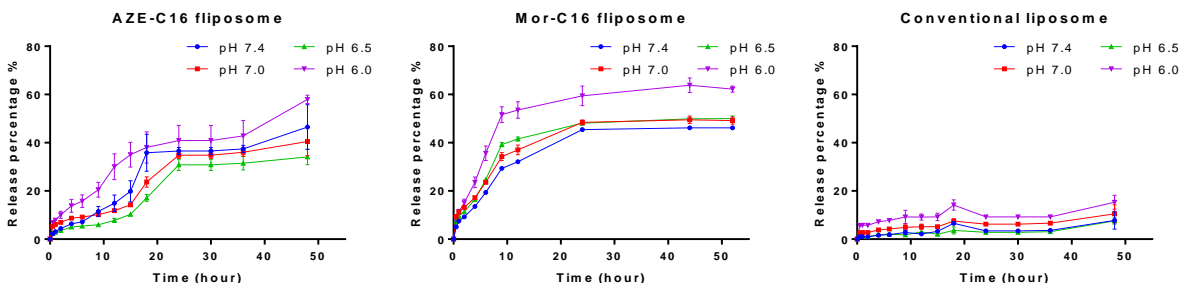
Figure 3.5. Release Percentage of calcein-loaded liposomes over 48h at defined pHs, 37°C (n=3).
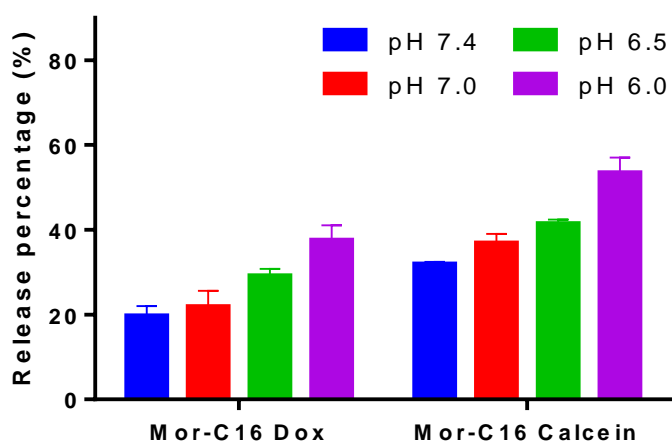
Figure 3.6. Release Percentage of DOX-loaded fliposomes and calcein-loaded fliposome after 12h at defined pHs, 37°C. Data presented as mean ± SD, N = 3.

Calcein, also known as fluorexon, is a widely used fluorescent probe in cell imaging by fluorescent microscopy [133]. Calcein is excited at 495 nm and emits at 515 nm. Calcein is highly water soluble and its fluorescence self-quenches when the concentration reaches above 70 mM (Figure 3.7), consistent to the literature report [134]. Therefore, calcein has been prominently utilized as a model probe for investigating drug release from liposomes and liposome-drug interaction. Generally, calcein, at the concentration above the self-quenching concentration, is entrapped inside the aqueous core of liposome by passive loading during hydration. When calcein is release from liposome, it is diluted to give de-quenched and thus

elevated fluorescent signal. Therefore, it is an excellent model to validate our doxorubicin

release assay on different fliposomes. Besides calcein, fluorescent dye-and-quencher pairs, such

as ANTS/DPX are also used in fluorescent assays on the release of liposomes [108, 135].
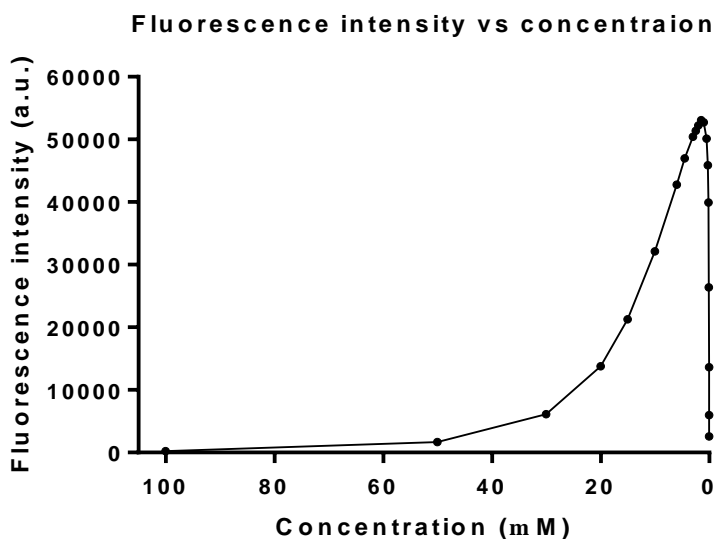
Figure 3.7. Fluorescence intensity vs calcein concentration profile.

3.4 Summary

We have studied several release assays for DOX-loaded liposomes, including traditional

dialysis methods, fluorescent methods and our new resin adsorption methods. Because of the

unique chemical properties of the cargo drug, doxorubicin, it is hard to find a direct method to

measure the released drug in sink condition, which is recognized as the golden standard in

industry. Despite certain drawbacks such as the potential interaction between resin and

formulation and the lack of mass balance, the direct resin adsorption method appears to be the

most practical and feasible method to kinetically monitor the release profile of pH-sensitive

liposomes *in vitro*. The advantage and disadvantage of the four release assay methods is

summarized in Table 3.4.

Table 3.4. Comparison of release assay methods

Method	Pros	Cons
Equilibrium microdialysis	• Quick • Small sample sizes	• Low recovery
Indirect Resin adsorption	• Higher accuracy	• Complicated process • Systemic error from sample size
Fluorescent dequenching	• High throughput	• Degradation
Direct Resin adsorption	• Acceptable error • Kinetic monitoring	• Possible interaction between resin and liposome

Chapter 4: Optimization of pH-sensitive Fliposomes

4.1 Introduction

In order to maximize the benefit of liposomes for anticancer therapy, many properties of such systems need to be optimized. In addition to triggered release, which is a focus for this dissertation, stability, small and homogeneous size, and adequate drug-loading capacity are all important properties of liposomes for anticancer therapy.

Particle size is an essential characteristic of nano drug delivery systems. The size is directly associated with stability, drug payload, release profile as well as pharmacokinetics of the drug delivery system [136]. Most importantly, an appropriate size range will allow the liposomes to extravasate from blood circulation into the tumor by the EPR effect, but not to be cleared by the body [120, 122]. As a reference, market product Doxil® has a size range of 80 - 100 nm [38]. It would be critical to include particle size as a parameter for optimization.

Polydispersity Index (PDI) is the term to describe the degree of heterogeneity in the size distribution of a nanoparticle sample [136, 137]. The value of PDI ranges from 0.0, which represents a perfectly uniform sample, to 1.0, which represent a total random distribution of the particle size. PDI values of 0.3 and below are typically accepted to indicate a nanoparticle formulation of reasonable quality [137]. From the perspective of liposomes for drug delivery, many efficiency and safety issues are related to the size of liposome, such as premature leakage. Successful liposome preparations, therefore, should contain homogenous populations of nanometer-range vesicle of an optimal size. The uniformity is another desirable attribute of the fliposomes for further application.

pH-sensitivity and stability are two diagonally opposite properties for quality control. Stability is the fundamental requirement for the design of nano-formulations because it prevents

many toxicity issues and allows the accumulation of the delivery system at the target site. It was

reported that 24-hour circulation is required for the manifestation of the EPR effect [138]. On

the other hand, pH-sensitivity enables the nano-formulation to respond to the acidic tumor

microenvironment, pH 6.0. Balancing the two opposing properties of the fliposomes is the focus

of this Chapter.

Drug-loading capacity is an easily overlooked but important property of a formulation.

The application of any drug formulation requires a minimum loading capacity to eventually

deliver enough treatment agent. In our case, it can be optimized to prepare formulation of

sufficient amount and concentration for the animal studies. The reference of 2 mg/ml

doxorubicin concentration in Doxil® is selected as our target.

The manufacture procedure can be modified to improve the above-mentioned properties.

Dispersion techniques, such as sonication and extrusion, could be options to optimize the

preparation. Lipid-to-drug ratio was also reported to be a key parameter to increase the

concentration of the drug payload [139]. Lipid composition is the focus of this study to optimize

the formulation for *in vitro* and *in vivo* studies. The aim of this chapter's studies is to identify the

factors influencing the outcomes of EPR effect and to optimize the formulation using

comprehensive method.

4.2 Materials and Methods

4.2.1 Materials. The lipids 1,2-dipalmitoyl-sn-glycero-3-phosphocholine (DPPC), 1,2-

distearoyl-sn-glycero-3-phosphocholine (DSPC), N-palmitoyl-sphingosine-1-

(succinyl[methoxy(polyethylene glycol)2000]) (PEG-ceramide (2000)), 1,2-dipalmitoyl-sn-

glycero-3-phosphoethanolamine-N-[azido(polyethylene glycol)-2000 (DPPE-PEG (2000)) were

purchased from Avanti Polar Lipids, Inc. (Alabaster, AL, USA). Cholesterol, copper(II) D-

gluconate, Dowex® 50WX-4, 2-Amino-2-(hydroxymethyl)propane-1,3-diol (Tris) and triethanolamine (TEA) were purchased from Sigma-Aldrich. Doxorubicin Hydrochloride was purchased from Biotang (Waltham, MA, USA).

4.2.2 Screening design for identification primary factors. Various liposomes with different lipid compositions were prepared by the thin-film hydration methods listed in 2.2.2.1. The size and ζ-potential of the liposomes were characterized by the methods listed in 2.2.4. The DOX concentration and drug encapsulation efficiency were determined by the methods listed in 2.2.5. pH-sensitivity and stability were evaluated by the direct resin adsorption release assay listed in 3.2.5. The primary factors that control the system were identified by the evaluation of colloidal stability and the pH-sensitivity with liposome charaterization.

4.2.3 Response surface methodology (RSM) for fliposome optimization. Central composite design (CCD) experiments were conducted to visualize the effects of independent variables on the select responses which represent the desired properties of the fliposomes. Two variables, percentage of Tach lipid and cholesterol, were identified as major independent factors through screening design and used in the design of the experiments by RSM. Five responses, size, PDI, pH-sensitivity, stability and maximum drug loading were selected to represent the desired properties of fliposomes, where pH-sensitivity was defined as equation below,

$$pH\ sensitivity\ (\%) = released\ DOX\ \%\ at\ pH\ 6.0 - released\ DOX\ \%\ at\ pH\ 7.4$$

after 48 hours; stability was defined as released DOX% at pH 7.4 after 48 hours.

CCD by 2 factors and 5 central points consisted of 13 runs with alpha level ($\alpha = 2^{k/4}$, k= number of factors) at 1.414 for two independent variables. The ranges and level of the variables are listed in Table 4.1. The complete CCD design matrix of experiments and the responses from

a total of 13 experiments were presented in the Table 4.6. CCD and response surface diagram

were constructed using Design-Expert (7.0.0) software.

Table 4.1. Factors and the correspondent values in coded and physical form

Factors	Code	Levels				
		$-\alpha$	-1	0	$+1$	$+\alpha$
AZE%	X1	25%	28.66%	37.5%	46.34%	50%
Chol%	X2	20%	23.66%	32.5%	41.34%	45%

All runs in CCD experiments were prepared by ethanol injection methods listed in

2.2.2.2. The liposomes were characterized by the methods listed in 2.2.4 while doxorubicin

concentration and drug encapsulation efficiency were determined by the methods listed in 2.2.5.

pH-sensitivity and stability were evaluated by direct resin adsorption release assays listed in

3.2.5.

4.2.4 Prediction by RSM. The optimal factor level as reflected by the AZE-C16 and

cholesterol molar percentage in the composition was predicted by Design-Expert (7.0.0) software

(Stat-Ease, Minneapolis, MN). The criteria of independent factors and response were listed in

Table 4.2. Point prediction was conducted with numerical solutions function.

Table 4.2. Optimization criteria for AZE-C16 based flipsomes

Factors	Goal	Lower limit	Upper limit	Lower weight	Upper weight	Importance
AZE%	In range	10	60	1	1	-
Chol%	In range	20	40	1	1	-
Size	Minimize	100	300	1	-	+++
PDI	Minimize	0.1	1	1	-	++++
pH sensitivity	Maximize	0	40	-	1	+++++
Stability	Minimize	0	50	1	-	++++
Drug loading	Maximize	1	2	-	1	+++

4.2.5 Data analysis. Data are presented as mean ± standard deviation (SD) for the

screening design study. The statistical analysis was performed by t-test for the pegylated lipid

composition study using GraphPad Prism 6.0 Software (GraphPad Software, La Jolla, CA).

Model selection and analysis of variance (ANOVA) for select model were performed using

Design-Expert 7.00 Software (Stat-Ease, Minneapolis, MN). The results with $p < 0.05$ were

accepted as statistically significant. Response surface plot and contour plot was generated by

Design-Expert (7.00) Software.

4.3 Results and Discussion

4.3.1 Effect of pegylated lipid composition. The effect of pegylated lipid in the bilayer

of liposomes on the size, PDI, drug loading and pH-sensitivity was evaluated with the select

compositions listed in Table 4.3. The fliposomes with two different pegylated lipids didn't show

much change on the size, PDI, drug loading capacity, as suggested in Table 4.3. A slight

increase of size was observed with the fliposomes prepared with PEG-ceramide, which is a

potential reason for the small increase of drug loading. Both fliposomes have similar PDI values

around 0.2, suggesting homogenous size distribution of the colloid system. Apparently, significant difference in pH-sensitivity was observed between the two pegylated lipids. In Figure 4.1, the fliposome with PEG-ceramide released 16% more than the one with PEG-DPPE after 24 hour incubation at 37°C. This drastic increase could be contributed by the charge of pegylated lipid molecule. PEG-Ceramide is neutral while PEG-DPPE is negatively charged. When the fliposome was exposed to the environment of lower pH, those negative charged phosphate group in PEG-DPPE would compete with TACH lipid to grab proton. Because there was 5% such molecules in the bilayer, the pH-sensitivity would be counterbalanced. This observation was also explained by potential ionic interaction between the phosphate group of DSPE-PEG and the protonated amine group in TACH C12 lipid [102], which is thought to compete with the formation of an intramolecular hydrogen bond by the TACH lipid. Therefore, PEG-ceramide was chosen over PEG-DPPE for further investigation of liposomes.

Table 4.3. Composition, size, PDI, EE and drug loading concentration of select DOX-loaded fliposomes with two pegylated lipid

Liposome	Mole ratio	Size (nm)	PDI.	EE (%)	Dox Conc. (mg/ml)
Mor-C16 : DPPC : PEG-DPPE	50 : 45 : 5	158.8	0.177	71.70	0.717
Mor-C16 : DPPC : PEG-Ceramide	50 : 45 : 5	180.1	0.208	82.57	0.826
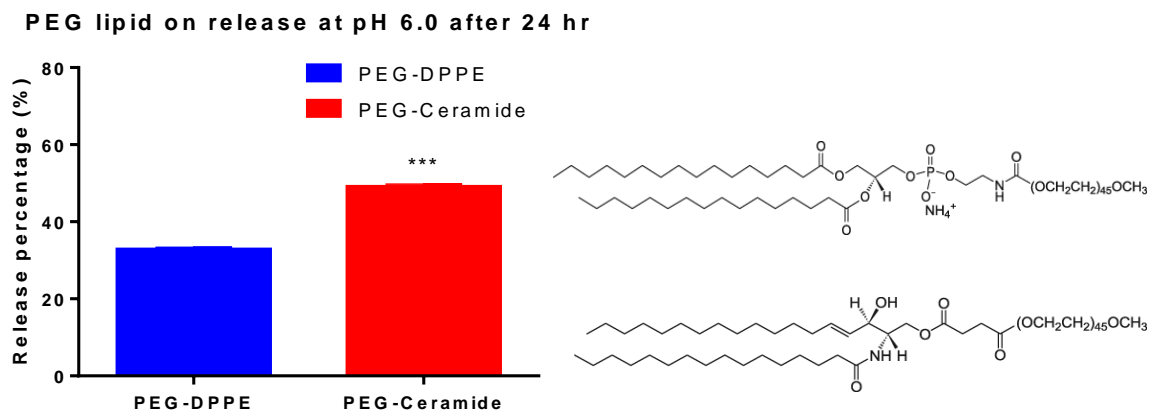
Figure 4.1. Pegylated lipid effect on release profile of DOX-loaded fliposomes at pH 6.0, 37°C after 24 hours. Data presented as mean ± SD, N = 3. *** p<0.001 for t-test.

4.3.2 Effect of cholesterol. The effect of cholesterol in the bilayer of liposomes on the size, PDI, drug loading and pH-sensitivity is evaluated with the select composition listed in Table 4.4. The liposomes with and without cholesterol in composition were characterized and result was listed in Table 4.4. Without cholesterol in the bilayer of liposomes, the size and PDI were larger than the liposomes with cholesterol. In addition, it was prominent that the drug loading was higher after adding cholesterol into the bilayer for the non-pH sensitive liposomes. Cholesterol also increased the stability of the liposomes, as indicated by the lower release of non-pH-sensitive liposomes at all pHs ranging from 6.0 to 7.4 (Figure 4.2).

Table 4.4. Composition, size, PDI, EE and drug concentration of DOX-loaded liposomes with and without cholesterol

Liposome	Mole ratio	Size (nm)	PDI.	EE (%)	Dox Conc. (mg/ml)
DPPC : PEG-DPPE	95 : 5	219.4	0.474	36.6	0.366
DPPC : Chol : PEG-DPPE	70 : 25 : 5	188.8	0.120	79.4	0.794
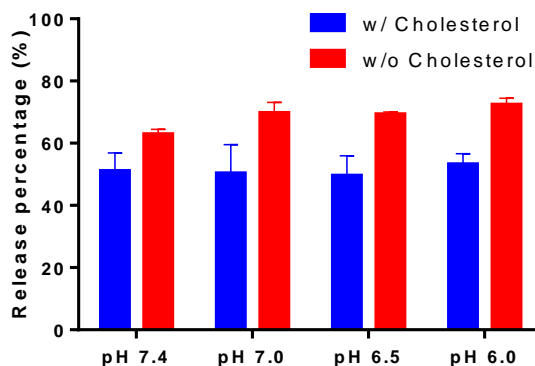
Figure 4.2. Cholesterol effect on release profile of DOX-loaded liposomes (DPPC : PEG-DPPE= 95 : 5, DPPC : Chol : PEG-DPPE = 70 : 25 : 5) at defined pHs, 37°C after 24 hours. Data presented as mean ± SD, N = 3.

It was reported that cholesterol can stabilize liposomal formulation when added into the bilayer structure [140, 141]. It was found that cholesterol controlled the fluidity of the liposome bilayer by occupying the cavities between the hydrocarbon chains of phospholipid, thereby inhibiting the free movement of those fatty acyl chains in the dispersed liquid crystalline phase [142]. In the gel phase, cholesterol can disturb the crystalline chain lattice in the bilayer, thereby increasing the permeability of the liposome [143]. Therefore, cholesterol would augment the liposome stability when the temperature is elevated above the transition temperature ($T > T_m$) and would enhance the drug retention during the high temperature of incubation. However, the incorporation of cholesterol would also decrease the pH-sensitivity because the fliposomes are exposed to the physiological temperature around 37°C *in vivo*, which is below their transition temperature. In addition, it has been reported that the higher ratio of cholesterol to DPPC (0.8 ~ 1.0) in the liposome bilayer will form an extraordinary lateral order, which is an extremely stable system without noticeable transition temperature [142].

With those prominent influences on the physicochemical properties and on the pH-sensitivity, cholesterol was chosen as primary factor for the further optimization.

4.3.3 Effect of phospholipid. The effect of phospholipid in the bilayer of liposomes on the size, PDI, release profile was evaluated with the select compositions listed in Table 4.5. The liposomes that were prepared with DPPC didn't show any significant difference with those with DSPC in the physicochemical properties, such as size and PDI, however, lower drug release, no matter within conventional liposomes or fliposomes, was observed in the presence of DSPC.

Table 4.5. Composition, size, PDI and release percentage of DOX-loaded liposomes with different phospholipids (n=3).

Liposome	Molar ratio	Size (nm)	PDI	pH	Release% after 12 hr
DSPC : Chol :PEG-Ceramide	70:25:5	134.3	0.093	6.5	41.5±1.6
DPPC : Chol :PEG-Ceramide	70:25:5	116.4	0.046	6.5	58.9±1.6
DSPC : Mor-C16 : PEG-Ceramide	70:25:5	122.1	0.084	7.4	42.2+1.0
DPPC : Mor-C16 : PEG-Ceramide	70:25:5	108.4	0.109	7.4	66.6±0.4

It was well acknowledged that the transition temperature (T_m) of a liposome system is mainly determined by the T_m of the component lipids. T_m is defined as the temperature at which the lipid bilayer has a physical change from the ordered gel phase to the disordered liquid crystalline phase[144]. The hydrocarbon length of the lipid tail and saturation/unsaturation of the fatty acyl chains of the lipids are the two main factors that determine the T_m. In Table 4.6, five different phospholipids with different T_m are listed. It was also reported that an increase in length of the hydrocarbon chain (and therefore transition temperature) is directly correlated to stability[145]. Therefore, incorporating DSPC or DPPC into the liposome bilayer to balance the stability and pH-sensitivity is considered as a key factor for further optimization.

Table 4.6. Transition Temperature of Phospholipids[146]

Lipid	Hydrocarbon length	Unsaturated bond	T_m (°C)
DLPC	12	0	-1
DMPC	14	0	23
DPPC	16	0	41
DSPC	18	0	55
DOPC	18	1	-20

4.3.4 Effect of flipids. The effect of flipid in the bilayer of liposomes on the size, PDI and pH-sensitivity was evaluated with the select composition listed in Table 4.7 and 4.8. Increase in size and PDI was observed along with an increase of molar percentage of flipids in the fliposome composition (Table 4.7). It was also accompanied by the drastic increase in the resistance during the extrusion. The PDI value was above 0.3, suggesting that the colloidal system was not stable, and/or that a large aggregation was forming. Together these phenomena indicated that TACH lipids were not compatible with the liposomal bilayer structure at high mole percentages. This may be caused by the steric hindrance of the amine head group as well as the cyclohexanol ring (Figure. 4.3). In addition, the close-to-zero surface charge of the liposomes may also contribute to the aggregation. On the other hand, a flipid was introduced to render the saturated and PEGylated liposomes pH-sensitive. It was apparent that the pH-sensitivity in this case, which is the difference between the release percentage at physiological pH 7.4 and tumor microenvironment pH 6.0, will be boosted with increasing flipid composition. It is demonstrated by the comparison in Table 4.8 that doubling the molar percentage of MOR-C16 lead to nearly 18% raise of the pH-triggered release.

Given the different effects of the flipid as discussed above, it is crucial to optimize the molar percentage of flipid to balance between pH-sensitivity and good colloidal properties of the

liposome. Therefore, mole percentage of flipid was selected as another primary variable for

further optimization.

Table 4.7. Composition, size, PDI of empty fliposomes of different mole percentage of the Tach-lipid.

Liposome	Molar ratio	size (nm)	PDI
DPPC : MOR-C16 :PEG-Ceramide	65:30:5	116.7	0.169
DPPC : MOR-C16 :PEG-Ceramide	55:40:5	179.3	0.459
DPPC : MOR-C16 :PEG-Ceramide	45:50:5	221	0.569

Table 4.8. Composition, size, PDI and release percentage of DOX-loaded fliposomes at different mole percentage of the TACH-lipid MOR (n=3).

Liposome	Molar ratio	Size (nm)	PDI	pH sensitivity %	Release % after 48 hr
DPPC : MOR-C16 :PEG-Ceramide	70 : 25 : 5	108.4	0.109	15.9±1.2	64.0±4.4
DPPC : MOR-C16 :PEG-Ceramide	45 : 50 : 5	182.4	0.309	34.1±3.4	94.3±1.8
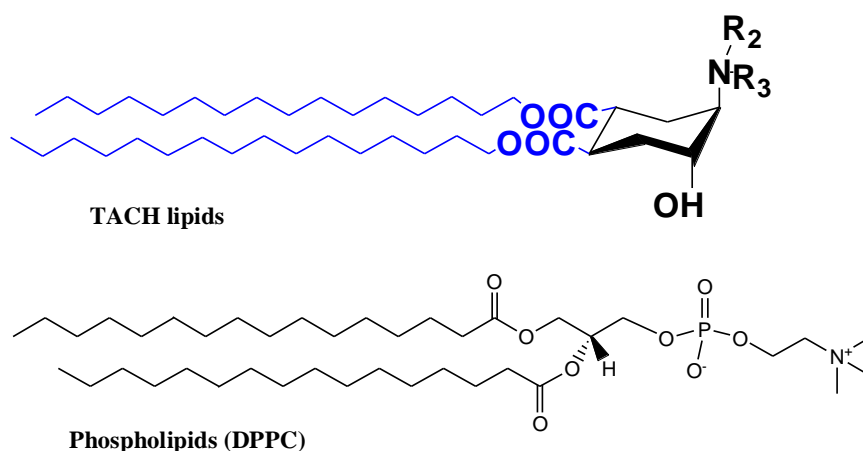
Figure 4.3. Chemical structure of TACH-lipid and phospholipids

4.3.5 Optimization of liposome composition with response surface methodology

(RSM). Based on the RSM approach, the total number of runs was calculated as $2^k + n_a + n_0$, where k is the number of independent factors, 2^k represents the full factorial design points, n_a represents the axial points determined by α level, and n_0 is the replicate number of center point. In this experiment, we had 2 factors, and 5 central points to give 13 total runs.

A general equation for the relation of independent variable and response is:

$Y=b_0＋b_1X_1+b_2X_2+b_3X_1X_2+b_4X_1^2+b_5X_2^2$.

Where Y is the dependent variable; X_1 and X_2 are the independent variables; b_0 is the intercept coefficient, which is the model constant; b_1 and b_2 are the estimated linear coefficients for the factor X_1 and X_2 respectively; b_3 is interaction coefficient and b_4 and b_5 are quadratic coefficients. The magnitude and the mathematical sign of coefficients suggested the degree of effect upon the dependent responses. The complete CCD design matrix of experiments and the responses from a total of 13 experiments were presented in the Table 4.9.

Table 4.9. CCD of experiments for optimization of AZE-C16 based fliposome utilizing DX-7 software.

Run No.	X_1 (AZE%)	X_2 (Chol%)	size (nm)	PDI	pH sensitivity (%)	Stability (%)	Drug loading (mg/ml)
1	37.50	32.50	178.1	0.279	28.05	34.63	1.42
2	28.66	41.34	173.3	0.255	15.70	27.63	1.73
3	37.50	45.00	283.2	0.515	8.43	48.87	1.51
4	46.34	41.34	187.9	0.328	8.64	44.04	1.42
5	37.50	32.50	258.5	0.606	7.53	46.27	1.47
6	37.50	32.50	212	0.359	17.15	48.89	1.10
7	37.50	32.50	163.5	0.198	24.33	44.20	1.60
8	46.34	23.66	228.7	0.575	18.00	51.38	1.30
9	37.50	20.00	158.8	0.173	10.73	43.40	1.85
10	50.00	32.50	175.8	0.195	12.90	42.71	1.13
11	37.50	32.50	166.6	0.316	21.68	48.07	1.26
12	28.66	23.66	139.9	0.308	13.63	46.71	1.42
13	25.00	32.50	146.3	0.31	4.72	49.27	1.08

Table 4.10. Coefficients of regression equations for the responses with actual factors

Dependent variable (Reponses)	Regression coefficients					
	b_0	b_1	b_2	b_3	b_4	b_5
Size (nm)	-90.44	16.56	-7.77	-0.237	-0.090	0.293
PDI	-	-	-	-	-	-
pH sensitivity (%)	-181.0	6.29	5.21	-0.037	-0.066	-0.061
Stability (%)	-	-	-	-	-	-
Drug loading (mg/ml)	2.017	0.097	-0.148	-6.01E-4	-1.10E-3	2.61E-3

According to the ANOVA test of model on all five dependent variables, none of them statistically fit to a quadratic model. Only size, pH-sensitivity and drug loading were suggested

by lack of fit tests to fit as a quadratic model, and the coefficients of general regression equations for the actual factors were listed in Table 4.10. Although the fitting was not good to have regression, the effect of two primary factors on key properties of the AZE-C16-based fliposome was still able to be evaluated.

4.3.5.1 Effect of AZE-C16 and cholesterol percentage on size. In order to fully utilize the EPR effect, size is the critical parameter which need to be well controlled during the preparation procedure. For the simplicity procedure, the extrusion of all fliposome in 13 runs were only conducted through 200 nm polycarbonate filters 5 times for the sake of the productivity. Therefore, all the sizes of fliposomes wouldn't be close to 100 nm. For the optimization purpose, it was one factor to reflect good quality of a colloidal system. It was apparent that the size increased along with the increase of AZE% and Chol%. It could also be reflected by the trends in response surface plot (Figure 4.4) and quadratic equation: size = -90.44 + 16.56 * AZE% - 7.77 * Chol% - 0.237 * AZE% * Chol% - 0.090 * (AZE%)^2 + 0.293* (Chol%)^2.
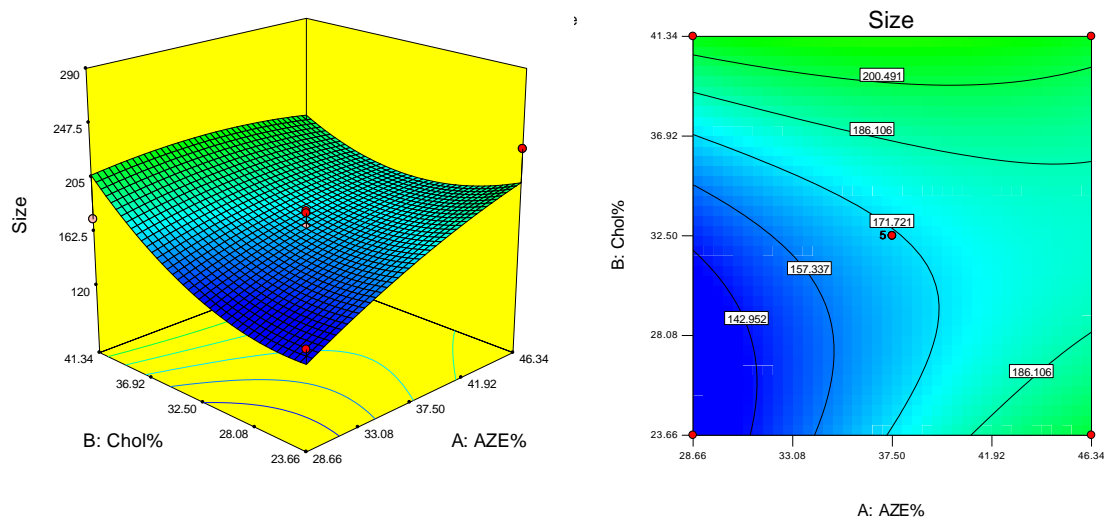
Figure 4.4. Response surface plot (3D) (left) and contour plot (right) showing the effect of AZE% and Chol% on Size.

4.3.5.2 Effect of AZE-C16 and cholesterol percentage on pH sensitivity. Rendering pH-sensitivity is our main approach to improve pegylated liposomes. According to the 3D response surface plot (Figure 4.5), the pH-sensitivity increased with the increase of AZE% or Chol% to certain extent, then the pH-sensitivity gradually decreases. It was reflected by larger values in the central concentric circle of the contour plot. The quadratic equation was pH sensitivity = -181.0 + 6.29 * AZE% + 5.21 * Chol% - 0.037 * AZE% * Chol% - 0.066 * (AZE%)^2 - 0.061* (Chol%)^2. Mathematically, after AZE% and Chol% went over certain value, the negative effect from the quadratic parts of the equation would counterbalance the positive contribution from the linear parts.
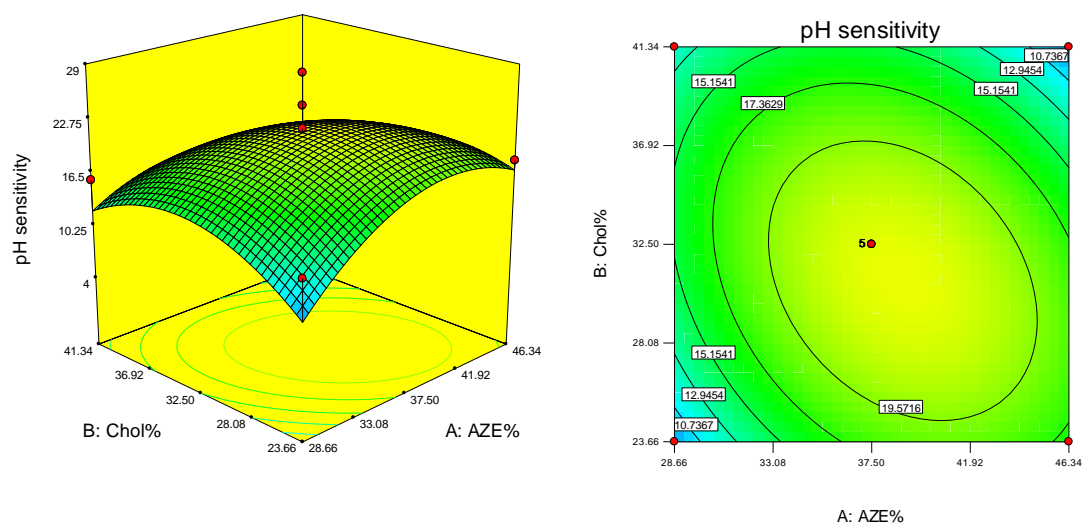
Figure 4.5. Response surface plot (3D) (Left) and contour plot (Right) showing the effect of AZE% and Chol% on pH sensitivity.

4.3.5.3 Effect of AZE-C16 and cholesterol percentage on drug loading. Drug loading was an important response of RSM we would like to look into because of the needs of the animal studies. Higher loading gave more flexibility to conduct animal experiments. The market product Doxil® is at 2 mg/ml doxorubicin concentration, therefore, the aim of our fliposome was

to get close to 2 mg/ml at non-optimized condition. Among three of the quadratic models, drug

loading was least significant relative to the noise. According to the equation from the modeling,

Drug loading = 2.017+ 0.097 * AZE% - 0.148 * Chol% - 6.01E-4 * AZE% * Chol% - 1.10E-3 *

$(AZE\%)^2$ + 2.61E-3 * $(Chol\%)^2$, where the intrinsic drug loading is close to 2 mg/ml at our

current lipid to drug ratio (4:1, wt : wt). The contribution from lipid composition was limited,

while the drug-loading would decrease along with more cholesterol in the liposome bilayer

(Figure 4.6). It can be easily explained by the fact that cholesterol by itself is not conducive to

the formation of the lipid bilayer, and thus would decrease the total number of liposome vehicles

available for drug loading with the increase of its molar ratio.
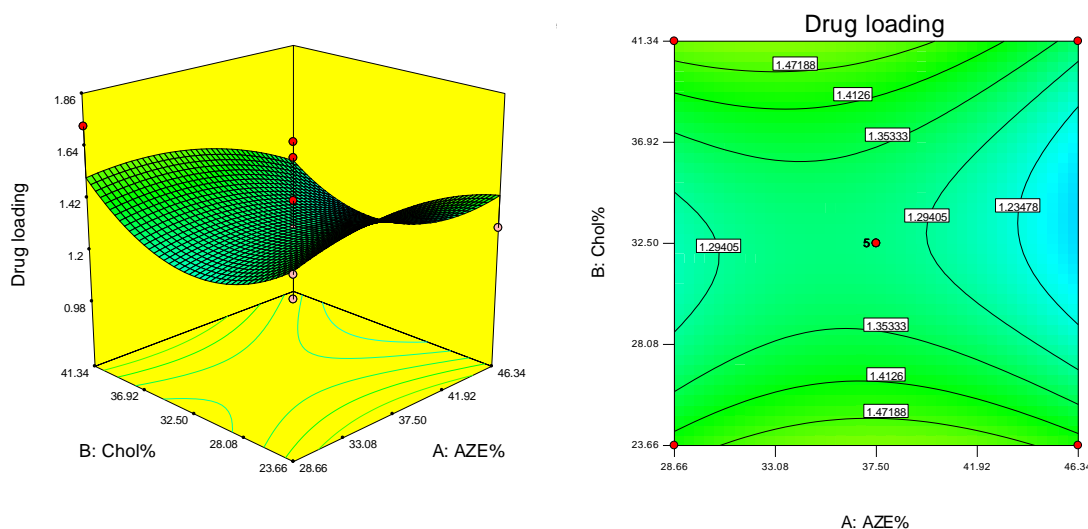
Figure 4.6. Response surface plot (3D) (Left) and contour plot (Right) showing the effect of
AZE% and Chol% on Drug loading.

4.3.5.4 Prediction of AZE-C16 based fliposome by RSM optimization. Based on the

constraints of the criteria set up, 30 starting points were simulated by Design-Expert. One

numerically optimized solution with the constraints of AZE% & Chol% in range and five

responses in target was obtained, of which the lipid composition is AZE: DSPC: Chol: PEG-Ceramide = 38: 32: 25: 5. The predict response is listed in Table 4.11.

Table 4.11. Predition of AZE-C16 based fliposome by RSM optimization

Response	Size (nm)	PDI	pH sensitivity (%)	Stability (%)	Drug loading (mg/ml)
Prediction	171.00	0.292	19.19	44.37	1.47

4.4 Summary

Several factors in the preparation of liposome formulation were investigated. The Neutral pegylated lipid, PEG-Ceramide was chosen for enhanced pH-sensitivity. Cholesterol and DSPC were necessary for the stability of the liposomes, including the AZE-C16-based fliposomes of quick response. RSM was utilized to further optimize the AZE-C16 based fliposome. AZE: DSPC: Chol: PEG-Ceramide = 38: 32: 25: 5 was predicted by RSM to have relatively high stability and pH-sensitivity. The optimized formulation was brought for further biological evaluation of efficacy together with another fliposome formulation MOR-C16: DPPC: PEG-Ceramide = 70: 25: 5, which had been previously identified in previous work [104].

Chapter 5: Evaluation of Anticancer Efficacy of Doxorubicin-loaded Fliposome *in vitro*

5.1 Introduction

The main stream strategy in the pharmaceutical industry to screen anticancer drugs and to validate their activities is to use two-dimensional models of cultured cells *in vitro* and animal models *in vivo*. Although *in vitro* 2D monolayer cell culture has many advantages such as convenience, high throughput and low-cost, their main drawback is the lack of cell-cell and cell-matrix interactions. In addition, although solid tumors usually carry variations in oxygen level, metabolite concentration and acidic extracellular pH, such features are all missing in 2D cell culture models [147]. More and more studies have discovered the poor correlation between the monolayer cell models *in vitro* and the animal models *in vivo*, which would explain the gap between findings at early stages of drug screening and late stages of drug development. Therefore, there is a great demand of cost-efficient and accurate *in vitro* models to bridge such a gap, especially in oncology.

3D MCS were established in the 1970s by Sutherland et al [148], and have now demonstrated many advantages over 2D cell culture models. 3D MCS are self-assembled under conditions that allow cells to grow and interact with their surroundings in three dimensions. A necrotic core can be observed in MCS when the size reaches 500 µm. The necrotic core is surrounded by a proliferative zone and a quiescent zone [149]. A typical configuration of 3D MCS (> 500 µm) with different areas is shown in Figure 5.1. 3D MCS include many features of solid tumors that are missing in 2D monolayer cells and thus have been proven to better mimic the native and complex tumor microenvironment [150].
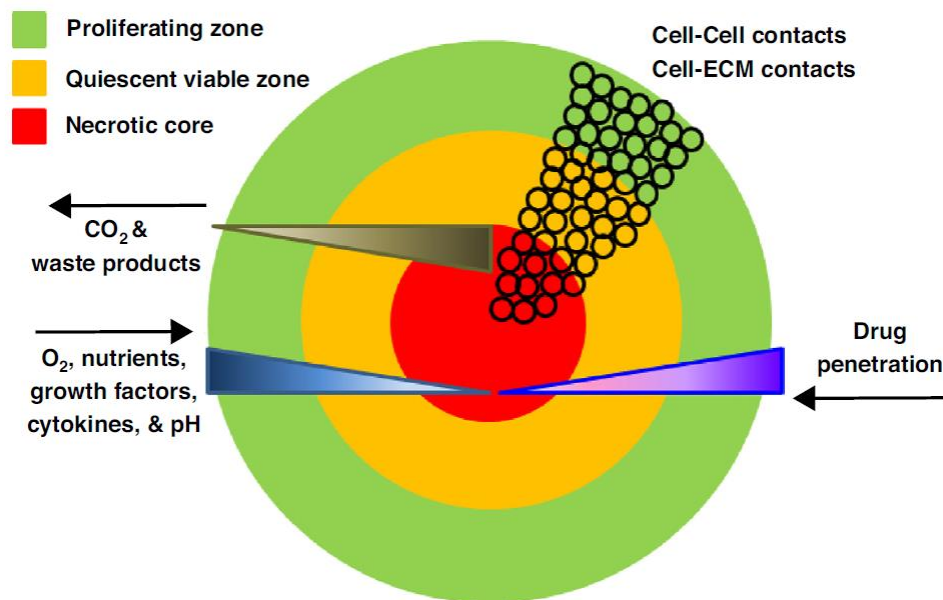
Figure 5.1. Illustration of the typical configuration of a 3D MCS over 500 µm in diameter [151]

The difference between using 3D MCS and 2D cell culture was demonstrated by many researches [152, 153]. Colley et al. [154] reported that the delivery of drugs into the core of the 3D MCS model of head and neck squamous cell carcinoma cells is crucial for the therapeutic effect while much lower exposure of the drug to the corresponding 2D monolayer cells substantially decreased the cancer cell viability. In breast cancer treatment, Pickl et al. [152] reported that the HER2 activation is enhanced in 3D MCS because the HER2 homodimer could be formed in the model whereas only HER2/HER3 heterdimer, but not the HER2 homodimer could be formed on the surface of monolayer cells. 3D MCS can be formed by many different breast cancer cell lines, including TNBC[155-157]. Moreover, a pH gradient has been demonstrated in 3D MCS model, a feature of the tumor microenvironment that would greatly facilitate the characterization of the pH-sensitive fliposomes [158].

Therefore, 3D MCS can serve as a better platform for cancer research by providing a more physiologically relevant microsystem. 3D MCS of TNBC can evaluate the efficacy of

fliposomes as a better prediction of fliposomes' anticancer activities *in vivo*. The aim of this chapter's studies is to construct and characterize TNBC 3D MCS and evaluate the anticancer efficacy on 3D MCS.

5.2 Materials and Methods

5.2.1 Materials. MDA-MB-231 and MDA-MB-468 cell lines were purchased from ATCC (Manassas, VA, USA). Advanced F12/DMEM, Non-Essential Amino Acid (NEAA), Collagen I, Bovine, Live/DEAD ^{TM} Cell Imaging Kit, Nigericin, Carboxy SNARF®-1, acetoxymethyl ester, acetate, and Trypsin-EDTA were purchased from Thermo-Fisher. 96-well Ultra-low Attachment Spheroid Microplates were purchased form Corning. HEPES and MES were purchased from Fisher. Tris was purchased from Sigma-Aldrich.

5.2.2 Cell culture condition.

5.2.2.1 Cell culture maintenance. TNBC cell lines MDA-MB-231 and MDA-MB-468 were maintained in Advanced F12/DMEM supplemented with 5% fetal bovine serum (Gemini, West Sacaramento, CA), 1% Penicillin-Streptomycin (Corning Life Science, Corning, NY) and 1% L-glutamine (Invitrogen, San Diego, CA). Cells were grown in 5% CO2 at 37 °C and passaged at 85% confluence. (3~4 days).

5.2.2.2 3D MCS formation. MDA-MB-231 (~3000 cells/well), MDA-MB-468 (~2500 cells/well) were seeded in the Corning ultra-low attachment 96 well plates with 1% collagen. The cells were centrifuged at 200 g for 15 minutes to facilitate the aggregation. The growth media was changed every other day by replacing 100 µL of the media in the well with 100 µL fresh media to maintain a 200 µL total media volume. The morphology of 3D MCS of each cell line was observed on an inverted microscope.

5.2.3 Live/dead cell assay. The LIVE/DEAD Viability/Cytotoxicity kit from ThermoFisher was used to assess the viability of the cells inside 3D MCS according to manufacturer protocol. Briefly, MDA-MB-468 cells (~2500 cells/well) were seeded in the Corning ultra-low attachment 96 well plate to form 3D MCS using the methods described above. At day 11-12 when the 3D MCS were at ~ 600 µm in diameter, three 3D MCS were transferred to a glass bottom dish containing 100 µL of total growth media for each cell line. The LIVE/DEAD cell imaging kit reagent was added to the 3D MCS at equal volume per well. The 3D MCS were incubated for 45 mins at room temperature, washed 3 times with PBS and imaged using a Leica DMIRE2 confocal microscope. The live cells give a green fluorescence signal at $\lambda_{ex} = 488$ nm and $\lambda_{em} = 515$ nm, while the dead cells give a nuclear read fluorescence signal at $\lambda_{ex} = 570$ nm and $\lambda_{em} = 602$ nm. Images were acquired using the MetaMorph software and analyzed using the ImageJ software.

5.2.4 pH gradient inside 3D MCS. The emission spectrum of Carboxy SNARF-1 shifts along with the change of pH so Carboxy SNARF-1 can be used to measure the pH gradient inside 3D MCS. Carboxy SNARF-1 is typically excited at one wave length between 488 nm and 530 nm and simultaneously emits fluorescent signal at two wavelengths, typically at about 580 nm and 640 nm. The pH can be determined by the ratio of these two fluorescent signals. MDA-MB-468 cells (~2500 cells/well) were seeded in the Corning ultra-low attachment 96 well plate to form 3D MCS using the methods described above. At day 11-12 when the 3D MCS were at ~ 600 µm in diameter, three 3D MCS were transferred to a glass bottom dish containing 100 µL of total growth media. SNARF-1 was dissolved in anhydrous DMSO at concentration of 100 µM and added to 3D MCS in the glass bottom dish to a final concentration of 10 µM. The 3D MCS were then incubated for 45 mins at 37°C, washed 3 times with PBS and imaged using a Leica

DMIRE2 confocal microscopy. At the end of an experiment, 3D MCS loaded with Carboxy

SNARF-1 was exposed to three calibration solutions of 10 µM nigericin at pH 5.5, 6.8 and 8.0.

The solutions were composed of 140 mM KCl, 1 mM MgCl$_2$, 0.5 mM EGTA and 20 mM MES

for pH 5.5, 20 mM Hepes for pH 6.8 or 20 mM Tris mM for pH 8.0. Three calibration images at

each pH were recorded in triplicate.
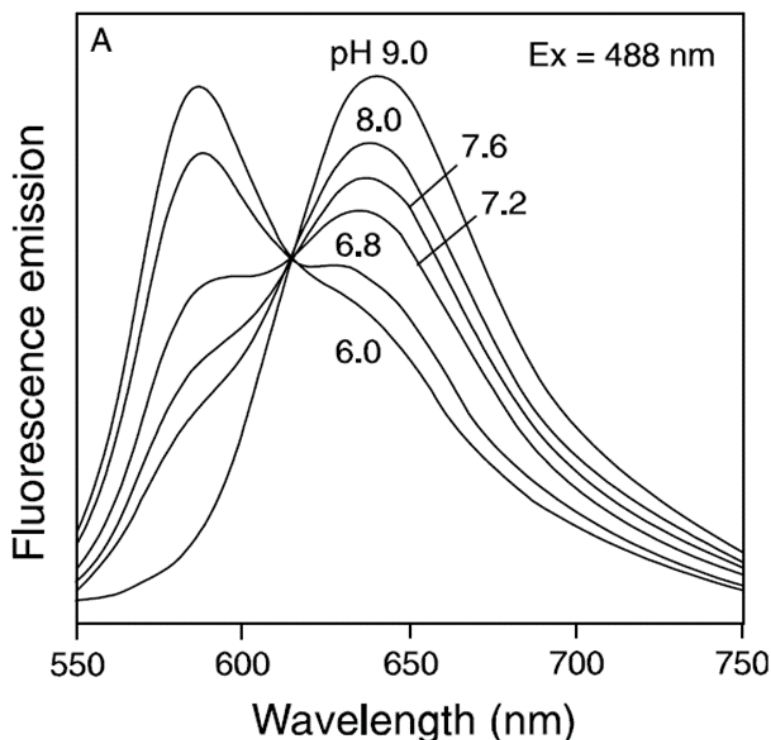
Figure 5.2. The emission Spectra of carboxy SNARF-1 indicates the correlation between pH and the ratio of fluorescence at 580/640 nm [159]

$$pH = pK_a - \log\left[\frac{R - R_B}{R_A - R} \times \frac{F_{B(\lambda 2)}}{F_{A(\lambda 2)}}\right] \qquad (1)$$

The pH at a given point in the fluorescent images can be estimated using the above

equation, where the pKa of carboxy SNARF-1 is ~ 7.5, R is the ratio of the fluorescence

intensities at the two wavelengths $\lambda 1 = 580$ nm and $\lambda 2 = 640$ nm ($F_{\lambda 1}/F_{\lambda 2}$). Subscripts A and B

represent the limiting values at the acidic and basic endpoints, respectively. From the equation

we can see pH is directly correlated to the R value - the higher R is, the lower pH would be.

However, the background signal needs to be subtracted before the calculation of R. Images were

acquired using MetaMorph software and analyzed using ImageJ software. One z-stack picture at

200 µm above the bottom of each 3D MCS was selected for the analyses and divided into five

areas using concentric circles. Each of the five areas was numbered 1 to 5 from the center to the

edge. The mean value of the two emission fluorescence signals of each region was measured.

The R value of each region was then calculated after subtracting the background noise. pH value

was then calculated by the above equation.

5.2.5 Cytotoxicity assays for DOX-loaded liposomes on 2D monolayer cells and on

3D MCS. MDA-MB-231 cells (~ 10,000 cells/well) and MDA-MB-468 cells (~ 5,000

cells/well) within 15 passages were seeded into 96-well plates and incubated at 37 °C with 5%

CO_2 overnight. The complete medium was then replaced, respectively, with 200 µL culture

mediums containing DOX-loaded liposomes and free DOX at incremental concentrations. After

incubation for 72 hours, 20 µL CellTiter 96® AQueous One Solution cell proliferation assay

(Promega Corp., WI, USA) was added to each well when 100 µL complete growth medium was

replaced to stop treatment. After further incubation at 37 °C with 5% CO_2 for 4 h, the

absorbance at 490 nm was recorded by Synergy HT microplate reader. The cells that were

exposed to only the growth media were assayed following the same procedure and taken as

100% viability reference. Samples were evaluated in quadruplicates.

MDA-MB-231 cells (~ 3,000 cells/well) and MDA-MB-468 cells (~ 2,500 cells/well)

within 15 passage were seeded into Corning ULA 96-well plate to form 3D MCS using the

method described above. After 11-13 days when the spheroids grew to ~600 µm in diameter, 3D

MCS were treated with free Dox and liposomal Dox at incremental concentrations in complete medium. After incubation for 72 h at 37°C with 5% CO_2, 3D MCS for each treatment group were transferred to an opaque-walled 96-well plate with 100 µl medium in each well. An equal volume of CellTiter-Glo 3D cell viability assay (Promega Corp., WI, USA) was added to each well. The plate was shaken for 5 minutes and incubated for an additional 20 minutes at room temperature to stabilize the luminescent signal. The luminescence was then recorded by a Synergy HT microplate reader. The cells that were treated only with the growth media were assayed following the same procedure and taken as 100% viability reference. Samples were evaluated in quadruplicates.

5.2.6 Drug distribution in 3D MCS. The distributions of free DOX and DOX-loaded liposomes within 3D MCS were determined by Laser confocal microscopy. MDA-MB-231 and MDA-Mb-468 3D MCS with a diameter of about 600 µm were harvested 11~ 13 days after seeding. All the 3D MCS were treated with 10 µg/ml free DOX or equivalent DOX-loaded liposomes and incubated at 37 °C with 5% CO_2 for 4 hours. The medium was then removed and MCS were washed with PBS. The spheroids were transferred to a glass bottom dish and observed on a Leica DMIRE2 laser confocal microscope with the following setup: Exposure (1s), Gain (1x), Image Scaling (1000-7000) and z step (10 µm). The excitation and emission were at 470 nm and 585 nm, respectively. Images were acquired using MetaMorph software and analyzed using ImageJ software. The semi-quantitative analysis of mean fluorescence intensity of free DOX, DOX-loaded liposomes in 3D MCS was made by calculating the mean fluorescence intensity of each multicellular spheroids. All pixels' fluorescence intensity of regions of interest were counted and normalized by the area.

5.2.7 Data analysis. Data are presented as mean ± standard deviation (SD) for the all

cytotoxicity assay study. IC_{50} was generated by nonlinear regression, log(inhibitor) vs. viability.

Response model using GraphPad Prism 6.0 Software (GraphPad Software, La Jolla, CA). The

statistical analysis was performed by one-way analysis of variance (ANOVA) for IC_{50}

comparison using GraphPad Prism 6.0 Software. Tukey's post hoc test analysis was performed

to compare between the treatment groups. The results with $p < 0.05$ were accepted as

statistically significant.

5.3 Results and Discussion

5.3.1 Formation of 3D MCS. Relatively tight multi-cellular spheroids of two TNBC cell

lines were successfully constructed at select seeding density after the application of

centrifugation and the use of collagen in the seeding media. As mentioned before, spheroids

with diameters larger than 500 µm commonly have a necrotic core surrounded by a viable layer

of quiescent zone and an outer shell of proliferating cells[160, 161]. The gradients of

metabolites, oxygen, nutrients and pH inside the 3D MCS make them a more physiologically

relevant platform for testing drug delivery systems than 2D cell models. The size of 3D MCS

gradually increased within 15 days and MDA-MB-231 formed tighter structure than MDA-MB-

468, shown in Figure 5.3. The growth curve of 3D MCS of MDA-MB-231 was validated with

the size and 3D viability assays (Figure 5.4).
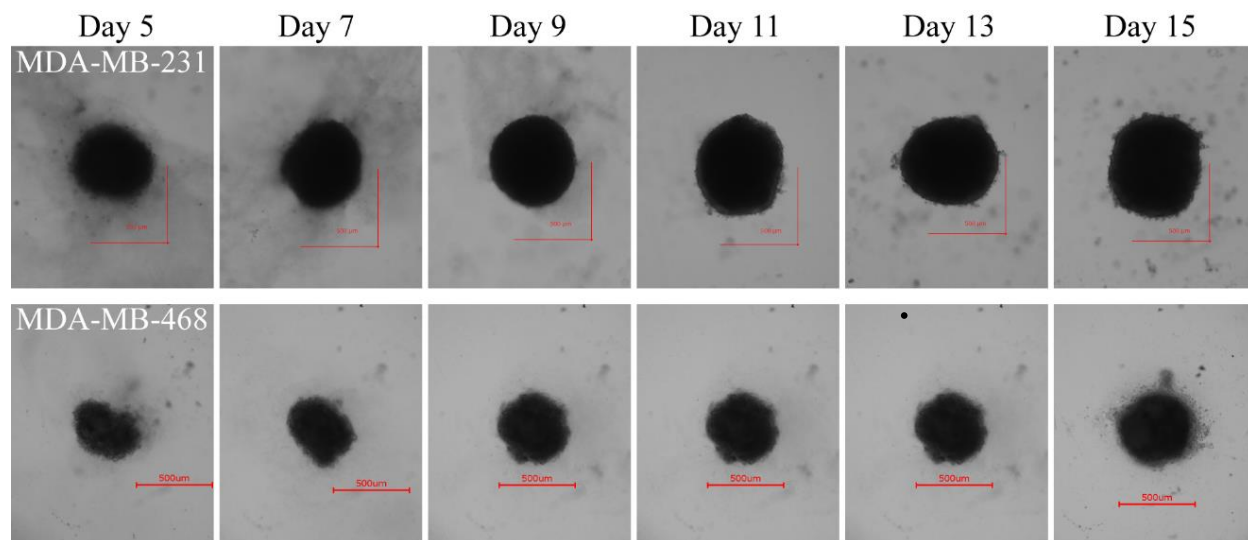
Figure 5.3. Morphology of MDA-MB-231 (3000 cells/well, upper) and MDA-MB-468 cells (2000 cells/well, lower) after 5, 7, 9, 11, 13, 15 days in the ULA 96 well plates.
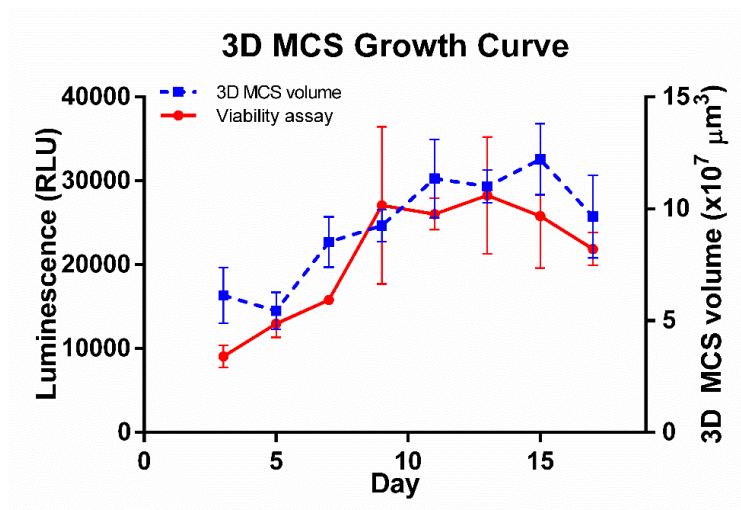
Figure 5.4. Growth Curve by size and 3D cell viability assay with MDA-MB-231 (3000 cells/well). Data presented as mean ± SD, N = 3.

5.3.2 Distribution of live and dead cells inside 3D MCS. Figure 5.5 shows the image of a 100 μm-deep cross section near the core of 3D MCS of MDA-MB-231 and MDA-MB-468 cells. The green signal from the fluorophore Calcein-AM represent the live cells while the red signals from the fluorophore ethidium homodimer-1 represent the dead cells. The confocal

images of both cell lines show that the green signals are concentrated in the peripheral areas,
indicating a proliferation zone while the red signals distribute mainly in the core, indicating a
necrotic zone. This phenomenon was also demonstrated by the semi- quantitative accumulation
of relative florescent signal at two wavelengths.
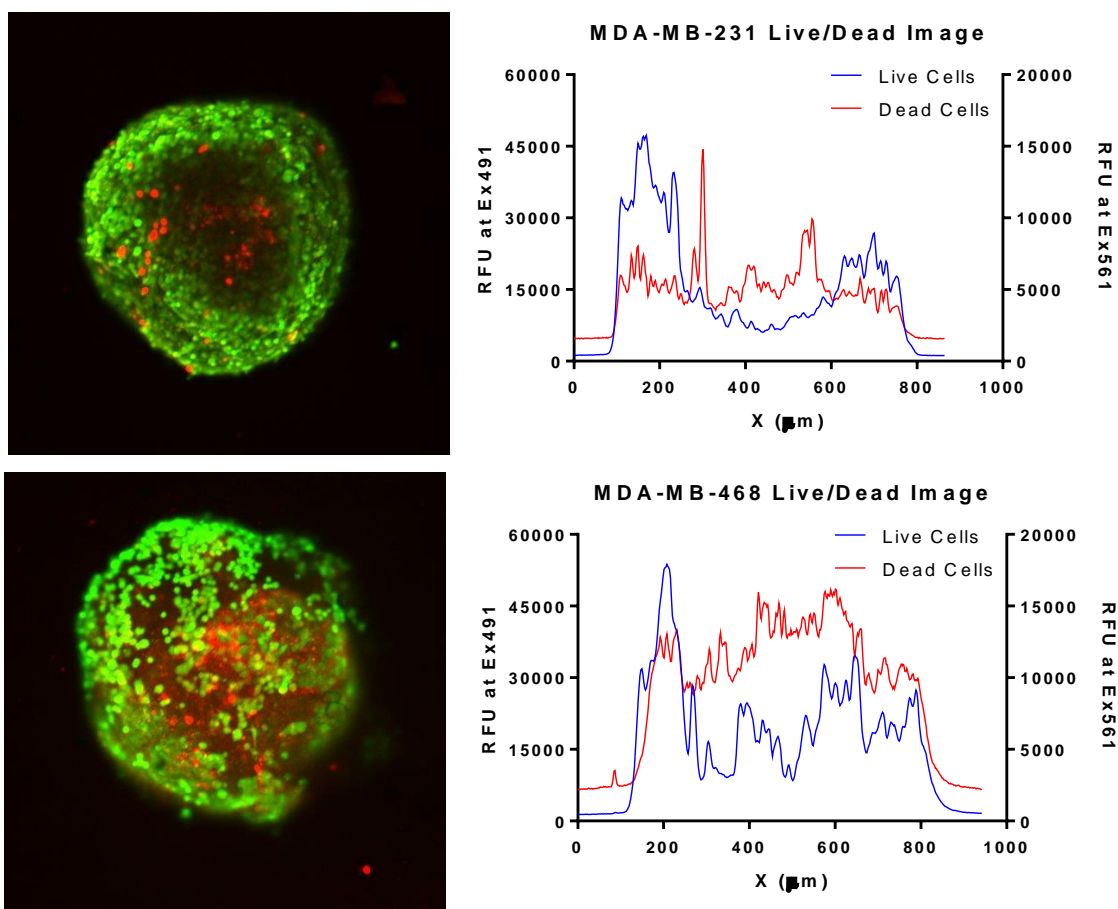
Figure 5.5. Confocal Image of the distribution of live and dead Cells in MDA-MB-231 (upper
left) and MDA-MB-468 (lower left) 3D MCS. Live cells fluoresce green, dead cells fluoresce
red. The fluorescence intensity profiles (right) for both channels show the different distribution
of live and dead cells in the spheroid structure.

5.3.3 pH gradient in 3D MCS. Based on the equation (1) listed in section 5.2.4, the R

value is inversely proportional to the pH value. For an identified sample, R_A, R_B, $F_{A(\lambda 2)}$ and

$F_{B(\lambda2)}$ are constant, which means the pH is a function of a single variable R. The descending

trend was observed from the central area to the peripheral area of the concentric circles (Area 1

to Area 5). At the limiting acidic and basic conditions, R_A, R_B, $F_{A(\lambda2)}$ and $F_{B(\lambda2)}$ were selected

from the area closer to the edge of the same z-stack, which was equilibrated to the calibration pH

by the K+/H+ ionophore nigericin[162]. The intra-MCS pH decreased along the radius from the

edge to the core, which was listed in Table 5.1. Although the calculated pH value was greatly

impacted by the morphology and tightness of 3D MCS, the descending trend of pH inside 3D

MCS was validated. Therefore, 3D MCS is an excellent model to evaluate the efficacy of DOX-

loaded, pH-sensitive fliposomes *in vitro*.
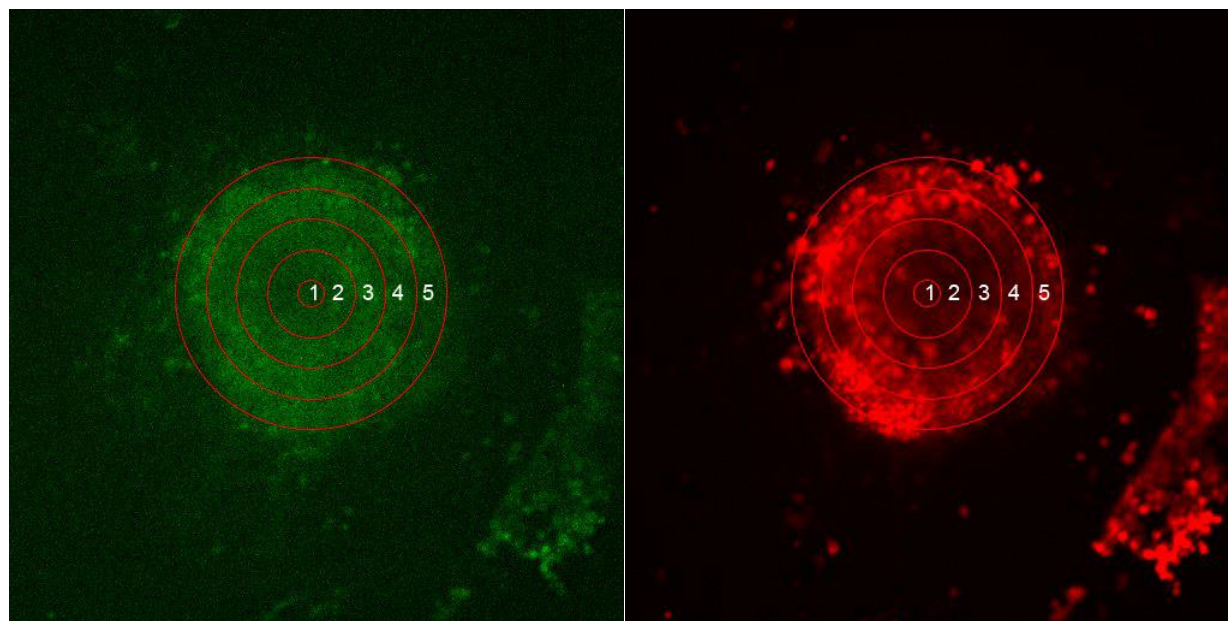
Figure 5.6. Confocal Images of MDA-MB-468 3D MCS with SNARF-1 at two channels (green: intensity at 580 nm channel, red: intensity at 640 nm channel)

Table 5.1. R value and calculated pH inside 3D MCS of MDA-MB-468

Area	1	2	3	4	5
R	0.47	0.45	0.32	0.25	0.27
pH	6.36	6.46	7.28	8.03	7.71

5.3.4 Cytotoxicity assay for DOX-loaded liposomes on 2D monolayer cells and on 3D MCS.
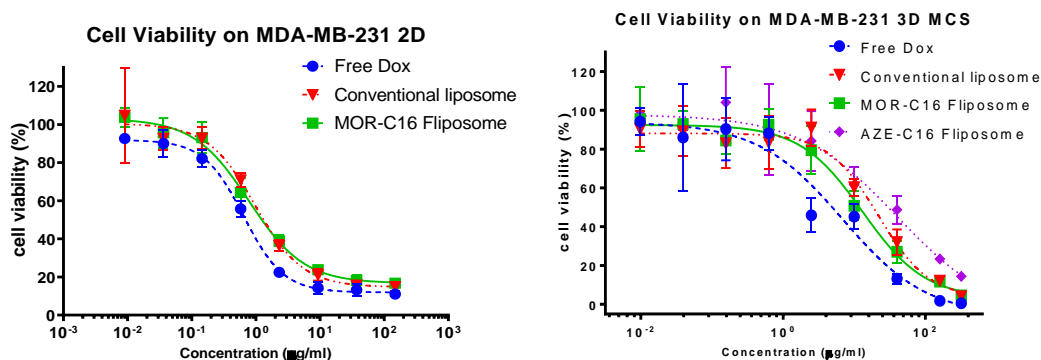
Figure 5.7. Viability of MDA-MB-231 monolayer cells (left) and MDA-MB-231 3D MCS (right) after 72 h drug exposure. Data presented as mean ± SD, N = 4.

Table 5.2. IC50 of Different Dox Formulations on 2D monolayer and 3D MCS of MDA-MB-231 cells after 72 h exposure. Data presented as mean ± SD, N = 4.

IC50 (µg/ml)	Free DOX	DOX-loaded Non pH-sensitive Liposome	MOR-C16 DOX-loaded Fliposome	AZE-C16 DOX-loaded Fliposome
2D	0.646 ± 0.091	0.973 ± 0.387	0.781 ± 0.207	-
3D	6.88 ± 6.06	21.88 ± 10.18	13.07 ± 5.81	39.97 ± 88.09

The fifty percent inhibitory concentration (IC$_{50}$) value of each DOX or DOX-loaded liposome formulation was calculated from data shown in Figure 5.7 using the GraphPad Prism software. Against 2D monolayer of MDA-MB-231 cells, free DOX, DOX-loaded non pH-sensitive liposome and fliposomes had similar IC$_{50}$ values, where no statistically significant difference was found among free DOX, non pH-senstivie liposome and MOR-C16 fliposome groups. There was the same trend of IC$_{50}$ values observed against 3D MCS of MDA-MB-231

cells. IC_{50} value of each treatment group didn't show statistical difference among all treatment groups due to the large standard deviations. Based on IC_{50} value, ranking of anticancer efficacy against 3D MCS was listed as free DOX > MOR-C16 fliposome > stealth liposome > AZE-C16 fliposome, as shown in Table 5.2.
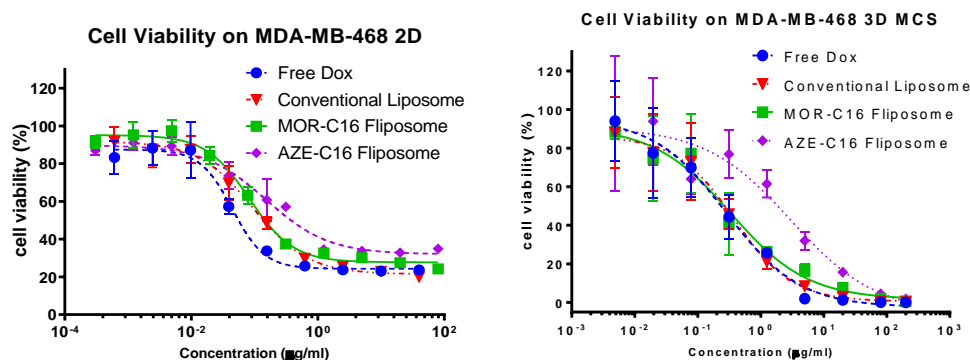
Figure 5.8. Viability of MDA-MB-468 monolayer cells (left) and MDA-MB-468 3D MCS (right) after 72 h drug exposure. Data presented as mean ± SD, N = 4.

Table 5.3. IC50 of Different Dox Formulations on 2D monolayer and 3D MCS of MDA-MB-468 cells after 72 h exposure. Data presented as mean ± SD, N = 4.

IC50 (µg/ml)	Free DOX	DOX-loaded Non pH-sensitive Liposome	MOR-C16 DOX-loaded Fliposome	AZE-C16 DOX-loaded Fliposome
2D	0.045 ± 0.012	0.095 ± 0.031	0.083 ± 0.017	0.153 ± 0.056
3D	0.285 ± 0.202	0.375 ± 0.215	0.333 ± 0.303	3.01 ± 3.44

The anticancer activities against MDA-MB-468 cells gave a completely different profile. IC_{50} value of free DOX was lower than any other treatment groups on 2D model. MOR-C16 Fliposome shared similar anticancer efficacy with conventional liposome, but only free DOX and MOR-C16 Fliposome were significantly better than AZE-C16 Fliposome ($p<0.05$). To compare IC_{50} values of different formulations of DOX against 3D MCS of MDA-MB-468 cells,

there was no statistically significant difference among the groups of free DOX, conventional liposome, MOR-C16 fliposome and AZE-C16 fliposome.

Comparing to evaluation anticancer efficacy by change of size and morphology [163-165], evaluation by IC_{50} against 3D MCS is more convenient and accurate. Generally, IC_{50} value of any treatment group against 3D MCS was much greater than the IC_{50} value against 2D monolayer cells. This could be explained by the fact that penetration resistance was much higher in the 3D MCS model, which reflected a much more realistic environment of tumor. However, different TNBC cell lines exhibited different degree of the increase of the IC_{50}. This phenomenon could be explained by the different tightness of the MCS of different cell lines, which affect the drug penetration and thus the drug activity. All of the results suggest that, after long time exposure, the cytotoxicity was enhanced in 3D MCS but not in monolayer cancer cells. This could be attributed to the enhanced release of DOX from the fliposomes, especially the MOR-C16 fliposome, in the acidic environment inside 3D MCS.

5.3.5 Drug distribution inside 3D MCS. The selected formulation demonstrated different levels of anticancer activity on the TNBC *in* vitro model between 2D monolayer cell and 3D MCS. The difference is caused by many factors, of which one potential factor is the drug penetration resistant in 3D MCS model. Full exposure of drug to 2D model enables the quick equilibrium and complete cytotoxic effect, which is not seem in the 3D MCS as well as solid tumor. The fluorescent signal of doxorubicin distributed inside 3D MCS gave us insight on how the penetration resistance affected efficacy.
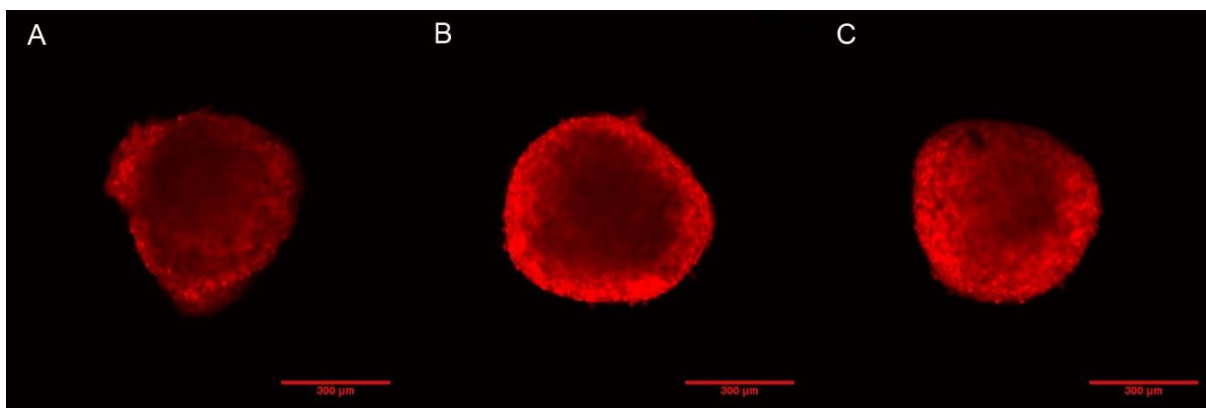
Figure 5.9. Confocal Images of MDA-MB-231 3D MCS (cross section at 120 µm deep) Treated with Free Dox (A), Dox-loaded Non pH-sensitive liposome (B) and Dox-loaded MOR-C16 Fliposome (C) for 4 h

After a 4 h incubation with different treatment groups of equivalent amount of DOX, confocal microscopy images of cross sections of MDA-MB-231 3D MCS at about 120 µm from the bottom were taken and the fluorescent signal of DOX was analyzed (Figure 5.9). Stronger fluorescent signals of MCS that were treated with liposomal DOX were observed in comparison to those treated with Free DOX. An intense ring of DOX accumulated was observed in the outer proliferative cells of each 3D MCS, indicating limited penetration of all formulations into MCS after 4 h incubation.
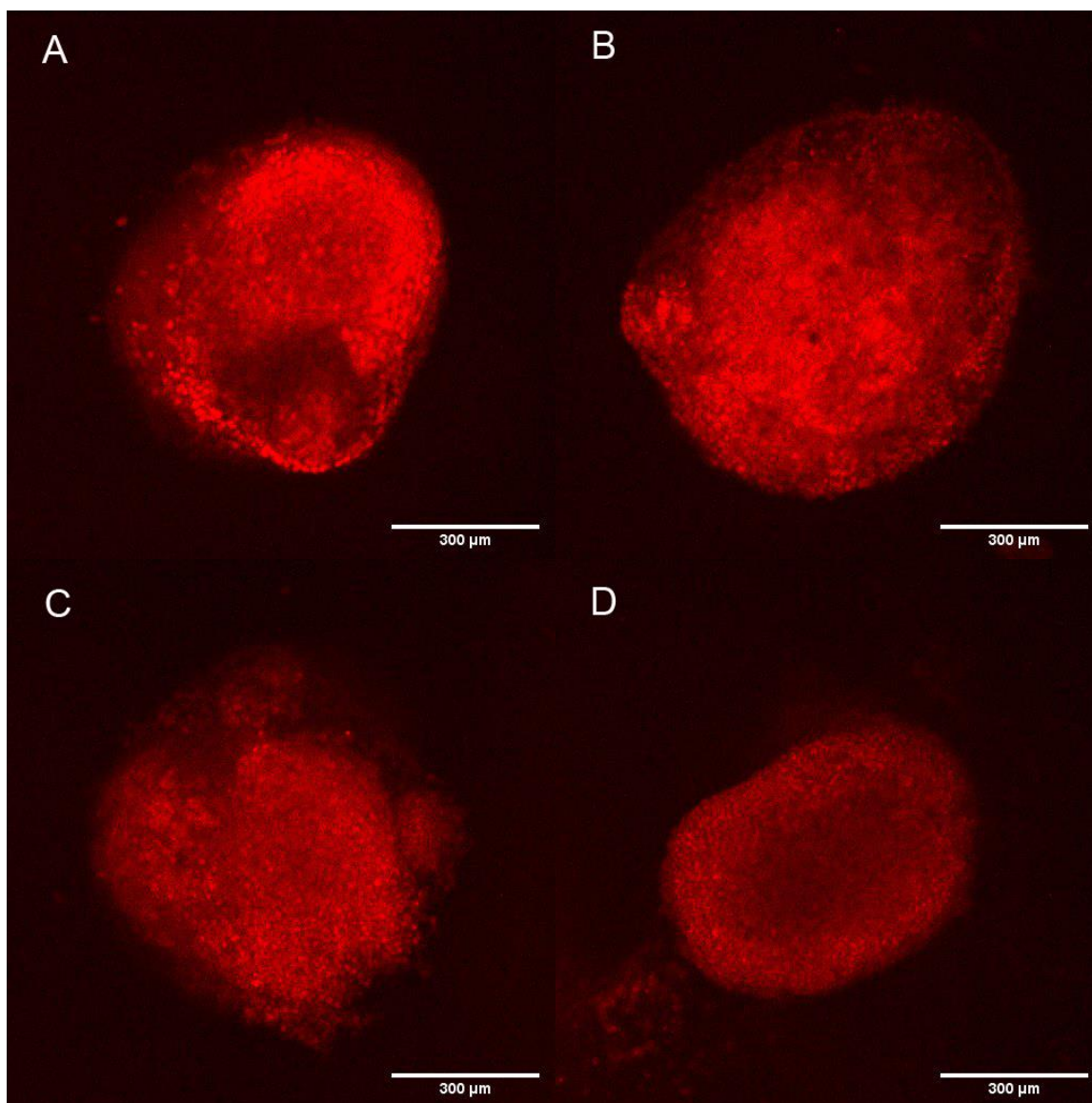
Figure 5.10. Confocal Images of MDA-MB-468 3D MCS (cross section at 120 µm deepth) treated with Free DOX (A), DOX-loaded conventional liposome (B), DOX-loaded MOR-C16 Fliposome (C) and DOX-loaded AZE-C16 Fliposome (D) for 4 h

No qualitive difference of fluorescent intensity was observed among groups of MDA-MB-468 3D MCS after treatment by free or liposomal DOX for 4 h except for AZE-C16 Fliposome (Figure 5.10). This result suggests that both free DOX and DOX-loaded liposomes could penetrate into MDA-MB-468 3D MCS with similar efficiency given 4 h of exposure time.

When the penetration of DOX into 3D MCS of two TNBC cell lines was compared with the penetration of liposomal DOX (4 hour of exposure time), the liposomal DOX groups showed more penetration than the free DOX in 3D MCS of MDA-MB-231 cell lines, but no qualitive difference of penetration into 3D MCS of MDA-MB-468 was observed between liposomal DOX and free DOX. This phenomenon indicated the association between the cell line that formed the 3D MCS and the DOX penetration into the 3D MCS, which was consistent with the report by Namhuk, et al. [163]. Cellular accumulation and uptake of a weakly-basic drug, such as doxorubicin has been reported to decrease along with lower extracellular pH [166-168]. At low pH in the MCS interstitium, such as area 2 in Figure 5.6, the ionized DOX has low lipid solubility and high electrical resistance, thus a greatly reduced membrane penetration. If one cell line could form tight spheroid, such as MDA-MB-231, the diffusion of free DOX would be limited by such resistance. However, if the cell line could only form loose aggregate, such as MDA-MB-468, the penetration wouldn't be the limiting step for the cytotoxic effect of the anticancer agent. Therefore, the enhanced cytotoxicity of the DOX-loaded fliposomes in comparison to conventional liposome, both of which has similar size and surface charge, could be attributed to the enhanced release of the fliposomes in response to the reduced pH inside the 3D MCS, rather than differences in liposomal drug distribution.

The confocal scanning of 3D MCS was performed with z-stack sectioning of 10 µm per step from the bottom to top. The 100 µm depth was chosen due to the limit of the confocal laser scanning technique [169]. The degree of light penetration is greatly affected and reduced by the scattering in the sample and the defocusing of the illumination beam when the light travels over 100 µm through sample [170, 171]. Therefore, the fluorescent signal at 100 µm depth from bottom was acceptable for comparison across different MCS without impact of light penetration

issues. Multiphoton microscopy can be utilized in the future studies since the excitation photon would be split into multi photons which carry the same energy as a sum but have much longer wavelength for deeper penetratioin [172]. Still this technique can only enhance the penetration of the excitation photons, but not the emission photons. Cryosection is another alternative way to address the light penetration issue by cutting the spheroids into sections of $10 - 20\,\mu m$ in thickness. High resolution images of each section can then be easily obtained using confocal microscopy [173]. The drug distribution in the cryosections could also be directly measured by MALDI Imaging Mass Spectrometry [174].

5.4 Summary

3D MCS of TNBC was successfully established for *in vitro* efficacy evaluation. Cell viability and pH gradient inside 3D MCS were validated to confirm that MCS possess the essential microenvironment as an appropriate model to evaluate pH-sensitive liposomes. Free DOX, DOX-loaded conventional liposome and DOX-loaded Fliposome were evaluated in 3D MCS model. DOX-loaded Fliposome, especially the MOR-C16 fliposome (DPPC : Mor-C16 : PEG-Ceramide = 70 : 25 : 5), showed improved efficacy than the conventional liposome (DPPC : Chol : PEG-Ceramide = 70 : 25 : 5) based on IC_{50} value.

Chapter 6: Evaluation of Anticancer Efficacy of Doxorubicin-loaded Fliposome in Mice

6.1 Introduction

Animal models are still the most important evaluation tools to bridge the gap between the discovery of drug candidates *in vitro* and their clinical development. Although many innovative techniques and mechanistic studies have emerged to allow better prediction of a drug candidate's efficacy and safety from its data *in vitro*, animal models, especially mice models in oncology are still essential in evaluating a drug candidate before any further trial in human [175]. The animal models in oncology are typically utilized to simulate a cancer's invasion, metastasis and therapeutic response to the new drug candidate. Therefore, robust and relevant animal models are paramount to test our hypothesis after tremendous work in formulation and *in vitro* evaluation.

Human tumor xenograft models in nude mice stand out from various animal models because of the low cost, ease to handle and numerous support information [176]. Since the first mouse leukemia models grown as ascites back to 1960, tremendous effort has been devoted to build various tumor models in mice by millions of scientists [177]. For breast cancer, the xenograft models was successfully established in 1969 [178] and the orthotopic metastatic breast cancer was established by transplanting a patient-derived xenograft fragment into the nude mouse fat pad in 1993 [179]. Generally, there are different types of *in vivo* mouse model of breast cancer, including cell-derived xenografts (CDX), patient-derived xenografts (PDX) and genetically engineered mouse models (GEMM) [175]. It is widely accepted that the xenograft models are inferior to the GEMM due to immunodeficiency, but CDX is widely accepted for evaluating the response of human tumor to the therapy because PDX is severely limited by the resource [180]. Among the CDX of breast cancer, the ectopic CDX model which implants

human tumor cells subcutaneously into the immunocompromised mouse is most commonly used because it is fast, cheap and technically simple but still involves human breast cancer cells. However, this subcutaneous model does not appropriately reflect the reality of breast cancer. In particular, the perfusion of blood in such subcutaneous tumor is more than the tumor *in situ*, which exaggerates the EPR effect. In contrast, an orthotopic CDX model of breast cancer implants human breast cancer cells in the murine mammary gland/fat pad, which would provide the xenograft a microenvironment similar to that of breast cancer while the xenograft tumor size is still measurable with calipers. In addition, sex hormone levels play a critical role in the tumorigenesis of TNBC, which makes the orthtopic TNBC xenograft mice model an excellent system to evaluate the efficacy of fliposome. Nevertheless, it must be noted that the immunodeficient mouse model of orthotopic implantation doesn't perfectly reproduce the tumorigenesis in human because the host immune cells at the tumor site would also play important roles in the genesis, progression and metastasis of a TNBC tumor [181].

Generally regression of tumor and longer survival is utilized in clinical studies to indicate the efficacy of the therapy. Some studies failed to achieve observable tumor regression because the administration of sub therapeutic doses, in which less cytotoxicity can prolong the duration of study. Overall tumor volumes were calculated and compared to non-treatment or reference treatment to assess efficacy. The timing of dosing the drug candidate is a key parameter that affects the outcome of such an experiment. A "tumor growth delay study" is more reliable for assessing the potential of a treatment because the first dose is initiated after the appearance of the solid tumor rather than before the appearance of a small solid tumor, which is known as "tumor growth inhibition study".

Preparation of doxorubicin in a liposomal formulation can change the pharmacokinetics and pharmacodynamics of the drug to achieve lower toxicity and higher efficacy of the therapy [38]. Hence, information on the pharmacokinetics of fliposome will help us better understand the correlation between its *in vitro* feature and *in vivo* efficacy and safety. The aim of this Chapter's studies is to determine the efficacy of the DOX-loaded pH-sensitive fliposome as compared to conventional liposomes against TNBC on the orthotopic xenograft mouse model.

6.2 Materials and Methods

6.2.1 Materials.

6.2.1.1 Chemical agents. Isoflurone, ketamine, xylazine, and heparin were purchased from Patterson Veterinary (Saint Paul, MN). High-performance liquid chromatography (HPLC)-grade acetonitrile, and acetic acid were purchased from Fisher Scientific (Fair Lawn, NJ).

6.2.1.2 Animals. For the pilot pharmacokinetic study, jugular vein-cannulated female athymic nude mice (NU- Foxn 1^{nu}) were obtained from Charles River at 8 weeks of age; for anticancer efficacy evaluation, female athymic nude mice (NU- Foxn 1^{nu}) were obtained from Charles River at 5 weeks of age. The *in vivo* study was performed based on the animal protocol (No. 16R0r) which was approved by the Institutional Animal Care and Use Committee (IACUC), University of the Pacific. The mice were housed in a temperature-controlled room with a 12-hour day/night lighting cycle and were housed individually if cannulated. All mice were fed standard murine chow and water *ad libitum*.

6.2.2 Pilot pharmacokinetic study.

6.2.2.1 Pilot pharmacokinetic study design. The DOX-loaded AZE-C16 fliposome listed in the 4.3.5 (5 mg/kg equivalent doxorubicin) was administered via jugular vein cannula to female mice. Blood samples (100 µL) were gently withdrawn from the jugular vein cannula

followed by fluid replacement (equivalent volume) with sterile saline at each time point. The

assignment of mice sampled, and the time point was shown in Table 6.1. The total blood volume

withdrawn (excluding terminal samples) was no greater than 10% of the animal's total blood

volume within first 24 hours. At terminal time point (48 or 72 hour), animals were anesthetized

(isoflurane: 2-3% induction and 1-2% maintenance) and blood sample was taken by cardiac

puncture. All blood samples were mixed with sterilized water at volume ratio 1:2 in order to lyse

all blood cells. The samples were then stored at -20°C until further analysis.

Table 6.1. Sequential assignment of sampling in pilot pharmacokinetic study (six mice coded by letter A through F)

Time(hr)	1	2	8	24	48	72
Mice to be sampled	A	A	D	E	A	B
	D	B	B	F	C	D
	E	F	C	C	E	F

6.2.2.2 Sample preparation. DOX (1000 µg/mL) and Daunorubicin (1000 µg/mL) were

prepared in methanol and stored at -20 °C. The solutions of DOX were further diluted with

methanol to give a series of standard solutions at 0, 1, 2, 20, 100, 200, 1000 µg/ml DOX

concentrations. Then 2.5 µl standard solutions were added into 47.5 µl lyzed blood to obtain the

standard whole blood working solutions with at 0, 0.1, 1, 5, 10, 50 µg/ml DOX concentrations.

Whole blood working solutions for quality control (QC) were prepared separately at 0.1, 5 and

50 µg/ml DOX for low QC, moderate QC and high QC, respectively. For standards and quality

controls, 2.5 µl of Daunorubicin (100 µg/ml) was added into 150 µl of water-lysed standard

whole blood working solution or QC solution. For each unknown lysed whole blood sample, 2.5

µl of Daunorubicin (100 µg/ml) was added to 150 µl lysed blood water mixture sample. 850 µl

of acetonitrile with 1% formic acid was added to all samples and standards to precipitate plasma

proteins. The DOX was de-chelated from Copper by sonication at 55°C for 25 minutes followed by centrifugation at 10000 rpm for 20 minutes at 4°C. 10 µl of the supernatant was aliquoted for analysis.

   6.2.2.3 LC/MS/MS assay. The LC/MS/MS system included an Agilent 1100 series HPLC consisting of an online degasser, a binary pump, and an auto-sampler (Agilent Technologies, Santa Clara, CA) and an MDS Sciex API 3000 triple – quadruple tandem mass spectrometer equipped with a turbo ion spray (Applied Biosystems, Foster City, CA). 10 µl of sample was injected into a PLRP-S C18 column (150 × 2.1 mm i.d., 3-µm particle size; Varian Palo Alto, CA) with a ZORBAX RELIANCE C18 Guard column (12.5 × 4.6 mm i.d., 5-µm particle size; Agilent, Santa Clara, CA). Mobile phase A was 0.1% formic acid in double-distilled water. Mobile phase B was 0.1% formic in acetonitrile. A gradient elution with a flow rate of 250 µl/min was used to separate the compounds (Table 6.2). The total running time is 15 minutes. The mass spectrometer was operated in positive ionization mode with multiple reaction monitoring. Table 6.3 shows the detail of the mass spectrometer parameters of Doxorubicin and Daunorubicin.

Table 6.2. Gradient elution program

Time (min)	0	4	4.03	5.3	6	15
A%	80	50	5	5	80	20
B%	20	50	95	95	80	20

Table 6.3. Mass spectrometer parameters for MRM of Doxorubicin

Parameter (units)	Doxorubicin	Daunorubicin
Q1/Q3	544.2/397.2	528.3/363.2
Declustering potentials (volts	11	16
Focusing Potential (volts)	70	120
Collision Enegery (volts)	15	33
Collision Cell exit potentials (volts)	22	30

6.2.2.4 Data analysis. Data are presented as mean ± standard deviation (SD) for the

pharmacokinetic study. Non-compartmental analysis of the whole blood concentration time

profiles was conducted in Phoenix WinNonLin to obtain AUC*inf*, Lambda_z and total clearance

(CL). Subsequently, the elimination half-life was calculated with the formula: $t_{1/2} =$

ln2/Lambda_z.

6.2.3 Anticancer efficacy evaluation on a TNBC orthotopic model.

6.2.3.1 Establishment of TNBC orthotopic xenograft model. The MDA-MB-468 cells

were cultured and maintained in the Advance DMEM/F12 medium as described previously. On

the day of the experiment, the cells were trypsinized and re-suspended in medium followed by

centrifugation at 200 g for 5 minutes. After aspiration of the supernatant, the cell pellet was

washed twice with PBS. A cell counting by a Scepter™ 2.0 Handheld Automated Cell Counter

(MilliporeSigma, Burlington, MA) was performed with the re-suspended cells in sterile PBS.

Lastly the cells were re-suspended in the cold HBSS/Matrigel® Matrix (vol : vol = 1:1) mixture

containing 0.04% Dnase, of which the cell density is approximately 8×10^8 cells/ml. The cells

suspension was maintained on ice until injection.

For the ease of performing the orthotopic injection of tumor cells, the mice were

anaesthesized (isoflurane: 2-3% induction and 1-2% maintenance). The MDA-MB-468 cells

(8,000,000 cells/ mouse) were injected into the mammalian fat pad using a 27 gauge needle on the second nipple around the left axillary region of mice. Following inoculation, the mice were observed daily for their general health and appearance of tumors.

6.2.3.2 Study design. The tumors were allowed to grow up to 70 - 100 mm^3 for 2 weeks after inoculation. The tumor bearing mice were randomly divided into five groups (control, doxorubicin solution, conventional liposome, MOR-C16 fliposome and AZE-C16 fliposome) with eight mice per group except for the control group (N=5). Stratified randomization was based on size of tumor. Afterwards, 5 mg/kg free doxorubicin, conventional liposome (5 mg/kg equivalent doxorubicin) and fliposomes (5 mg/kg equivalent doxorubicin) were diluted in sterilized PBS and administered to the mice once a week for 4 weeks, while PBS (100 μL) was administered as a control to evaluate the effect of no treatment. The animals were anesthetized with isoflurane and the formulations were injected through tail vein. Body weight was recorded and monitored to evaluate the safety; tumor size (in mm^3) was measured with calipers every other day, and the tumor volume was calculated using the formula:

$$Tumor\ volume\ (mm^3) = \frac{1}{2} \times L \times S^2$$

where L the long axis and S is the short axis of the tumor lump. The tumor and hearts were removed and weighted when the animals were euthanized by anesthetics overdose after 63 days post first dosing.

6.2.3.3 Data analysis. Data are presented as mean ± standard error of mean (SEM) for the anticancer efficacy study due to large deviation of tumor volume based on measurement. The statistical analysis was performed by two-way analysis of variance (ANOVA) for the antitumor efficacy study using GraphPad Prism 6.0 Software (GraphPad Software, La Jolla, CA). Tukey's post hoc test analysis was performed to compare between the treatment groups. The

correlation analysis was performed for comparing the tumor volume measurement and the tumor weight. The results with $p < 0.05$ were accepted as statistically significant.

6.3 Results and Discussion

6.3.1 Doxorubicin LC-MS/MS assay. The retention time for Doxorubicin and Daunorubicin was 6.65 and 7.18 minutes respectively. The standard curve in blood is from 0.1 to 50 µg/ml Doxorubicin (Figure 6.1) based on weighted regression (1/y) analysis ($r^2 > 0.99$) of the peak area ratio (Doxorubicin/Daunorubicin) versus Doxorubicin concentration. LOD and LOQ is 0.01 and 0.1 µg/ml, respectively.
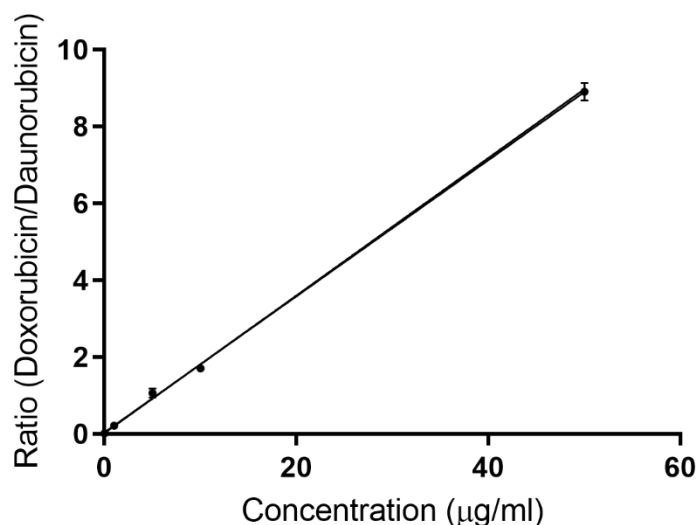
Figure 6.1. Standard curve (0.1 to 50 µg/ml) of AZE-C16 fliposome Doxorubicin in blood (n=3, $r^2 = 0.9970$)

6.3.2 Pilot pharmacokinetic analysis. Figure 6.2 shows the average Doxorubicin concentration in blood of 6 mice (n =3/ timepoint) versus time after 5 mg/kg IV administration. Due to the low sensitivity of analysis assay, the concentration of the last three time points fell below the LOQ but above LOD, therefore the point of 24 hour was presented as the LOQ and 48 and 72 hours were not used for analysis. The concentration of DOX in blood dropped quickly to

lower than 0.3 µg/ml (the IC_{50} value on 3D MCS) within 12 hours. The pharmacokinetic curve

showed the feature of two-compartmental model, which was not consistent with the reported

three-compartmental model in the literature [182]. The values of area under the plasma

concentration-time curve (AUC) and total clearance were in between of the values of pegylated

liposome and free doxorubicin reported in the literature [183]. Elimination half-life calculated

from the 8- and 24-h values was approximately 6.5 h, which was close to the value of free dox

[184]. Comparing to the data listed in the literature [182-184], the pharmacokinetic profile of

AZE-C16 fliposome was more similar with free doxorubicin other than pegylated liposomal

doxorubicin, suggesting doxorubicin may leak prematurely from AZE-C16 fliposome during

circulation before accumulation at the tumor site.
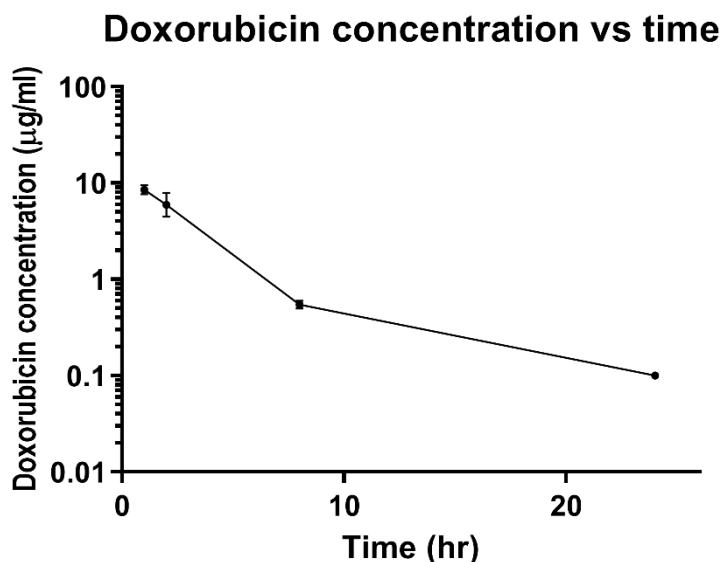
Figure 6.2. Doxorubicin blood concentrations following intravenous administration of DOX-loaded AZE-C16 fliposome (5 mg/kg equivalent doxorubicin) to female nude mice. Data presented as mean ± SD, N = 3.

6.3.3 Anticancer efficacy of pH-sensitive liposomes on TNBC orthotopic model. The anticancer activity of fliposome was investigated using the above-mentioned orthotopic MDA-MB-468 xenografts nude mouse model. The treatment was started at a mean tumor size of 75 mm^3, and no tumor regression was observed. Figure 6.3 shows the effect of different formulations on tumor volumes measured every other day for nine weeks. The statistical analysis was performed using two-way ANOVA with data up to 61 days post first dose, after which the deviation within each group was getting larger. Turkey post test comparisons between treatment groups showed that tumor volume of MOR-C16 treatment group was significantly ($p < 0.05$) smaller than the one of free DOX treatment group from day 57 to 61, and significantly ($p < 0.05$) smaller than the one of conventional liposome group at day 61. There was a clear trend that the tumor progression of fliposome (MOR-C16 and AZE-C16) treatment groups was delayed compared to free DOX and conventional treatment group, which suggested the pH-sensitive liposome did improve the anticancer activity against TNBC in an orthotopic xenograft model. In addition, the tumor weight was correlated with the tumor volume at the end of the experiment, confirming that the tumor volume measurement accurately reflected the tumor progression with $R = 0.7833$ and $p < 0.001$ (Figure 6.4).
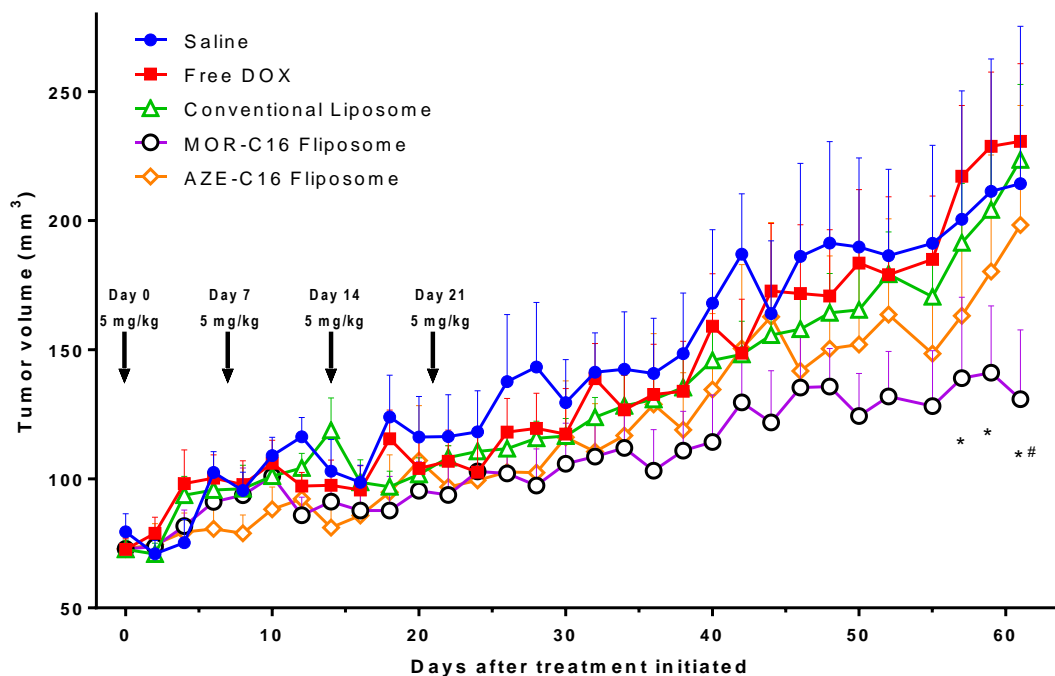
Figure 6.3. Anticancer efficacy of DOX formulations in mouse orthotopic xenografts bearing MDA-MB-468 breast cancer. MDA-MB-468 cells were inoculated into the mammalian fat pad in the axillary of femal athymic nude mice. The animals received ~100 µL of normal saline as control or 5 mg/kg of DOX in PBS or 5 mg/kg of equivalent DOX-loaded liposome on 0, 7, 14, 21 days (indicated by arrows). The data represent mean ± SEM of results calculated from 5 or 8 animals. * Significant difference (p<0.05 for two-way ANOVA) observed between MOR-C16 and Free DOX group, # Significant difference (p<0.05 for two-way ANOVA) observed between MOR-C16 and conventional liposome group.
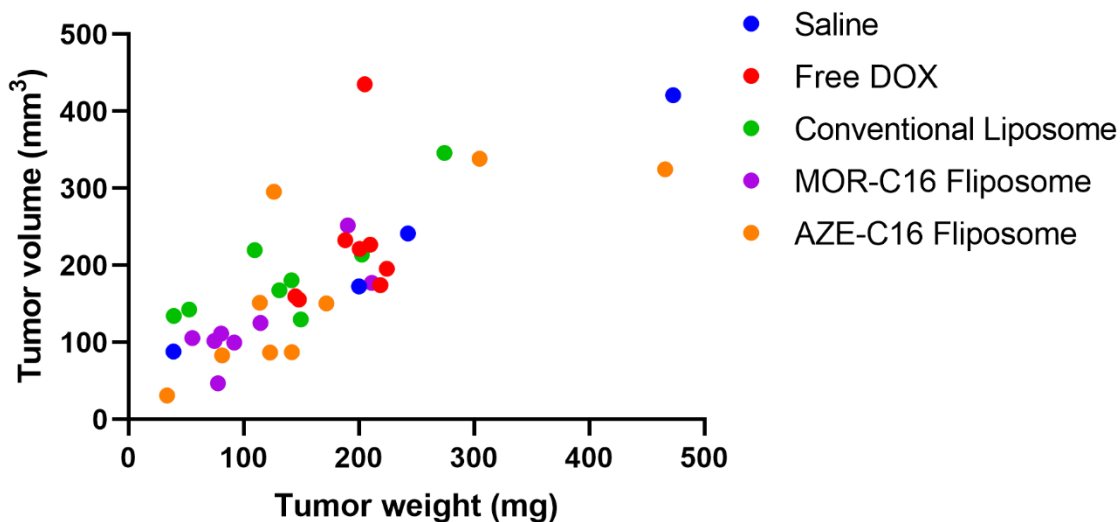
Figure 6.4. Correlation analysis of tumor weight and tumor volume at the end of experiment on Day 63 after the first IV injection (n = 37 total).

Although there was statistically significant difference shown in limited days between the fliposome groups and the other groups, a benefit of pH-triggered release as a passive targeting strategy was still observed. There are several areas that could be improved for future investigations. First, the orthotopic breast cancer model could be improved by injecting TNBC cell at exponential phase under more robust conditions, which will facilitate tumor progression so that the tumor volume will have more apparent difference between different groups, which would provide better chance to observe statistically significant differences. 3D MCS of breast cancer cells could also be inoculated into the mammalian fat pad instead of the suspended cancer cells to form a more uniform size of tumor, which will reduce the deviation within each group. Secondary, another TNBC cell line could be chosen for further animal studies. According to our cell culture studies, the liposomal doxorubicin will be more advantageous in the anticancer activities when the cell line could form tighter spheroids rather than loose aggregates in culture. The fold of increase of the IC_{50} value from 2D monolayer to 3D MCS would be a good indicator

to construct animal models that bears tighter solid tumors. Thirdly, the therapeutic benefits of pH-triggered release against solid tumors rely first on the intratumoral accumulation of the formulation by the EPR effect. Therefore, sufficient duration of circulation in blood, which is a key indicator of liposome stability *in vivo* is a major concern for the design of triggerable liposomes. It was reported that 24 hour circulation is required for the manifestation of the EPR effect[138], and the total amount of DOX eventually displaying a therapeutic effect at tumor site would determine the utmost contribution by triggered release. According to the pilot pharmacokinetic study, the AZE-C16 fliposome, which has better and quicker response upon lower pH , was less stable in the blood circulation than the reported conventional liposomes [184]. The less efficacy obtained of AZE-C16 fliosome compared to MOR-C16 could be explained by unexpected premature leakage during the blood circulation, leading to the quick dropping of drug concentration in blood within 8 hours and the insufficient intratumoral accumulation through the EPR effect. As an improvement, the optimization of formulation should highlight stability as a priority, especially stability at 24 hours to provide a fundament for sufficient circulation of the delivery system under study.

6.3.4 Cardiotoxicity evaluation. During the whole experiment, no mice showed drastic decrease of the body weight. It is also reported that heart weight to body weight ratio would decrease when doxorubicin accumulated excessively into the heart [185, 186]. In this study, the heart weight to body weight ratio among all treatment groups had no significant difference compared to the non-treatment group (Figure 6.5). All the animals possessed steady body weight. It was reported that the median cumulative cardiotoxic dose of doxorubicin was 36.4 mg/kg found in the mouse [187], which was much higher than our experiment design. In order to get better tumor regression efficacy, higher dosage of liposomal doxorubicin could be used in

future research. Lastly, the administration of free DOX induces the accumulation of reactive

oxygen species in heart. Therefore, cardiotoxicity would be another safety issue that warrants

further investigation in the future.
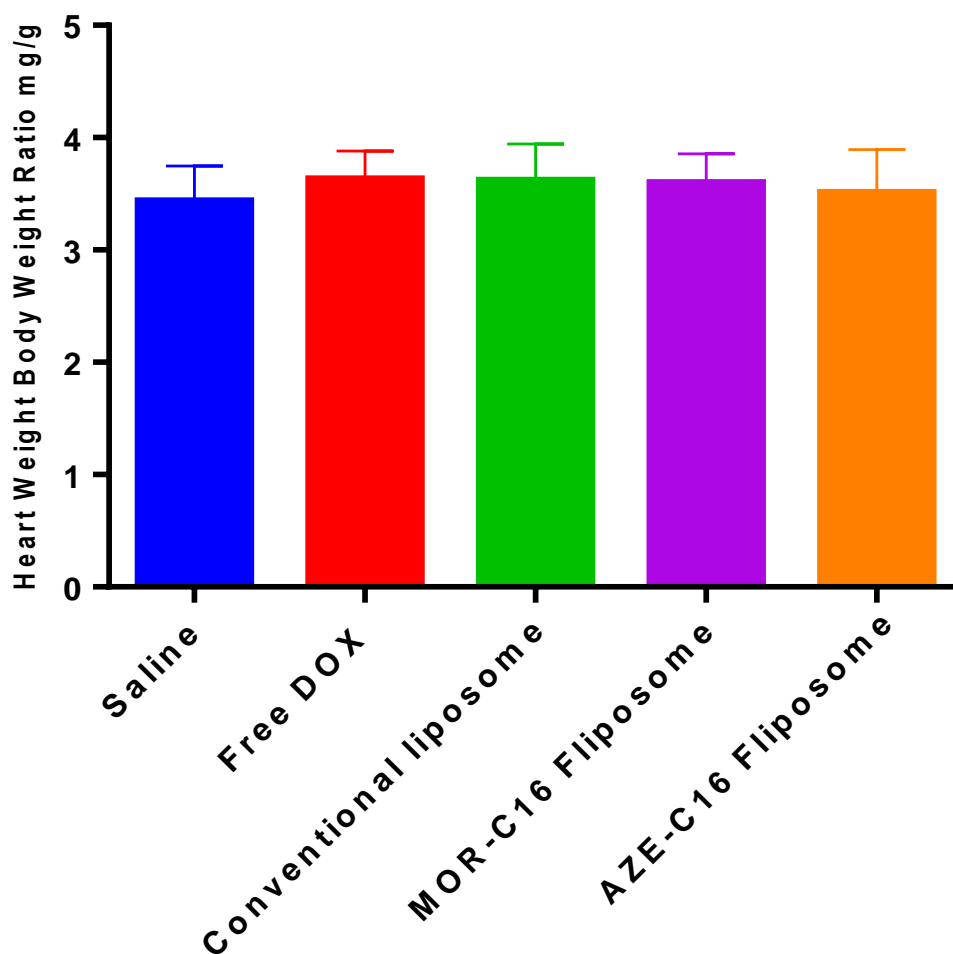
Figure 6.5. Effect of doxorubicin and liposomal DOX on the heart weight to body weight ratio as an indicator of doxorubicin-induced cardiotoxicity in nude mice on Day 63 after the first IV injection. The data represent mean ± SD of results calculated from 8 animals (Saline group N=5). One-way ANOVA followed by Tukey's multiple comparison test suggested no significant differences between different treatment groups.

6.4 Summary

An orthotopic TNBC xenograft mice model was successfully established for *in vivo* efficacy evaluation. Anticancer activity of free DOX, DOX-loaded conventional liposome and DOX-loaded Fliposome was evaluated in the orthotopic xenograft model by monitoring the tumor progression for 61 days. DOX-loaded Fliposome, especially the MOR-C16 fliposome (DPPC : Mor-C16 : PEG-Ceramide = 70 : 25 : 5), showed improved efficacy than the conventional liposome (DPPC : Chol : PEG-Ceramide = 55 : 40 : 5) which was suggested by the delay of the tumor progression. The AZE-C16 fliposome was less effective than the MOR-C16 fliposome probably due to its lower stability, which was observed in its *in vitro* release profile and in the pilot pharmacokinetic study. The quick response of AZE flipids to lower pH, also suggested by the estimated pKa value of 6.8, compromised the stability of liposome. Further investigation is needed to balance the pH-sensitivity and stability *in vivo.*

Chapter 7: Summary and Future Work

Breast cancer is a major health care concern and the second leading cause of death affecting American women. Triple negative breast cancer is characterized by lack of expression of the estrogen receptor (ER), the progesterone receptor (PR) and the human epidermal growth factor receptor (HER2 /neu). It is the leading fatal subtype of breast cancer with the poorest prognosis. Chemotherapy, individually or in combination with surgery or radiotherapy is predominantly given to TNBC patients since TNBC is not responsive to targeted therapies. Doxorubicin is one of the most effective drugs used in the treatment of TNBC, but it has serious adverse effects, especially cardiotoxicity associated with the accumulation use of free drug. Liposomes are one of the widely used drug delivery systems to facilitate physical targeting, in which preferred accumulation is achieved by the EPR effect for the treatment of solid tumors. Stimuli-response, such as a reverse pH gradient at tumor site, can ramp up the release rate of anticancer agent, consequently makes more free drug available to exert its biological effect. A combination of a physical targeting approach with a pH triggered release strategy can have a significant impact on overall effectiveness of the therapy against TNBC. The objective of this dissertation work was to develop and evaluate doxorubicin loaded pH-sensitive liposomes for drug delivery against TNBC.

pH-sensitive fliposomes with conformational switch lipids were successfully prepared by thin film hydration. In order to have a standardized procedure, ethanol injection followed by tangential flow filtration was developed to prepare fliposomes. The metal ion remote loading method was developed to circumvent the increasing proton concentration caused by the traditional ammonium gradient remote loading methods. Fliposomes carried high encapsulation

efficiency (>80%), small mean particle size (<200 nm) and small PDI (<0.3), indicating the robustness of the preparation procedure.

It is critical to have a reliable method to evaluate pH-sensitivity of fliposomes *in vitro* since the release of our delivery system is triggered by the reverse pH gradient at the tumor site. Several release assays for DOX-loaded liposomes, including traditional dialysis methods, fluorescent methods and our new resin adsorption methods were evaluated. Adsorption of positive charged doxorubicin onto the cellulose membrane of dialysis tubing made dialysis not reflect the real release profile while various degradation rates of DOX in different pH buffer reversed the intensity of fluorescent measurement. Taking the complexity of the operation procedure into consideration for high throughput evaluation, the direct resin adsorption method appears to be the most practical and feasible method to kinetically monitor the release profile of pH-sensitive liposomes *in vitro*. The pH-sensitivity of fliposomes evaluated by direct resin adsorption method was validated with calcein loaded fliposomes, in which calcein is a commonly used water-soluble fluorescent probe for investigating drug release from liposomes. The pH-sensitive release of doxorubicin from fliposomes was similar with the release of calcein in fliposomes.

In order to maximize the benefit of liposomes for anticancer therapy, the properties of fliposomes need to be optimized to achieve effective physical targeting and pH-sensitive release. In addition to triggered release, which is a focus for this dissertation, stability, small and homogeneous size, and adequate drug-loading capacity are all important properties of liposomes for anticancer therapy. All those physical properties except for size are related to components of liposomes other than the preparation procedure. Therefore, identification of the factors impacting the outcome of physical targeting and the optimization of fliposomes were based on

the lipid composition in this dissertation. The neutral pegylated lipid, PEG-Ceramide was chosen for enhanced pH-sensitivity. Cholesterol and long hydrocarbon tail phospholipid, such as DSPC were necessary for the stability of the liposomes, while the incorporation of cholesterol and DSPC compromised the release in response to the desired pH. With an increasing mole percentage of flipid, the pH-sensitivity of fliposomes was increased, while the homogeneity, and consequently *in* vivo stability was sacrificed, indicated by a drastic increase of size and PDI. In early studies, AZE-C16-based fliposomes showed quick response of release to the desired pH, but less stability. RSM was utilized to further optimize the AZE-C16 based fliposome. AZE: DSPC: Chol: PEG-Ceramide = 38: 32: 25: 5 was predicted by RSM to have relatively high stability and pH-sensitivity.

Before evaluating the efficacy in an *in vivo* model, we evaluated the anticancer efficacy of fliposome *in vitro*. 3D MCS are self-assembled cultures of tumor cells formed in conditions where cell-cell interactions predominate over cell-substrate interactions. 3D MCS include many features of solid tumors that are missing in 2D monolayer cells, especially the reverse pH gradient. Therefore, 3D MCS mimic the native and complex tumor microenvironment, thus can serve as a valid and clinically relevant *in vitro* model to evaluate efficacy of fliposomes. Two 3D TNBC MCS, MDA-MB-231 and MDA-MB-468, were successfully established for *in vitro* efficacy evaluation. Cell viability and the pH gradient inside 3D MCS were validated by laser confocal microscopy to confirm that MCS possess the essential microenvironment. Free DOX, DOX-loaded conventional liposomes and DOX-loaded fliposomes were evaluated in the 3D MCS model for anticancer efficacy. IC_{50} value for all treatment groups against 3D MCS was much greater than the IC_{50} value against 2D monolayer cells, which could be explained by the fact that penetration resistance was much higher in the 3D MCS model. DOX-loaded

Fliposomes, especially the MOR-C16 fliposome (DPPC : Mor-C16 : PEG-Ceramide = 70 : 25 : 5), showed improved efficacy than the conventional liposome based on IC_{50} value.

A pilot pharmacokinetic study of AZE-C16 fliposome was conducted in female athymic nude mice due to concerns of stability with AZE-C16 fliposomes. The results showed that the concentration of DOX in blood dropped quickly lower than 0.3 µg/ml (the IC_{50} value on 3D MCS) within 12 hours. The pharmacokinetic profile of AZE-C16 fliposomes was similar with free doxorubicin, which indicated premature leakage from AZE-C16 fliposomes in circulation. A pharmacokinetic study of MOR-C16 fliposomes is also needed to correlate with the *in vitro* stability and pharmacokinetic study with the eventual efficacy results and compare the outcome of AZE-C16 and MOR-C16 fliposome. Increasing the dose or improvement in the analytical assay could possibly solve the problem of LOQ, which will give better insight into fliposome *in vivo*. The antitumor efficacy of pH-sensitive fliposomes was evaluated in an orthotopic MDA-MB-468 xenograft in a nude mouse model, which was the first time that the DOX-loaded liposomal formulation conducted the treatment on TNBC orthotopic model. DOX-loaded Fliposomes, especially the MOR-C16 fliposomes showed improved efficacy compared to conventional liposomes at day 61 post-first dose, which was suggested by the delay in tumor progression.

As potential work for comprehensive development of fliposome, the further optimization of fliposome by RSM, including MOR-C16 flipsome, is very critical. The stability within 24 hours should be ranked as the highest priority compared to pH-sensitivity based on current research. In addition, the percentage of components should cover wider range for better prediction. If needed, the independent variables could be added to three factors (flipid%, phospholipid% and cholesterol%), by which more interaction could be investigated. On the

other hand, the biodistribution and comprehensive pharmacokinetic studies are necessary to investigate doxorubicin exposure to the TNBC as well as normal tissue. Doxorubicin exposure through the EPR effect can be obtained by comparing the drug concentration in tumor of fliposome and one of pegylated liposome, therefore the contribution from pH-triggered release can be estimated if there is difference suggested in the efficacy with two treatments. Regarding the efficacy evaluation, dose escalation to achieve better tumor regression is another potential study for comprehensive experiment design once the final optimization is done.

There is another perspective need further investigation, which is the correlation between *in vitro* characteristics and *in vivo* outcome. The characterization of fliposomes *in vitro*, such as stability or pH sensitivity, is the most common and convenient method to investigate the property of fliposomes. We also have developed the 3D MCS platform to evaluate the anticancer efficacy of fliposomes. How to link different tools *in vitro* with the outcome of *in vivo* model is critical, for instance, the identification of which characteristic *in vitro* has the most impact on the exposure in 3D MCS, consequently influencing half-life *in vivo*. Once the correlation is established, different strategies aiming at various *in vivo* profile can be achieved by manipulation of parameters of fliposomes, such as size and particular components.

In conclusion, pH-sensitive fliposomes were successfully prepared by thin film hydration and ethanol injection methods with appropriate properties for physical targeting. Direct Resin adsorption method was established to evaluate pH-sensitivity of fliposome *in vitro*. 3D MCS and orthotopic TNBC models were successfully established for efficacy evaluation. Doxorubicin-loaded fliposomes, especially the MOR-C16 fliposome showed improved anticancer efficacy over non pH-sensitive liposome *in vitro* and in an orthotopic TNBC xenografts mouse model.

REFERENCES

1. American Cancer Society. Cancer Facts & Figures 2018. Atlanta: American Cancer Society; 2018.
2. Wolrd Health Organization, Cancer Fact Sheets. 2018; Available from: https://www.who.int/cancer/en/
3. Siegel, R.L., K.D. Miller, and A. Jemal, C*ancer statistics, 2019.* CA Cancer J Clin, 2019. 6**9**(1): p. 7-34.
4. Tate, C.R., et al., T*argeting triple-negative breast cancer cells with the histone deacetylase inhibitor panobinostat.* Breast Cancer Res, 2012. 1**4**(3): p. R79.
5. Chavez, K.J., S.V. Garimella, and S. Lipkowitz, T*riple negative breast cancer cell lines: one tool in the search for better treatment of triple negative breast cancer.* Breast Dis, 2010. 3**2**(1-2): p. 35-48.
6. Yersal, O. and S. Barutca, B*iological subtypes of breast cancer: Prognostic and therapeutic implications.* World J Clin Oncol, 2014. 5(3): p. 412-24.
7. Fallahpour, S., et al., B*reast cancer survival by molecular subtype: a population-based analysis of cancer registry data.* CMAJ Open, 2017. 5(3): p. E734-E739.
8. Brewster, A.M., M. Chavez-MacGregor, and P. Brown, E*pidemiology, biology, and treatment of triple-negative breast cancer in women of African ancestry.* Lancet Oncol, 2014. 1**5**(13): p. e625-34.
9. Abdulkarim, B.S., et al., I*ncreased risk of locoregional recurrence for women with T1-2N0 triple-negative breast cancer treated with modified radical mastectomy without adjuvant radiation therapy compared with breast-conserving therapy.* J Clin Oncol, 2011. 2**9**(21): p. 2852-8.
10. Yao, H., et al., T*riple-negative breast cancer: is there a treatment on the horizon?* Oncotarget, 2017. 8(1): p. 1913-1924.
11. Wahba, H.A. and H.A. El-Hadaad, C*urrent approaches in treatment of triple-negative breast cancer.* Cancer Biol Med, 2015. 1**2**(2): p. 106-16.
12. Dumontet, C. and M.A. Jordan, M*icrotubule-binding agents: a dynamic field of cancer therapeutics.* Nat Rev Drug Discov, 2010. 9(10): p. 790-803.
13. Rohena, C.C. and S.L. Mooberry, R*ecent progress with microtubule stabilizers: new compounds, binding modes and cellular activities.* Nat Prod Rep, 2014. 3**1**(3): p. 335-55.
14. Martin, M., et al., M*olecular predictors of efficacy of adjuvant weekly paclitaxel in early breast cancer.* Breast Cancer Res Treat, 2010. 1**23**(1): p. 149-57.
15. Hastak, K., E. Alli, and J.M. Ford, S*ynergistic chemosensitivity of triple-negative breast cancer cell lines to poly(ADP-Ribose) polymerase inhibition, gemcitabine, and cisplatin.* Cancer Res, 2010. 7**0**(20): p. 7970-80.
16. Zhang, J., et al., C*hemotherapy of metastatic triple negative breast cancer: Experience of using platinum-based chemotherapy.* Oncotarget, 2015. 6(40): p. 43135-43.
17. Carey, L.A., et al., T*he triple negative paradox: primary tumor chemosensitivity of breast cancer subtypes.* Clin Cancer Res, 2007. 1**3**(8): p. 2329-34.
18. Omarini, C., et al., N*eoadjuvant treatments in triple-negative breast cancer patients: where we are now and where we are going.* Cancer Manag Res, 2018. 1**0:** p. 91-103.

19. Wang, C., et al., P*revalence of BRCA1 mutations and responses to neoadjuvant chemotherapy among BRCA1 carriers and non-carriers with triple-negative breast cancer.* Ann Oncol, 2015. 2**6**(3): p. 523-8.

20. Schmid, P., et al., A*tezolizumab and Nab-Paclitaxel in Advanced Triple-Negative Breast Cancer.* N Engl J Med, 2018. 3**79**(22): p. 2108-2121.

21. Arcamone, F., et al., A*driamycin, 14-hydroxydaunomycin, a new antitumor antibiotic from S. peucetius var. caesius.* Biotechnol Bioeng, 1969. 1**1**(6): p. 1101-10.

22. Young, R.C., R.F. Ozols, and C.E. Myers, T*he anthracycline antineoplastic drugs.* N Engl J Med, 1981. 3**05**(3): p. 139-53.

23. Burke, T.G. and T.R. Tritton, S*tructural basis of anthracycline selectivity for unilamellar phosphatidylcholine vesicles: an equilibrium binding study.* Biochemistry, 1985. 2**4**(7): p. 1768-1776.

24. Bellarosa, D., et al., A*poptotic events in a human ovarian cancer cell line exposed to anthracyclines.* J Pharmacol Exp Ther, 2001. 2**96**(2): p. 276-83.

25. Thirumaran, R., G.C. Prendergast, and P.B. Gilman, C*hapter 7 - Cytotoxic Chemotherapy in Clinical Treatment of Cancer,* in C*ancer Immunotherapy,* G.C. Prendergast and E.M. Jaffee, Editors. 2007, Academic Press: Burlington. p. 101-116.

26. Pharmacists, T.A.s.o.H.-S. D*oxorubicin Hydrochloride.* 2018; Available from: https://www.drugs.com/monograph/doxorubicin-hydrochloride.html#moreResources.

27. Tacar, O., P. Sriamornsak, and C.R. Dass, D*oxorubicin: an update on anticancer molecular action, toxicity and novel drug delivery systems.* J Pharm Pharmacol, 2013. 6**5**(2): p. 157-70.

28. Momparler, R.L., et al., E*ffect of adriamycin on DNA, RNA, and protein synthesis in cell-free systems and intact cells.* Cancer Res, 1976. 3**6**(8): p. 2891-5.

29. Thorn, C.F., et al., D*oxorubicin pathways: pharmacodynamics and adverse effects.* Pharmacogenet Genomics, 2011. 2**1**(7): p. 440-6.

30. Ross, W.E., D.L. Glaubiger, and K.W. Kohn, P*rotein-associated DNA breaks in cells treated with adriamycin or ellipticine.* Biochim Biophys Acta, 1978. 5**19**(1): p. 23-30.

31. Bodley, A., et al., D*NA topoisomerase II-mediated interaction of doxorubicin and daunorubicin congeners with DNA.* Cancer Res, 1989. 4**9**(21): p. 5969-78.

32. Wang, S., et al., A*ctivation of nuclear factor-kappaB during doxorubicin-induced apoptosis in endothelial cells and myocytes is pro-apoptotic: the role of hydrogen peroxide.* Biochem J, 2002. 3**67**(Pt 3): p. 729-40.

33. https://www.pharmgkb.org/pathway/PA165292163

34. Cortazar, P., et al., U*S Food and Drug Administration approval overview in metastatic breast cancer.* J Clin Oncol, 2012. 3**0**(14): p. 1705-11.

35. Wang, S., et al., D*oxorubicin induces apoptosis in normal and tumor cells via distinctly different mechanisms. intermediacy of H(2)O(2)- and p53-dependent pathways.* J Biol Chem, 2004. 2**79**(24): p. 25535-43.

36. Ganz, W.I., et al., R*eview of tests for monitoring doxorubicin-induced cardiomyopathy.* Oncology, 1996. 5**3**(6): p. 461-70.

37. Rivankar, S., A*n overview of doxorubicin formulations in cancer therapy.* J Cancer Res Ther, 2014. 1**0**(4): p. 853-8.

38. Barenholz, Y., D*oxil(R)--the first FDA-approved nano-drug: lessons learned.* J Control Release, 2012. 1**60**(2): p. 117-34.

39. Jain, R.K., N*ormalization of tumor vasculature: An emerging concept in antiangiogenic therapy.* Science, 2005. 3**07**(5706): p. 58-62.

40. Wu, M., et al., T*he effect of interstitial pressure on tumor growth: coupling with the blood and lymphatic vascular systems.* J Theor Biol, 2013. 3**20:** p. 131-51.

41. Tredan, O., et al., D*rug resistance and the solid tumor microenvironment.* J Natl Cancer Inst, 2007. 9**9**(19): p. 1441-54.

42. Netti, P.A., et al., R*ole of extracellular matrix assembly in interstitial transport in solid tumors.* Cancer Res, 2000. 6**0**(9): p. 2497-503.

43. Kobayashi, H., R. Watanabe, and P.L. Choyke, I*mproving conventional enhanced permeability and retention (EPR) effects; what is the appropriate target?* Theranostics, 2013. 4(1): p. 81-9.

44. Torchilin, V.P., P*assive and Active Drug Targeting: Drug Delivery to Tumors as an Example,* in D*rug Delivery,* M. Schäfer-Korting, Editor. 2010, Springer Berlin Heidelberg: Berlin, Heidelberg. p. 3-53.

45. Bazak, R., et al., P*assive targeting of nanoparticles to cancer: A comprehensive review of the literature.* Mol Clin Oncol, 2014. 2(6): p. 904-908.

46. Maeda, H., T*oward a full understanding of the EPR effect in primary and metastatic tumors as well as issues related to its heterogeneity.* Adv Drug Deliv Rev, 2015. 9**1:** p. 3-6.

47. Maeda, H., T*umor-selective delivery of macromolecular drugs via the EPR effect: background and future prospects.* Bioconjug Chem, 2010. 2**1**(5): p. 797-802.

48. Perry, J.L., et al., M*ediating Passive Tumor Accumulation through Particle Size, Tumor Type, and Location.* Nano Letters, 2017. 1**7**(5): p. 2879-2886.

49. van Vlerken, L.E., T.K. Vyas, and M.M. Amiji, P*oly(ethylene glycol)-modified nanocarriers for tumor-targeted and intracellular delivery.* Pharm Res, 2007. 2**4**(8): p. 1405-14.

50. Yamaoka, T., Y. Tabata, and Y. Ikada, D*istribution and tissue uptake of poly(ethylene glycol) with different molecular weights after intravenous administration to mice.* J Pharm Sci, 1994. 8**3**(4): p. 601-6.

51. Greish, K., E*nhanced Permeability and Retention (EPR) Effect for Anticancer Nanomedicine Drug Targeting,* in C*ancer Nanotechnology: Methods and Protocols,* S.R. Grobmyer and B.M. Moudgil, Editors. 2010, Humana Press: Totowa, NJ. p. 25-37.

52. Maki, S., T. Konno, and H. Maeda, I*mage enhancement in computerized tomography for sensitive diagnosis of liver cancer and semiquantitation of tumor selective drug targeting with oily contrast medium.* Cancer, 1985. 5**6**(4): p. 751-7.

53. Nagamitsu, A., K. Greish, and H. Maeda, E*levating blood pressure as a strategy to increase tumor-targeted delivery of macromolecular drug SMANCS: cases of advanced solid tumors.* Jpn J Clin Oncol, 2009. 3**9**(11): p. 756-66.

54. Yuan, F., et al., V*ascular permeability and microcirculation of gliomas and mammary carcinomas transplanted in rat and mouse cranial windows.* Cancer Res, 1994. 5**4**(17): p. 4564-8.

55. Thurber, G.M., M.M. Schmidt, and K.D. Wittrup, A*ntibody tumor penetration: transport opposed by systemic and antigen-mediated clearance.* Adv Drug Deliv Rev, 2008. 6**0**(12): p. 1421-34.

56. Deckert, P.M., C*urrent constructs and targets in clinical development for antibody-based cancer therapy.* Curr Drug Targets, 2009. 1**0**(2): p. 158-75.

57. Danhier, F., O. Feron, and V. Preat, T*o exploit the tumor microenvironment: Passive and active tumor targeting of nanocarriers for anti-cancer drug delivery.* J Control Release, 2010. 1**48**(2): p. 135-46.

58. Patra, C.R., et al., T*argeted delivery of gemcitabine to pancreatic adenocarcinoma using cetuximab as a targeting agent.* Cancer Research, 2008. 6**8**(6): p. 1970-1978.

59. Bazak, R., et al., C*ancer active targeting by nanoparticles: a comprehensive review of literature.* J Cancer Res Clin Oncol, 2015. 1**41**(5): p. 769-84.

60. Eloy, J.O., et al., L*iposomes as carriers of hydrophilic small molecule drugs: strategies to enhance encapsulation and delivery.* Colloids Surf B Biointerfaces, 2014. 1**23:** p. 345-63.

61. Samad, A., Y. Sultana, and M. Aqil, L*iposomal drug delivery systems: an update review.* Curr Drug Deliv, 2007. 4(4): p. 297-305.

62. Allen, T.M. and P.R. Cullis, L*iposomal drug delivery systems: from concept to clinical applications.* Adv Drug Deliv Rev, 2013. 6**5**(1): p. 36-48.

63. Torchilin, V.P., R*ecent advances with liposomes as pharmaceutical carriers.* Nature Reviews Drug Discovery, 2005. 4(2): p. 145-160.

64. ElBayoumi, T.A. and V.P. Torchilin, C*urrent Trends in Liposome Research,* in L*iposomes: Methods and Protocols, Volume 1: Pharmaceutical Nanocarriers,* V. Weissig, Editor. 2010, Humana Press: Totowa, NJ. p. 1-27.

65. Khaw, B.A., et al., I*ntracytoplasmic gene delivery for in vitro transfection with cytoskeleton-specific immunoliposomes.* J Control Release, 2001. 7**5**(1-2): p. 199-210.

66. Krown, S.E., et al., U*se of liposomal anthracyclines in Kaposi's sarcoma.* Seminars in Oncology, 2004. 3**1:** p. 36-52.

67. Jesorka, A. and O. Orwar, L*iposomes: technologies and analytical applications.* Annu Rev Anal Chem (Palo Alto Calif), 2008. 1**:** p. 801-32.

68. Scherphof, G.L., et al., U*ptake and intracellular processing of targeted and nontargeted liposomes by rat Kupffer cells in vivo and in vitro.* Ann N Y Acad Sci, 1985. 4**46:** p. 368-84.

69. Alving, C.R., et al., T*herapy of leishmaniasis: superior efficacies of liposome-encapsulated drugs.* Proc Natl Acad Sci U S A, 1978. 7**5**(6): p. 2959-63.

70. Agrawal, A.K. and C.M. Gupta, T*uftsin-bearing liposomes in treatment of macrophage-based infections.* Adv Drug Deliv Rev, 2000. 4**1**(2): p. 135-46.

71. Senior, J. and G. Gregoriadis, I*s half-life of circulating liposomes determined by changes in their permeability?* 1982. 1**45**(1): p. 109-114.

72. Immordino, M.L., F. Dosio, and L. Cattel, S*tealth liposomes: review of the basic science, rationale, and clinical applications, existing and potential.* Int J Nanomedicine, 2006. 1(3): p. 297-315.

73. McIntosh, T.J., T*he effect of cholesterol on the structure of phosphatidylcholine bilayers.* Biochim Biophys Acta, 1978. 5**13**(1): p. 43-58.

74. Gabizon, A. and D. Papahadjopoulos, L*iposome formulations with prolonged circulation time in blood and enhanced uptake by tumors.* Proc Natl Acad Sci U S A, 1988. 8**5**(18): p. 6949-53.

75. Allen, T.M., S*tealth Liposomes: Five Years On.* Journal of Liposome Research, 1992. 2(3): p. 289-305.

76. Needham, D., T.J. McIntosh, and D.D. Lasic, R*epulsive interactions and mechanical stability of polymer-grafted lipid membranes.* Biochim Biophys Acta, 1992. 1**108**(1): p. 40-8.

77. Johnston, M.J., et al., T*herapeutically optimized rates of drug release can be achieved by varying the drug-to-lipid ratio in liposomal vincristine formulations.* Biochim Biophys Acta, 2006. 1**758**(1): p. 55-64.

78. Laginha, K.M., et al., D*etermination of doxorubicin levels in whole tumor and tumor nuclei in murine breast cancer tumors.* Clin Cancer Res, 2005. 1**1**(19 Pt 1): p. 6944-9.

79. Karanth, H. and R.S. Murthy, p*H-sensitive liposomes--principle and application in cancer therapy.* J Pharm Pharmacol, 2007. 5**9**(4): p. 469-83.

80. Chatzipanteli, K., et al., I*mportance of posttraumatic hypothermia and hyperthermia on the inflammatory response after fluid percussion brain injury: biochemical and immunocytochemical studies.* J Cereb Blood Flow Metab, 2000. 2**0**(3): p. 531-42.

81. Davidsen, J., et al., S*ecreted phospholipase A(2) as a new enzymatic trigger mechanism for localised liposomal drug release and absorption in diseased tissue.* Biochim Biophys Acta, 2003. 1**609**(1): p. 95-101.

82. Huang, S.L. and R.C. MacDonald, A*coustically active liposomes for drug encapsulation and ultrasound-triggered release.* Biochim Biophys Acta, 2004. 1**665**(1-2): p. 134-41.

83. Luo, D., et al., D*oxorubicin encapsulated in stealth liposomes conferred with light-triggered drug release.* Biomaterials, 2016. 7**5:** p. 193-202.

84. Garcia-Jimeno, S., et al., R*eversible and irreversible aggregation of magnetic liposomes.* Nanoscale, 2017. 9(39): p. 15131-15143.

85. Elersic, K., et al., E*lectric-field controlled liposome formation with embedded superparamagnetic iron oxide nanoparticles.* Chem Phys Lipids, 2012. 1**65**(1): p. 120-4.

86. Gao, W., J.M. Chan, and O.C. Farokhzad, p*H-Responsive nanoparticles for drug delivery.* Mol Pharm, 2010. 7(6): p. 1913-20.

87. Webb, B.A., et al., D*ysregulated pH: a perfect storm for cancer progression.* Nat Rev Cancer, 2011. 1**1**(9): p. 671-7.

88. Huber, V., et al., C*ancer acidity: An ultimate frontier of tumor immune escape and a novel target of immunomodulation.* Semin Cancer Biol, 2017. 4**3:** p. 74-89.

89. Swietach, P., et al., T*he chemistry, physiology and pathology of pH in cancer.* Philos Trans R Soc Lond B Biol Sci, 2014. 3**69**(1638): p. 20130099.

90. Bellone, M., et al., T*he acidity of the tumor microenvironment is a mechanism of immune escape that can be overcome by proton pump inhibitors.* Oncoimmunology, 2013. 2(1): p. e22058.

91. Damaghi, M., J.W. Wojtkowiak, and R.J. Gillies, p*H sensing and regulation in cancer.* Front Physiol, 2013. 4**:** p. 370.

92. Lee, E.S., et al., T*umor pH-responsive flower-like micelles of poly(L-lactic acid)-b-poly(ethylene glycol)-b-poly(L-histidine).* J Control Release, 2007. 1**23**(1): p. 19-26.

93. Ferreira, S.M., et al., T*echnetium-99m-labeled ceftizoxime loaded long-circulating and pH-sensitive liposomes used to identify osteomyelitis.* Bioorg Med Chem Lett, 2012. 2**2**(14): p. 4605-8.

94. Morilla, M.J., et al., E*tanidazole in pH-sensitive liposomes: design, characterization and in vitro/in vivo anti-Trypanosoma cruzi activity.* J Control Release, 2005. 1**03**(3): p. 599-607.

95. Andresen, T.L., S.S. Jensen, and K. Jorgensen, A*dvanced strategies in liposomal cancer therapy: problems and prospects of active and tumor specific drug release.* Prog Lipid Res, 2005. 4**4**(1): p. 68-97.

96. Drummond, D.C., M. Zignani, and J. Leroux, C*urrent status of pH-sensitive liposomes in drug delivery.* Prog Lipid Res, 2000. 3**9**(5): p. 409-60.

97. Parente, R.A., S. Nir, and F.C. Szoka, Jr., M*echanism of leakage of phospholipid vesicle contents induced by the peptide GALA.* Biochemistry, 1990. 2**9**(37): p. 8720-8.

98. Polozova, A. and F.M. Winnik, C*ontribution of hydrogen bonding to the association of liposomes and an anionic hydrophobically modified poly(N-isopropylacrylamide).* Langmuir, 1999. 1**5**(12): p. 4222-4229.

99. Meyer, O., D. Papahadjopoulos, and J.C. Leroux, C*opolymers of N-isopropylacrylamide can trigger pH sensitivity to stable liposomes.* Febs Letters, 1998. 4**21**(1): p. 61-64.

100. Drummond, D.C. and D.L. Daleke, S*ynthesis and Characterization of N-Acylated, Ph-Sensitive Caged Aminophospholipids.* Chemistry and Physics of Lipids, 1995. 7**5**(1): p. 27-41.

101. Chen, H., et al., N*ovel pH-sensitive cationic lipids with linear ortho ester linkers for gene delivery.* Eur J Med Chem, 2012. 5**2:** p. 159-72.

102. Samoshina, N.M., et al., F*liposomes: pH-Sensitive Liposomes Containing a trans-2-morpholinocyclohexanol-Based Lipid That Performs a Conformational Flip and Triggers an Instant Cargo Release in Acidic Medium.* Pharmaceutics, 2011. 3(3): p. 379-405.

103. Liu, X., et al., F*liposomes: pH-triggered conformational flip of new trans-2-aminocyclohexanol-based amphiphiles causes instant cargo release in liposomes.* J Liposome Res, 2012. 2**2**(4): p. 319-28.

104. Zhao S., Design and in vitro Characterization of Lipids with a pH-sensitive Conformational Switch and Their Liposomes for Anticancer Drug Delivery. Dissertation, 2018

105. Liu X., Fliposomes: pH-sensitive liposomes comprising novel trans-2-aminocyclohexanol-based amphiphiles as conformational switches for the liposome membrane. Dissertation, 2013

106. Zheng, Y., et al., F*liposomes: trans-2-aminocyclohexanol-based amphiphiles as pH-sensitive conformational switches of liposome membrane - a structure-activity relationship study.* Chem Phys Lipids, 2017.

107. Zheng, Y., et al., t*rans-2-Aminocyclohexanol-based amphiphiles as highly efficient helper lipids for gene delivery by lipoplexes.* Biochim Biophys Acta, 2015. 1**848**(12): p. 3113-25.

108. Zheng, Y., et al., F*liposomes: pH-controlled release from liposomes containing new trans-2-morpholinocyclohexanol-based amphiphiles that perform a conformational flip and trigger an instant cargo release upon acidification.* Nat Prod Commun, 2012. 7(3): p. 353-8.

109. Bangham, A.D., M.M. Standish, and G. Weissmann, T*he action of steroids and streptolysin S on the permeability of phospholipid structures to cations.* J Mol Biol, 1965. 1**3**(1): p. 253-9.

110. Riaz, M., L*iposomes preparation methods.* Pak J Pharm Sci, 1996. 9(1): p. 65-77.

111. Elizondo, E., et al., L*iposomes and other vesicular systems: structural characteristics, methods of preparation, and use in nanomedicine.* Prog Mol Biol Transl Sci, 2011. 1**04:** p. 1-52.

112. Laouini, A., et al., P*reparation, Characterization and Applications of Liposomes: State of the Art.* Journal of Colloid Science and Biotechnology, 2012. 1(2): p. 147-168.

113. Akbarzadeh, A., et al., L*iposome: classification, preparation, and applications.* Nanoscale Res Lett, 2013. 8(1): p. 102.

114. Liu, L. and T. Yonetani, P*reparation and characterization of liposome-encapsulated haemoglobin by a freeze-thaw method.* J Microencapsul, 1994. 1**1**(4): p. 409-21.

115. Pick, U., L*iposomes with a large trapping capacity prepared by freezing and thawing of sonicated phospholipid mixtures.* Arch Biochem Biophys, 1981. 2**12**(1): p. 186-94.

116. Charcosset, C., et al., P*reparation of liposomes at large scale using the ethanol injection method: Effect of scale-up and injection devices.* Chemical Engineering Research & Design, 2015. 9**4:** p. 508-515.

117. Benny C. L. Cheung, T.H.T.S., Johanna M. Leenhouts, Pieter R. Cullis, L*oading of doxorubicin into liposomes by forming Mn2+-drug complexes.* Biochimica et Biophysica Acta (BBA) - Biomembranes, 1998. **Volume 1414**(Issues 1–2): p. Pages 205-216.

118. Amselem, S., A. Gabizon, and Y. Barenholz, O*ptimization and upscaling of doxorubicin-containing liposomes for clinical use.* J Pharm Sci, 1990. 7**9**(12): p. 1045-52.

119. Amselem, S., Y. Barenholz, and A. Gabizon, O*ptimization and Upscaling of Doxorubicin-Containing Liposomes for Clinical Use.* Journal of Pharmaceutical Sciences, 1990. 7**9**(12): p. 1045-1052.

120. Bertrand, N. and J.C. Leroux, T*he journey of a drug-carrier in the body: an anatomo-physiological perspective.* J Control Release, 2012. 1**61**(2): p. 152-63.

121. Blasi, P., et al., S*olid lipid nanoparticles for targeted brain drug delivery.* Adv Drug Deliv Rev, 2007. 5**9**(6): p. 454-77.

122. Nakamura, Y., et al., N*anodrug Delivery: Is the Enhanced Permeability and Retention Effect Sufficient for Curing Cancer?* Bioconjug Chem, 2016. 2**7**(10): p. 2225-2238.

123. Caracciolo, G., C*linically approved liposomal nanomedicines: lessons learned from the biomolecular corona.* Nanoscale, 2018. 1**0**(9): p. 4167-4172.

124. Kheirolomoom, A., et al., C*opper-doxorubicin as a nanoparticle cargo retains efficacy with minimal toxicity.* Mol Pharm, 2010. 7(6): p. 1948-58.

125. Kheirolomoom, A., et al., I*ntracellular trafficking of a pH-responsive drug metal complex.* J Control Release, 2016. 2**43:** p. 232-242.

126. Abend, A., et al., D*issolution Testing in Drug Product Development: Workshop Summary Report.* AAPS J, 2019. 2**1**(2): p. 21.

127. Dokoumetzidis, A. and P. Macheras, A *century of dissolution research: from Noyes and Whitney to the biopharmaceutics classification system.* Int J Pharm, 2006. 3**21**(1-2): p. 1-11.

128. Waters, N.J., et al., V*alidation of a rapid equilibrium dialysis approach for the measurement of plasma protein binding.* J Pharm Sci, 2008. 9**7**(10): p. 4586-95.

129. Motlagh, N.S.H., et al., F*luorescence properties of several chemotherapy drugs: doxorubicin, paclitaxel and bleomycin.* Biomedical optics express, 2016. 7(6): p. 2400-2406.

130. Mohan, P. and N. Rapoport, D*oxorubicin as a molecular nanotheranostic agent: effect of doxorubicin encapsulation in micelles or nanoemulsions on the ultrasound-mediated intracellular delivery and nuclear trafficking.* Molecular pharmaceutics, 2010. 7(6): p. 1959-1973.

131. Wu, D.C. and C.M. Ofner, 3rd, A*dsorption and degradation of doxorubicin from aqueous solution in polypropylene containers.* AAPS PharmSciTech, 2013. 1**4**(1): p. 74-7.

132. Eliaz, R.E. and F.C. Szoka, L*iposome-encapsulated doxorubicin targeted to CD44: A strategy to kill CD44-overexpressing tumor cells.* Cancer Research, 2001. 6**1**(6): p. 2592-2601.

133. Maherani, B., et al., C*alcein release behavior from liposomal bilayer; influence of physicochemical/mechanical/structural properties of lipids.* Biochimie, 2013. 9**5**(11): p. 2018-33.

134. Hamann, S., et al., M*easurement of Cell Volume Changes by Fluorescence Self-Quenching.* 2002. 1**2**(2): p. 139-145.

135. Düzgüneş, N., H. Faneca, and M.C.P. de Lima, M*ethods to Monitor Liposome Fusion, Permeability, and Interaction with Cells,* in L*iposomes: Methods and Protocols, Volume 2: Biological Membrane Models,* V. Weissig, Editor. 2010, Humana Press: Totowa, NJ. p. 209-232.

136. Danaei, M., et al., I*mpact of Particle Size and Polydispersity Index on the Clinical Applications of Lipidic Nanocarrier Systems.* Pharmaceutics, 2018. 1**0**(2).

137. Rane, S.S. and P. Choi, P*olydispersity index: How accurately does it measure the breadth of the molecular weight distribution?* Chemistry of Materials, 2005. 1**7**(4): p. 926-926.

138. Iyer, A.K., et al., E*xploiting the enhanced permeability and retention effect for tumor targeting.* Drug Discov Today, 2006. 1**1**(17-18): p. 812-8.

139. Johnston, M.J., et al., I*nfluence of drug-to-lipid ratio on drug release properties and liposome integrity in liposomal doxorubicin formulations.* J Liposome Res, 2008. 1**8**(2): p. 145-57.

140. Lu, T., et al., I*nfluence of polymer size, liposomal composition, surface charge, and temperature on the permeability of pH-sensitive liposomes containing lipid-anchored poly(2-ethylacrylic acid).* Int J Nanomedicine, 2012. 7**:** p. 4917-26.

141. Ladbrooke, B.D., R.M. Williams, and D. Chapman, S*tudies on lecithin-cholesterol-water interactions by differential scanning calorimetry and X-ray diffraction.* Biochim Biophys Acta, 1968. 1**50**(3): p. 333-40.

142. Redondo-Morata, L., M.I. Giannotti, and F. Sanz, I*nfluence of cholesterol on the phase transition of lipid bilayers: a temperature-controlled force spectroscopy study.* Langmuir, 2012. 2**8**(35): p. 12851-60.

143. Kheirolomoom, A. and K.W. Ferrara, C*holesterol transport from liposomal delivery vehicles.* Biomaterials, 2007. 2**8**(29): p. 4311-20.

144. Avanti Polar Lipids, I., W*hat is the transition temperature of the lipid.* 2018.

145. Anderson, M. and A. Omri, T*he effect of different lipid components on the in vitro stability and release kinetics of liposome formulations.* Drug Deliv, 2004. 1**1**(1): p. 33-9.

146. Avanti Polar Lipids, I., P*hase_Transition_Temps_for_Glycerophospholipids.* 2018.

147. Lovitt, C.J., T.B. Shelper, and V.M. Avery, A*dvanced cell culture techniques for cancer drug discovery.* Biology (Basel), 2014. 3(2): p. 345-67.

148. Inch, W.R., J.A. McCredie, and R.M. Sutherland, G*rowth of nodular carcinomas in rodents compared with multi-cell spheroids in tissue culture.* Growth, 1970. 3**4**(3): p. 271-82.

149. Cox, M.C., et al., T*oward the Broad Adoption of 3D Tumor Models in the Cancer Drug Pipeline.* ACS Biomaterials Science & Engineering, 2015. 1(10): p. 877-894.

150. Wang, C., et al., T*hree-dimensional in vitro cancer models: a short review.* Biofabrication, 2014. 6(2): p. 022001.

151. Sant, S. and P.A. Johnston, T*he production of 3D tumor spheroids for cancer drug discovery.* Drug Discov Today Technol, 2017. 2**3:** p. 27-36.
152. Pickl, M. and C.H. Ries, C*omparison of 3D and 2D tumor models reveals enhanced HER2 activation in 3D associated with an increased response to trastuzumab.* Oncogene, 2009. 2**8(**3): p. 461-8.
153. Sun, T., et al., C*ulture of skin cells in 3D rather than 2D improves their ability to survive exposure to cytotoxic agents.* Journal of Biotechnology, 2006. 1**22(**3): p. 372-381.
154. Colley, H.E., et al., P*olymersome-mediated delivery of combination anticancer therapy to head and neck cancer cells: 2D and 3D in vitro evaluation.* Mol Pharm, 2014. 1**1(**4): p. 1176-88.
155. Benton, G., et al., I*n vitro microtumors provide a physiologically predictive tool for breast cancer therapeutic screening.* PLoS One, 2015. 1**0(**4): p. e0123312.
156. Li, Q., et al., 3*D models of epithelial-mesenchymal transition in breast cancer metastasis: high-throughput screening assay development, validation, and pilot screen.* J Biomol Screen, 2011. 1**6(**2): p. 141-54.
157. Ivascu, A. and M. Kubbies, D*iversity of cell-mediated adhesions in breast cancer spheroids.* Int J Oncol, 2007. 3**1(**6): p. 1403-13.
158. Swietach, P., et al., N*ew insights into the physiological role of carbonic anhydrase IX in tumour pH regulation.* Oncogene, 2010. 2**9(**50): p. 6509-6521.
159. S, T.S., S*narf pH indicators.* Available from: https://www.thermofisher.com/order/catalog/product/C1270, 2003.
160. Lin, R.Z. and H.Y. Chang, R*ecent advances in three-dimensional multicellular spheroid culture for biomedical research.* Biotechnol J, 2008. 3(9-10): p. 1172-84.
161. Kunz-Schughart, L.A., et al., T*he use of 3-D cultures for high-throughput screening: the multicellular spheroid model.* J Biomol Screen, 2004. 9(4): p. 273-85.
162. Sun, B., C.H. Leem, and R.D. Vaughan-Jones, N*ovel chloride-dependent acid loader in the guinea-pig ventricular myocyte: part of a dual acid-loading mechanism.* J Physiol, 1996. 4**95 (Pt 1):** p. 65-82.
163. Baek, N., et al., M*onitoring the effects of doxorubicin on 3D-spheroid tumor cells in real-time.* Onco Targets Ther, 2016. 9**:** p. 7207-7218.
164. Wang, X., et al., D*oxorubicin delivery to 3D multicellular spheroids and tumors based on boronic acid-rich chitosan nanoparticles.* Biomaterials, 2013. 3**4(**19): p. 4667-79.
165. Kim, T.H., et al., T*he delivery of doxorubicin to 3-D multicellular spheroids and tumors in a murine xenograft model using tumor-penetrating triblock polymeric micelles.* Biomaterials, 2010. 3**1(**28): p. 7386-97.
166. Raghunand, N., et al., E*nhancement of chemotherapy by manipulation of tumour pH.* Br J Cancer, 1999. 8**0(**7): p. 1005-11.
167. Gerweck, L.E., S.V. Kozin, and S.J. Stocks, T*he pH partition theory predicts the accumulation and toxicity of doxorubicin in normal and low-pH-adapted cells.* Br J Cancer, 1999. 7**9(**5-6): p. 838-42.
168. Gerweck, L.E., S. Vijayappa, and S. Kozin, T*umor pH controls the in vivo efficacy of weak acid and base chemotherapeutics.* Mol Cancer Ther, 2006. 5(5): p. 1275-9.
169. Graf, B.W. and S.A. Boppart, I*maging and analysis of three-dimensional cell culture models.* Methods Mol Biol, 2010. 5**91:** p. 211-27.
170. Schmitt, J.M., A. Knuttel, and M. Yadlowsky, C*onfocal microscopy in turbid media.* J Opt Soc Am A Opt Image Sci Vis, 1994. 1**1(**8): p. 2226-35.

171. Smithpeter, C.L., et al., P*enetration depth limits of in vivo confocal reflectance imaging.* Appl Opt, 1998. 3**7**(13): p. 2749-54.

172. Centonze, V.E. and J.G. White, M*ultiphoton Excitation Provides Optical Sections from Deeper within Scattering Specimens than Confocal Imaging.* Biophysical Journal, 1998. 7**5**(4): p. 2015-2024.

173. Eetezadi, S., et al., E*ffects of Doxorubicin Delivery Systems and Mild Hyperthermia on Tissue Penetration in 3D Cell Culture Models of Ovarian Cancer Residual Disease.* Mol Pharm, 2015. 1**2**(11): p. 3973-85.

174. Lukowski, J.K., E.M. Weaver, and A.B. Hummon, A*nalyzing Liposomal Drug Delivery Systems in Three-Dimensional Cell Culture Models Using MALDI Imaging Mass Spectrometry.* Anal Chem, 2017. 8**9**(16): p. 8453-8458.

175. Holen, I., et al., I*n vivo models in breast cancer research: progress, challenges and future directions.* Dis Model Mech, 2017. 1**0**(4): p. 359-371.

176. Jung, J., H*uman tumor xenograft models for preclinical assessment of anticancer drug development.* Toxicol Res, 2014. 3**0**(1): p. 1-5.

177. Teicher, B.A., T*umor models for efficacy determination.* Mol Cancer Ther, 2006. 5(10): p. 2435-43.

178. Rygaard, J., H*eterotransplantation of a human malignant tumour to "Nude" mice - Commentary.* Apmis, 2007. 1**15**(5): p. 607-608.

179. Fu, X., P. Le, and R.M. Hoffman, A *metastatic orthotopic-transplant nude-mouse model of human patient breast cancer.* Anticancer Res, 1993. 1**3**(4): p. 901-4.

180. Richmond, A. and Y. Su, M*ouse xenograft models vs GEM models for human cancer therapeutics.* Dis Model Mech, 2008. 1(2-3): p. 78-82.

181. Qiu, W. and G.H. Su, D*evelopment of orthotopic pancreatic tumor mouse models.* Methods Mol Biol, 2013. 9**80:** p. 215-23.

182. Lu, W.L., et al., A *pegylated liposomal platform: pharmacokinetics, pharmacodynamics, and toxicity in mice using doxorubicin as a model drug.* J Pharmacol Sci, 2004. 9**5**(3): p. 381-9.

183. Anders, C.K., et al., P*harmacokinetics and efficacy of PEGylated liposomal doxorubicin in an intracranial model of breast cancer.* PLoS One, 2013. 8(5): p. e61359.

184. Johansen, P.B., D*oxorubicin pharmacokinetics after intravenous and intraperitoneal administration in the nude mouse.* Cancer Chemother Pharmacol, 1981. 5(4): p. 267-70.

185. Warpe, V.S., et al., C*ardioprotective effect of ellagic acid on doxorubicin induced cardiotoxicity in wistar rats.* Journal of Acute Medicine, 2015. 5(1): p. 1-8.

186. Kim, S.H., et al., C*omparision of doxorubicin-induced cardiotoxicity in the ICR mice of different sources.* Lab Anim Res, 2017. 3**3**(2): p. 165-170.

187. Bertazzoli, C., et al., Q*uantitative experimental evaluation of adriamycin cardiotoxicity in the mouse.* Cancer Treat Rep, 1979. 6**3**(11-12): p. 1877-83.